UNIVERSIDADE FEDERAL DO RIO GRANDE DO NORTE

CENTRO DE CIENCIAS EXATAS E DA TERRA

PROGRAMA DE POS-GRADUACAO EM CIENCIA E ENGENHARIA DE MATERIAIS

DOCTORAL THESIS

OBTAINING TRIPLE LAYER POLYCRYSTALLINE DIAMOND COMPACT BY HPHT METHOD

Meysam Mashhadikarimi

Advisor:
Prof. Dr. Uilame Umbelino Gomes

July 2017
Natal - RN

Dr. Meysam Mashhadikarimi

OBTAINING TRIPLE LAYER POLYCRYSTALLINE DIAMOND COMPACT BY HPHT METHOD

Thesis submitted to the Postgraduate Program in Materials Science and Engineering at UFRN as a part of the requirements for obtaining a PhD degree in Materials Science and Engineering.

Advisor: Prof. Dr. Uilame Umbelino Gomes

Universidade Federal do Rio Grande do Norte – UFRN
Sistema de Bibliotecas – SISBI
Catalogação da Publicação na Fonte - Biblioteca Central Zila Mamede

Mashhadikarimi, Meysam.
Obtaining Triple Layer Polycrystalline Diamond Compact by HPHT Method
Meysam Mashhadikarimi. - 2017.
127 f.: il.

Tese (Doutorado) – Universidade Federal do Rio Grande do Norte, Centro de Ciencias Exatas e da Terra. Pós-Graduacao em Ciencia e Engenharia de Materiais. Natal, RN, 2017.
Orientador: Prof. Dr. Uilame Umbelino Gomes.

1. Polycrystalline diamond compact – Tese. 2. High pressure high temperature – Tese. 3. Diamond – Tese. 4. Compacto de diamante policristalino - Tese. 5. Alta pressão e alta temperatura - Tese. 6. Diamante - Tese I. Gomes, Uilame Umbelino. II. Título.

RN/UFRN/BCZM CDU 621.762/.763

Programa de Pós-Graduação em PPgCEM Ciência e Engenharia de Materiais

UNIVERSIDADE FEDERAL DO RIO GRANDE DO NORTE
PROGRAMA DE PÓS-GRADUAÇÃO EM CIÊNCIA E ENGENHARIA DE MATERIAIS-PPGCEM

ATA Nº 195/2017 DE REALIZAÇÃO DA DEFESA DE TESE DE DOUTORADO DO ALUNO **MEYSAM MASHHADIKARIMI** DO PROGRAMA DE PÓS-GRADUAÇÃO EM CIÊNCIA E ENGENHARIA DE MATERIAIS DA UNIVERSIDADE FEDERAL DO RIO GRANDE DO NORTE.

Aos dez dias do mês de julho de dois mil e dezessete, às sete horas, no auditório do Departamento de Física Teórica e Experimental (DFTE) da Universidade Federal do Rio Grande do Norte (UFRN), realizou-se a Defesa de Tese de Doutorado intitulada "OBTENÇÃO DE COMPACTO DE DIAMANTE POLICRISTALINO DE CAMADA TRIPLAR POR MÉTODO HPHT", do Doutorando Meysam MashhadiKarimi, do Programa de Pós-Graduação em Ciência e Engenharia de Materiais (PPGCEM), tendo como Orientador o Prof. Dr. Uilame Umbelino Gomes. A Banca Examinadora foi composta por: Uilame Umbelino Gomes (Orientador e Presidente da Banca) - UFRN; Rubens Maribondo do Nascimento (Examinador Interno ao Programa) – UFRN; Francine Alves da Costa (Examinador Externo ao Programa) – UFRN; Marcello Filgueira (Examinador Externo à Instituição) – UENF; e Clodomiro Alves Junior (Examinador Externo à Instituição) – UFERSA. Inicialmente, o Orientador expôs aos presentes o roteiro formal da Defesa de Tese de Doutorado e, em seguida, deu início aos trabalhos da Banca, passando a palavra ao Candidato para que desse início a apresentação de seu trabalho, marcando o tempo médio de cinquenta minutos para a devida explanação. Concluída a exposição do Candidato, o Presidente passou a palavra aos Examinadores, que deram início ao exame oral. Terminada a arguição oral, solicitou aos presentes e ao Doutorando que se retirassem do recinto para que a Banca proferisse o julgamento. Posteriormente, solicitou o retorno do Candidato e, em seguida, foi comunicado que o aluno Meysam MashhadiKarimi foi APROVADO na Defesa de Tese de Doutorado de acordo com as normas vigentes na UFRN. A versão final do trabalho deverá ser submetida, via SIGAA, para fins de homologação, no prazo de 5 dias, contendo as modificações sugeridas pela Banca Examinadora. Conforme o artigo 46 da Resolução nº 197/2013 - CONSEPE, o candidato não terá o título se não cumprir as exigências acima. Nada mais tendo sido tratado, a Ata da Sessão Pública de Defesa de Tese de Doutorado foi assinada pelos Membros da Banca Examinadora e pelo Candidato ao título.

Prof. Dr. Uilame Umbelino Gomes
Orientador e Presidente da Banca

Prof. Dr. Rubens Maribondo do Nascimento
Examinador Interno ao Programa

Prof. Dr. Francine Alves da Costa
Examinador Externo ao Programa

Prof. Dr. Marcello Filgueira
Examinador Externo à Instituição

Prof. Dr. Clodomiro Alves Junior
Examinador Externo à Instituição

Meysam MashhadiKarimi
Candidato

Every challenging work needs self effort as well as support of others specially those who were very close to our heart,

My effort, I dedicate to my loving

Mother & Father

Whose affection, love and encouragement make me able to get such success and honor.

Acknowledgments

I would like to thank my advisors, Prof. Dr. Uiilame Umbelino Gomes for guiding and supporting me over the years. You have set an example of excellence as a researcher, mentor and instructor.

I express deep gratitude toProf. Dr. Marcello Filgueira for making me the opportunity to do main tests at State University of North Fluminense (UENF), for all his time dedicated to guidance, for the important discussions and valuable suggestions, personally or even at a distance, that were essential to define each step of the project.

I am grateful for the support I had from all professors at Federal University of Rio Grande do Norte especially Prof. Dr. Rubens Maribondo do Nascimento for all their supports during my study in Brazil.

I would also like to acknowledge all laboratory technicians and responsible Professors at Federal University of Rio Grande do Norte especially at LABPEMOL and Laboratorio de Caracterização estrutural dos materiais.

I feel the need to specially recognize the professors and staffs at State University of North Fluminense (UENF) especially Dr. Michel Picanço Oliveira and Renan Guimarães at LAMAV for all their help during my stay in Campus.

I would especially like to thank my amazing family for the love, support, and constant encouragement I have gotten over the years. In particular, I would like to thank my parents, my siblings, and my uncle Prof. Dr. Arab. You are the salt of the earth, and I undoubtedly could not have done this without you.

I would like to acknowledge my undergraduate and master research advisors, Prof. Dr. Ali Habibollah zade and Prof. Dr. Shahram Kheirandish for their constant enthusiasm and encouragement.

I really appreciate all the help I have received from my colleagues at LMCME who helped me directly or indirectly throughout my doctoral period for all their friendship and support for adapting to the new city and new workplace.

Finally, I would like to thank Coordination for the Improvement of Higher Education Personnel (CAPES) foundation for supporting the project.

"The knowledge of anything, since all things have causes, is not acquired or complete unless it is known by its causes"

Avicenna

LIST OF CONTENTS

LIST OF FIGURES

LIST OF TABLES

SYMBOLS AND ABBREVIATIONS

$A1_2O_3$ - Alumina

ASTM - American Society for Testing and Materials.

B_2O_3 - Boron trioxide

BC - Before Christ

BSE ‑ Backscattered electron.

CaO – Calcium oxide.

Co – Cobalt.

CVD – Chemical vapor deposition.

Di – Diamond.

EDS - Energy Dispersive Spectroscopy.

Fe – Iron.

GPa - Giga Pascal.

g/cm^3 - grams per cubic centimeter.

gf – gram force.

Gr - Graphite.

HEM – High energy milling.

HPHT – High pressure high temperature.

HV - Hardness Vickers.

IFT - Indentation fracture toughness.

K_2O - Potassium oxide.

kgf - kilogram-force.

LPS – Liquid phase sintering.

min – Minute.

MPa - Mega Pascal.

Na2O – Sodium oxide.

Nb – Niobium.

Ni – Nickel.

OM – Optical Microscope.

P - Pressure

PCD - Polycrystalline diamond.

PDC – Polycrystalline diamond compact.

SEM – Scanning Electron Microscope.

SiC - Silicon carbide

SiO_2 - Silicon dioxide

u. a. - Dimensionless units.

Vol- volume.

WC – Tungsten carbide.

wt – Weight.

XRD – X-Ray diffraction.

ZnO – Zinc oxide.

K – Degree Kelvin.

°C – Degree Celsius.

μm ‑ micrometer.

ABSTRACT

The primary objective of this thesis was to obtain a triple layer polycrystalline diamond compact (PDC) containing a polycrystalline diamond as top layer, a WC 10 wt% Co substrate, and a WC 20 wt% Nb/Ni interface to bond these two layers via high pressure high temperature (HPHT) sintering. To achieve this objective, the project has been done in three different stages. The first stage was producing diamond sintered body with a suitable binder, and finding the best sintering parameters. The second stage of project was done to study the WC 10 wt% Co hardmetal substrate at different sintering conditions, and the third and last stage was done according to the results achieved from previous stages to obtain a triple layer PDC. At the first stage, four different binders were used to sinter diamond under HPHT condition. Binders were Nb/Fe, Nb/Co, Nb/Ni and pure Nb and 10 wt% binder was used. Sintering was carried out at different temperature and under different pressure and holding time. Obtained samples were studies according to relative density, microstructure, and hardness to find the optimum binder and sintering parameters. Studies at this stage showed that Nb is the best binder and T=1750 °C, 7.7 GPa with holding time more than 6 minutes are the best sintering parameters. At the second stage a powder mixture of WC 10 wt% Co was sintered via HPHT at 1500, 1600, 1700, 1800, and 1900°C under 7.7 GPa pressure for 2 and 3 minutes. Microstructural/structural analyses were performed by SEM/EDS and XRD and hardness, Indentation Fracture Toughness (ITF) and compression tests were also carried out to understand effects of different sintering parameters. At this stage, it was found that full density can achieved for high sintering temperature along with abnormal grain growth. High hardness was observed in range starting from 1250 up to 1650 HV. At the third stage, to obtain PDC, a thin layer of WC 20 wt% Nb/Ni was used as an interface between top layer of diamond with pure Nb binder and WC 10 wt% Co substrate. Sintering was done via HPHT method at 1750°C under 7.7 GPa of pressure. Two different holding time of 6 (three successive 2 minutes) and 9 (three successive 3 minutes) were used. Hardness was measured and microstructural/structural studies were done via SEM/EDS. The overall results showed that this new kind of PDC can successfully produce using a new pure Niobium binder for diamond without any graphitization. It was also found that using an interface having the resemblance to both substrate and sintered diamond body caused good adhesion between layers that can results in enhanced performance and improving durability of PDC.

Keywords: Polycrystalline diamond compact, PDC, High pressure high temperature, Diamond, Interface, WC/Co substrate.

Resumo

Neste trabalho de pesquisa, foi obtido um compacto de diamante policristalino (PDC), constituído de uma camada superior de diamante policristalino sob um substrato de WC-10% em peso de Co e uma interface de WC-20% em peso de Nb/Ni entre as camadas, através de método de sinterização de alta pressão e alta temperatura (HPHT). Para alcançar esse objetivo, foram realizadas três etapas distintas. Na primeira etapa, foi sinterizado o corpo de diamante com um ligante adequado, e foram obtidos os melhores parâmetros de sinterização. Na segunda etapa, foi realizado o estudo de diferentes condições de sinterização para o substrato de metal duro WC-10% p.Co. E, na terceira e última etapa, foi produzido, de acordo com os resultados alcançados nas etapas anteriores, o compacto de diamante policristalino de camada tripla (PDC). Na primeira etapa, quatro ligantes diferentes foram usados para sinterizar o diamante através do método HPHT. Os ligantes utilizados foram o Nb/Fe, Nb/Co, Nb/Ni e Nb puro, sendo 10% em peso de ligante utilizado para cada composição. A sinterização foi realizada a diferentes temperaturas e sob diferentes pressões e tempos. As amostras obtidas foram analisadas através das medidas de densidade relativa e dureza, além das imagens eletrônicas de varredura, para encontrar os melhores parâmetros de sinterização e ligante. Os estudos mostraram que o Nb apresentou o melhor comportamento, e que os melhores parâmetros de sinterização foram: T = 1750 °C, P = 7,7 GPa, t = 6 minutos. Na segunda etapa, uma mistura em pó de WC-10% em peso de Co foi sinterizado através de HPHT sob pressão de 7,7 GPa, variando temperatura (1500 ºC, 1600 ºC, 1700 ºC, 1800 ºC, 1900 ºC) e tempo (2 e 3 minutos). As análises microestruturais e estruturais foram realizadas através de MEV/EDS e DRX. Ensaios de dureza, tenacidade (ITF) e de resistência à compressão, também, foram realizados para entender os efeitos de diferentes parâmetros de sinterização nas propriedades dos sinterizados, verificando-se densificação total das amostras sinterizadas a altas temperaturas. Entretanto, foi observado um crescimento anormal de grãos para estas mesmas temperaturas. Altos valores de dureza foram observados, aproximadamente, entre 1250 a 1650 HV para todas as amostras sinterizadas. Na terceira etapa, para a obtenção do PDC, uma camada fina de WC-20% em peso de Nb/Ni foi utilizada para a formação da interface entre a camada superior de diamante com ligante de Nb pura e o substrato de WC 10% em peso de Co. A sinterização foi feita através do método HPHT à temperatura de 1750 °C sob 7,7 GPa de pressão. Foram utilizados dois tempos diferentes, de 6 min. (três sucessivos 2 minutos) e 9 min. (três sucessivos 3 minutos). A dureza foi medida e os estudos estruturais/microestruturais foram realizados através de

análises de MEV/EDS. Em suma, os resultados mostraram que este novo tipo de PDC pode ser produzido com sucesso, usando um novo ligante, o niobio puro, para o diamante, sem qualquer presença de grafitização. Verificou-se também que o uso de uma interface com os mesmos elementos constituintes do substrato e do corpo de diamante sinterizado resultou numa boa adesão entre as camadas, o que pode resultar em melhor desempenho e melhorar a durabilidade do PDC.

Palavras-chave: Compacto de diamante policristalino, PDC, Alta pressão e alta temperatura, Diamante, Interface, Substrato de WC/Co.

Chapter 1:

Introduction

1. Introduction

The main tools employed in the drilling industry are roller cone and drag bits. Roller cone bits work by impact excavation and are currently used in hard rock formations because of a convenient wear resistance. Drag bits rather operate by shear mode in softer rock to medium hard formations. Nevertheless, they suffer from thermal abrasive wear and impact damage while drilling interbedded formations. As excavation rate is directly related to the overall cost, the drag bits using Polycrystalline Diamond Compact (PDC) cutters are really attractive compared to roller cone bits. In fact, PDC bits could drill twice faster and longer than roller bits even in hard formations [1].

The introduction of the man-made polycrystalline diamond cutting element, marketed by General Electric under the name STRATAPAX, heralded a revolution in the drill bit industry. Cutting elements, or compacts, of sintered diamond grains could be made in large, convenient sizes and did not have the cleavage planes of natural diamonds. The drag bit, a concept which had lain almost dormant for many years, was revived. New designs were fitted with the improved cutters, and they were run in almost every conceivable formation. As with most new technologies in high-risk enterprises, there were heartening successes and spectacular failures, but two features made these bits extremely attractive for geothermal use. Monolithic construction meant no moving parts, thus eliminating the problems of high-temperature bearings, seals, and lubricants; and a fundamentally different way of removing the rock (shearing, not crushing) drastically improved rate of penetration. PDC bits also became very popular in the oil patch in the early 1980's more than 20 companies were manufacturing them in a variety of configurations. The bits had some success in geothermal drilling where the formations were sedimentary, but most of our effort has been directed toward making them effective in the hard, fractured rocks so characteristic of hot reservoirs [2].

Petroleum and hydrothermal investigations in deep geological formations lead to manufacturing new bits materials able to drill at higher temperature, in more abrasive and harder geological fields. Such innovating materials, sintering processes and design, recently developed to improve drill bits hardness and fracture toughness [3].

Growing demand for hydrocarbons, and thus increase in their price has caused rapid development of drilling technology. For this reason also, wells are being drilled in an increasingly demanding geological conditions. All these factors contribute to the increased cost of drilling

operations and the need to reduce the duration of drilling. It entailed intense competition among the major manufacturers bringing continuous development in drill bit technology. Drilling in a deeper in more harsh conditions well requires a more advanced drilling technology and equipments. Therefore, the efficiency of drilling tools is increased by improving their quality, allows a further increase in rate of penetration. This is particularly important when drilling deep wells, especially in the case of drilling in hard formations. Drilling bit is the main part of drill string which is placed at the bottom of it. Bits are used to crush or cut the rock formation [4].

These cutters are composed of a layer of polycrystalline diamond bonded in-situ on to a Tungsten carbide substrate. The bonding is done during a high pressure and high temperature sintering process. The polycrystalline diamond layer is also created during this process to form a sintered material characterized by strong diamond to diamond bonding [5]. However, despite their extensive use and excellent abrasion resistance, PDC tools are still highly susceptible to fractures [6-11]. This is mainly a result of their relatively low fracture toughness [12].

In addition to new design for cutters to improve serviceability, study on new materials and producing method is really important. New PDCs with improved microstructure in both diamond layer and hardmetal substrate along with good bonding between layers can produce a tool with enhanced properties for available application as well as new ones. Solving problems of conventional PDCs such as graphitization and interlayer fracture, is possible either with new technology and design or using new materials.

The scope and objective of this thesis comprises both literature studies and experimental activities to obtain a triple layer polycrystalline diamond compact with new composition. The activities are:

- Literature study on polycrystalline diamond compacts, their properties and problems.
- Finding a binder for sintering diamond powder via HPHT method.
- Study hardmetal substrate at different sintering conditions.
- Using an interface to bond diamond layer and hardmetal substrate in order to improve overall properties.

This project aims to produce PDC wherein the substrate comprises cemented WC with a Co binder phase and the top layer is polycrystalline diamond with suitable binder.

Binding these two layer using an adequate interface is the main goal of the project that can provide a higher performance cutter for use in drilling, mining and quarrying.

The produced PDC can have an advantage over the prior art, in that, the lower and more uniform residual stresses provided by the thin and very uniform interface layer of hardmetal bonded to the substrate, materially reduces diamond layer delamination.

Another advantage is using an interface with composition close to the substrate and diamond layer that improve the adhesion of the both diamond and substrate to the interface.

Also in this project a new binder (pure Nb) is also used for sintered diamond layer. This binder can improve properties of the layer and as the interface also includes Niobium, it can have better adhesion as well.

Chapter 2:

Literature review

2. Literature review

2.1 Diamond

Diamond, an allotropic form of carbon, is the hardest mineral known to man [13, 14]. The flawless, or virtually flawless, pieces of diamond, when cut and polished, have always been valued as the most precious gems. Except rarity of gemstones and their decorative merits, there are also many other properties which make diamond a unique material [15]. It has the highest thermal conductivity at room temperature, the highest bulk modulus and the highest critical tensile stress for cleavage, an extremely high thermal conductivity, very low coefficients of friction and thermal expansion, and it is relatively inert to chemical attack by common acids and bases.

Until now, only few of these properties have fully been exploited in advanced industrial applications due to limited size and high price of diamond. The latest progress in diamond synthesis, however, is starting to remove the existing barriers, opening new opportunities for diamond as an advanced engineering material [16].

A great deal of research has already been undertaken to understand the properties and defect structures of both natural and synthetic diamond grains with excellent coverage given in the following references [17–20]. What emerges from these fundamental studies is that the properties of both natural and synthetic diamonds can vary significantly and the choice of the most appropriate source material for tool manufacture depends on the application to which diamonds will be put. In particular, diamond powder is extensively utilized as an abrasive for practical use and for nucleus formation in the fabrication of diamond films by the chemical vapor deposition (CVD) method [21].

As regards the diamond abrasive, its type, size and concentration are factors that have the greatest significance. Diamond manufacturers provide the toolmakers with a wide range of natural and synthetic grits of varying properties such as mechanical strength, thermal stability and matrix retention characteristics (Figure 2.1). The major difference between the natural and synthetic diamond is in the impurity content and particle shape. Natural grits, made by crushing mined diamond board, are free from metallic inclusions and hence show markedly higher thermal stability. They can retain strength throughout the whole range of PM processing temperatures, whereas synthetic grits begin to lose strength beyond 800°C. From the matrix retention viewpoint, crushed crystals possess excellent bonding characteristics, which result from the many re-entrant surfaces. This makes the natural diamond advantageous

for certain applications, e.g. frame sawing of sedimentary and metamorphic stones. On the other hand, the irregular diamond surface impairs mechanical strength [16].

Figure 2.1 Natural (a) and synthetic diamond abrasives produced by using Cobalt-base (b) and Nickel-base catalyst (c).

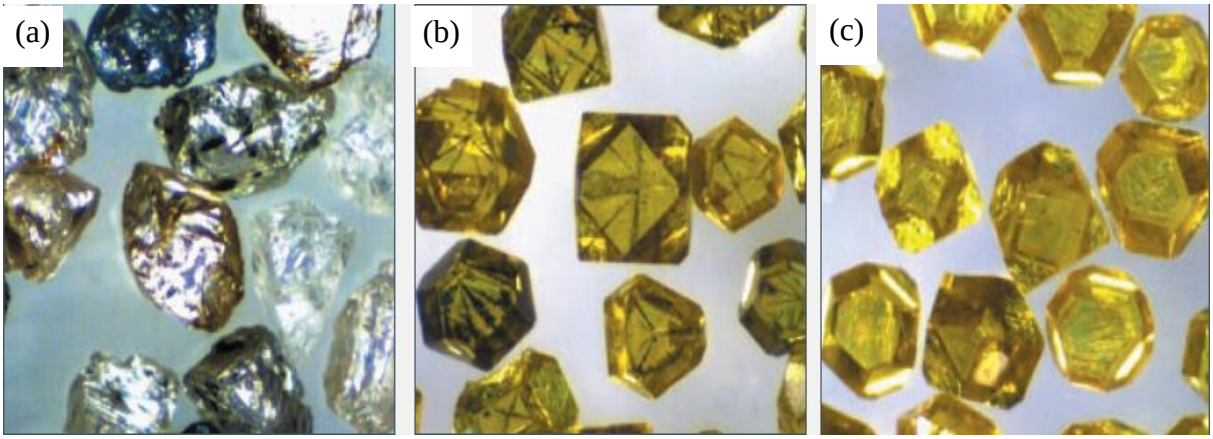

Source: [16].

The processed material primarily determines the type of diamond abrasive used in the tool. A good general rule is the harder the work piece, the stronger the diamond grit has to be selected. Diamond manufacturers provide the toolmakers with a wide range of natural and synthetic grits of varying properties such as mechanical strength, thermal stability and matrix retention characteristics [16].

Natural grits, made by crushing mined diamond board, are free from metallic inclusions and hence, they show excellent thermal stability. Natural diamond particle scan retain their original mechanical strength even up to around 1400 °C whereas synthetic grits begin to lose strength beyond around 800 °C [22]. From the matrix retention viewpoint, crushed crystals possess excellent bonding characteristics, which result from the many re-entrant surfaces. This makes the natural diamond advantageous for frame sawing of marble, limestone and other less hard stones. On the other hand, the irregular diamond surface impairs mechanical strength. In more rigorous applications, this drawback may successfully be dealt with by using rounded diamonds, which are designed and processed to cope with high-impact forces [22]. The rounded shape implies, however, that higher cutting forces are generated and hence rigid and more powerful machines are required. It is reasonable to choose rounded natural grits for manufacturing processes, which involve high hot pressing temperatures and give priority to low tool fabrication costs. The two mentioned natural diamond abrasives are illustrated in Figure 2.2.

Figure 2.2 Natural diamond abrasives with (a) re-entrant surfaces and (b) rounded.

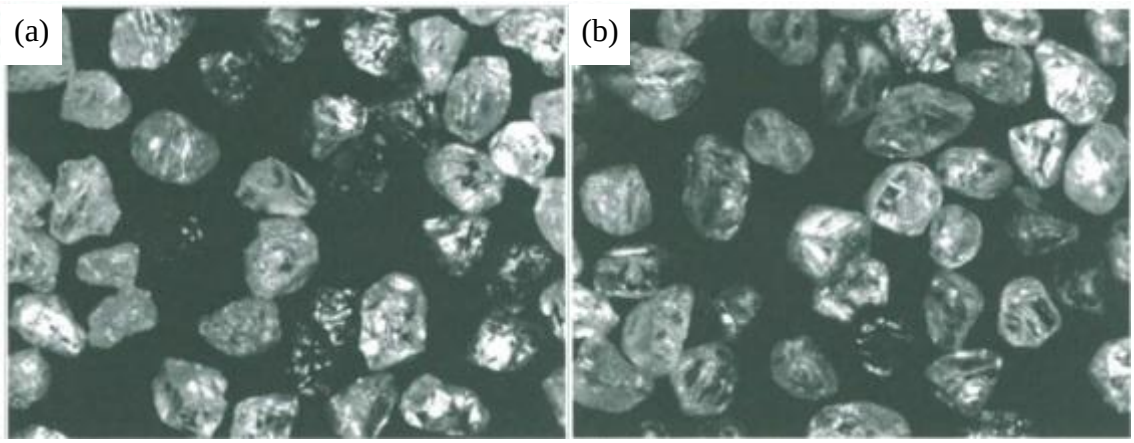

Source: [16].

The main advantage of using synthetic diamond is that it can be designed and manufactured to satisfy virtually any specific application requirements [16]. There are three main diamond manufacturing process: (1) high pressure, high temperature (HPHT) synthesis, usually operating in the diamond stability field [14, 23], (2) chemical vapor deposition (CVD) [24, 25] and (3) detonation synthesis [26]. Three important characteristics of diamond grit/grain used in composite manufacture are: (1) grain size, (2) grain shape and (3) strength [16]. Other physical properties that have important implications for the performance of diamond composites are: thermal stability, thermal fatigue strength, fracture toughness and - impact strength. As these properties have been reviewed elsewhere [17-19] they will only be referred to indirectly whenever they relate to the wear behavior of diamond composites.

2.2 Diamond and Graphite, Allotropic Form of Carbon

In 1961 Professor H. Tracy Hall [27] from Brigham Young University, in his research paper "The Synthesis of Diamond", describes the differences between diamond and graphite. In his paper, he explains that the difference at the atomic level between diamond and graphite could not be observed until the decade of 1910 to 1920, when the X-ray diffraction technique was developed to help study the crystal structures.

Diamond consists of carbon atoms aligned in hexagonal rings lying in the crystallographic plane 111, which is the natural cleavage plane of the diamond. These carbon rings are piled one on top of the other, duplicating every four times the initial sequence. Then every central atom is bounded by four other atoms at equal distances. All distances between atoms are 1.54Å.

In the case of graphite, the arrangement of the atoms is comparable to that of diamond in the sense that the layers are heaped in a parallel way one on top of the other creating hexagonal rings. The main difference is that they are not creased as closely as the diamond. The distance between the atoms in the same layer is closer than in the diamond formation at 1.42Å, but the individual planes are spaced farther apart at 3.37Å.

The bonding between the atoms for diamond is predominately covalent due to the formation of sp^3 hybrid bonds. All bonds are aliphatic in character, and equal, meaning that they are aligned at equivalent distances from each other. In the case of graphite, it has double bond character in its rings, so the molecule is aromatic in character. By comparing the two crystal arrangements, it can be deduced that graphite can be converted into diamond by utilizing high pressure to shorten the distance between the graphite bonds, forcing the rings to crease closer to each other to emulate the ones in the diamond crystal lattice. It must be considered that this transformation is reversible and at a certain condition diamond also can transform to graphite, this reverse transformation is called graphitization [27].

2.3 Transformation Problems

The process of changing graphite to diamond is more complex than just applying force to the graphite to realign its atom's bonding. As expressed by Professor Hall in his paper [27], there are two main problems when we are talking about a change in the polymorphic form of a material. These two problems are: the thermodynamic problem and the chemical kinetic problem.

It is important to have both in consideration when we are trying to convert graphite into diamond. Thermodynamics is concerned with the relative energies of the reactants and the resultants of a chemical response. So, if we want to change graphite into diamond, we need to ensure that we have a negative relative energy in order to have the thermodynamic permission to convert one to the other. In case of having a very large negative relative energy number, meaning that the free energy from the reactant is much greater than the free energy of the product, the reaction will still happen, but it will be difficult to control the process. Here is where the kinetics comes into place.

We now know that at atmospheric pressure the diamond is thermodynamically unstable with respect to graphite. So if we increase the temperature of the diamond it will convert back to graphite (graphitization). To prevent this reaction and to keep the relative energy negative, when sintering diamond it is necessary to increase the pressure

proportionally to the increase in temperature. The higher the temperature utilized, the higher the pressure that needs to be applied [27].

In 1976 the equilibrium boundary between diamond and graphite was determined over a temperature range that included 1100°C and 1625°C, and the pressure was computed in force/area measurements. Scott Kennedy and George Kennedy [28] published a research work in which an equilibrium equation for the diamond-graphite boundary was formulated and tested. The equation is:

$$P(\text{kbar}) = 19.4 + T(°\text{C})/40 \text{ kbar} \qquad \text{(equation 2.1)}$$

The results of the equation were plotted, and they matched the results from previous research works done on determining the diamond-graphite temperature-pressure phase diagram. Figure 2.3 shows the comparison of Kennedy's work and the prior work published by General Electric Company's research group. All G.E.'s work was done on a "belt" press, which is quite hard to calibrate for a precise internal pressure measurement. Kennedy's work was done in a piston-cylinder apparatus with a "Zero-friction" cell design, to ensure a better pressure representation [28].

This graphite-diamond phase diagram is a good source of information on which researchers and diamond manufacturers to base their processes. More recent work shows that spontaneous transformations from one solid phase to another can happen at room temperature, but it gets reverted to graphite after decompression [14].

The use of a solvent-catalyst, like Nickel, Cobalt, or Iron is required to take the carbon atoms apart from the graphite into a solution allowing them to rearrange, precipitating as diamond crystals.

In the case of sintering diamond to carbide Tungsten substrates, as in the manufacturing of polycrystalline diamond compact inserts (that is the objective of this work), the Cobalt utilized as a binder in the cemented carbide infiltrates through the diamond crystals with the function of catalyst on the nucleation of the Graphite to Diamond. Without the help of the Cobalt, the synthesis of the diamond crystals will be almost impossible but in the other hand using Cobalt can cause graphitization (transforming diamond to graphite) during the service especially at high temperature [29].

Figure 2.3 Graphite-diamond equilibrium graph showing the comparison between Kennedy's work (This work) and previous published work by G.E's researchers. Note: 10kbar = 1 GPa.

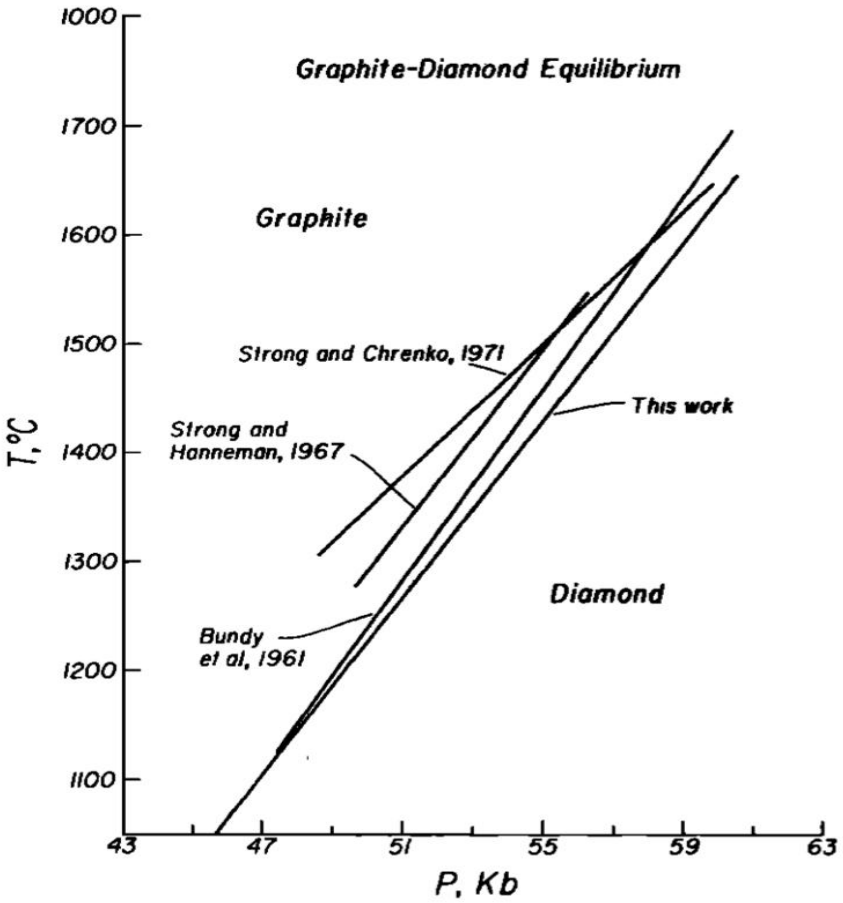

Source: [28].

2.4 History of Diamond Tools

The modern application of diamond tools is roughly a century old although the early use of diamond as an engraving tool goes back to 350 BC [30]. In Christ's time, splinters from broken diamonds were first applied as a set in Iron handles, i.e. metal bonded diamond tools [30, 31].

The next milestone in the history of diamond tools was to take place in 1819, when the first patent for a diamond wire-drawing die was granted to Brockendon in England [16]. At that time, however, it proved impossible to implement this invention into practical use and it took around 40 years until the first diamond wire-drawing die was successfully made and utilized by Milan and Balloffet in France [30].

Meanwhile, in 1824, Pritchard started to use shaped diamond wheels to grind and polish microscope lenses [30-32]. These wheels were made by hammering diamond grits, of adequate fineness, into the surface of a cast Iron body [31].

In 1854 a French engineer Hermann applied for a patent for a single-crystal diamond tool for cutting, turning and shaping hard stones which, upon improvements made a year later, were converted into a tool with multiple diamonds [30]. A few years later, in 1862, Leschot of Geneva was granted a patent covering a complete drilling rig which was to find practical application on a broader scale more than a century after the first description of a primitive diamond rock drill had appeared in Diderot's Encyclopedia [30, 32].

The first diamond circular sawblades for cutting stone were developed by Fromholt in France in 1885. Thirteen years later, a large diameter blade was first used in practice in the Euville stone quarries. The early blades used Brazilian carbonado diamonds set around their periphery. Carbonado was a valued material at that time [32] because, being a cryptocrystalline mass of small crystals locked in random directions; it was strong and resistant to cleavage. Such carbonado blades were utilized to cut limestone and marble during the construction of large buildings in Paris in the 1900s [30].

Further progress in the tool production routes took place in the period between 1927 and 1931, when the earliest patents describing the manufacture of metal matrix abrasive tools, by making them from powders, were issued in the USA and Great Britain. According to Gauthier (1927) [33], the powder mix was to be consolidated by cold pressing only, whereas Neven (1931) was probably the first to suggest hot pressing [34]. The first metal powder used was electrolytic Iron.

The idea of bonding diamond by means of metal powders dates back to 1883, when Gay described the manufacture of abrasive materials by incorporating traditional abrasives, such as quartz or emery, in a metal matrix [34]. He mentioned the use of brass, Iron or steel powders and proposed to make a good use of powder metallurgy techniques, such as hot pressing or infiltration, to form the matrix [34]. It had taken, however, a few decades until the inventions of the 1920s and 1930s made refinements to the Gay's ideas and apparently speeded up the development of diamond grit impregnated tools which were finally introduced to industrial application around 1940 [2].

Bonds other than metal were also being developed during this period. In 1925 the Bakelite Corporation took out a patent on the first phenolic resin bond [35]. In the early 1930s

resin-bonded wheels, containing 'fragmented' natural diamond grit, were patented by Wickman Ltd. in England (1933), Voegeli & Wirz in Switzerland (1934) [30], and Norton Co. in the USA (1934) [36].

Until the early 1950s the developments in diamond tools were relatively slow. In that period only mined diamond crystals were available. These were formed millions of years ago, under conditions of intense heat and pressure acting on the carbon, and later ejected to the surface by volcanic eruptions [16].

Much faster developments in the tool manufacturing technology, which have been seen over the last 50 years or so, may chiefly be attributed to the 'invention' of synthetic diamond. Efforts to manufacture synthetic diamond crystals date back at least several hundred years. They had remained fruitless until 1953, when positive and fully reproducible results were obtained by a team of researchers at ASEA [37]. Quite independently, and entirely without knowledge of what ASEA had been doing, General Electric announced its capability to manufacture synthetic diamonds on an industrial scale in 1955 [38]. While ASEA kept the diamond experiments secretive, GE was first to describe the process in the scientific literature [39] and patented it [40].

Permanent progress in the manufacturing technologies fostered the commercial importance of synthetics, which is now accounting for over 95% of all industrial diamonds consumed [41]. It is worthwhile to mention that the last five decades witnessed a spectacular, 50-fold or so, increase in the total consumption of industrial diamond. Over this time modern production techniques based on diamond tooling have been implemented into evolving areas of industrial activity enabling to do the job faster, more accurately and at less cost. They revolutionized machinery and processing techniques in the stone and construction industries, road repair, petroleum exploration, woodworking, cutting frozen foods, production of various parts and components made of glass, ceramics, metals, plastic and rubber, etc.

2.5 Classification of Diamond Tools

The term 'diamond tools' has a very broad meaning. The existing classifications of diamond tools are based on various criteria, such as the quantity of diamond involved and its origin, outward appearance and internal structure of the tool, its application, etc.

For the purpose of this thesis, like other sources, it is convenient to arrange the tool types into categories which would be distinctive with respect to the various manufacturing methods involved. Such a classification is shown in Figure 2.4.

Figure 2.4 Classification of diamond tools.

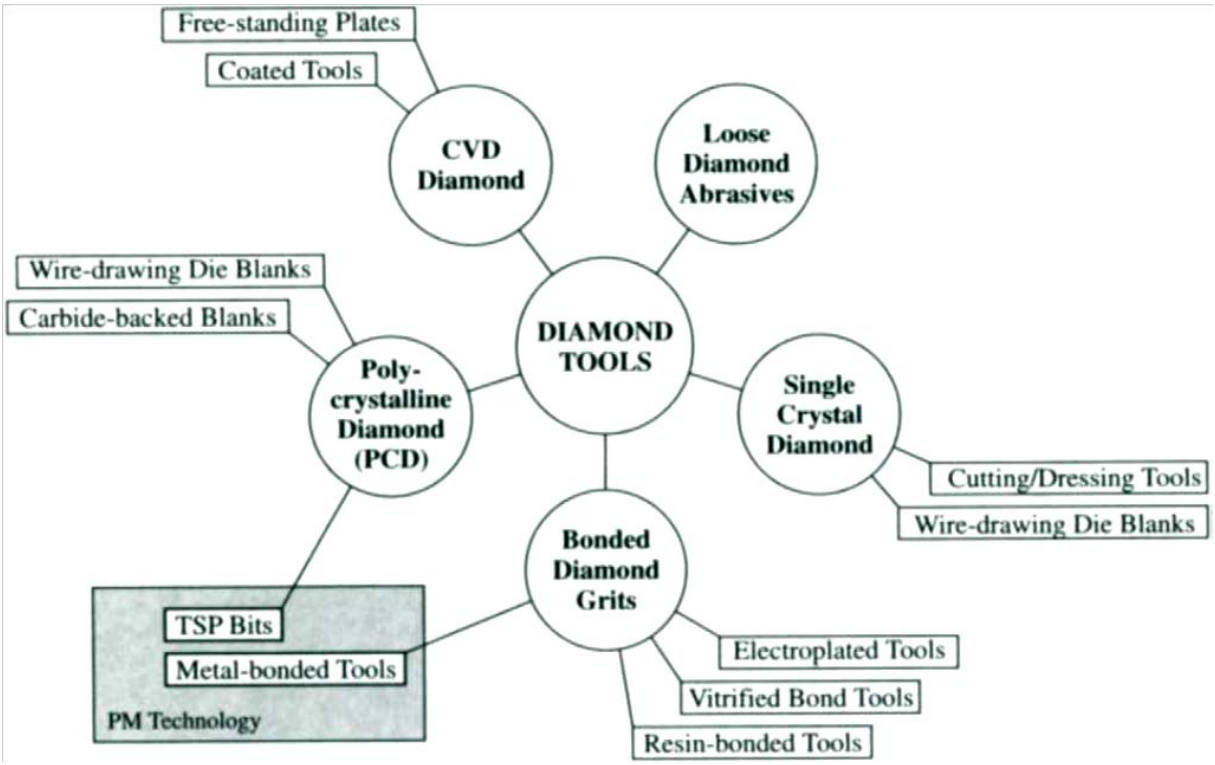

Source: [16].

2.5.1. *Loose Diamond Abrasives*

A loose diamond micron powder constitutes the simplest diamond tool (Figure 2.5). The existing diamond sizing standards define micron powders as nominally finer than around 84 μm although various sizing criteria and techniques are utilized [42]. Both natural and synthetic micron abrasives, mostly in a paste or liquid suspension form, are used for a wide variety of fine grinding and polishing operations. The most typical applications are preparation of metallographic, ceramic and mineralogical specimens [43], finishing of diamond cutting tools [44], profiling and calibration of diamond wire-drawing dies [45], polishing gemstones, sizing and finishing hardened steel and Tungsten carbide tool components [46], etc.

2.5.2. *Single-Crystal Diamond*

Single-crystal diamond tools, both natural and synthetic, are used as cutting tools, dressers and wire-drawing dies. Poor availability of large natural stones, variations in their quality, and time-consuming diamond selection and tool tip preparation procedures have, however, markedly restricted the consumption of natural stones over the last decade or so. The recent developments in high pressure-high temperature diamond technology make it

possible to produce synthetic single-crystal diamonds having sufficient size and consistency of shape, crystallographic orientation and performance not achievable with natural products [47-49].

Figure 2.5 Loose diamond micron powder products.

Source: www.eastwinddiamondabrasives.com

Diamond cutting blanks and dresser logs are produced by laser cutting of raw monocrystals [50]. Synthetic diamonds are more regular in shape than natural stones and the crystallographic orientations of each crystal are easy to define. Therefore large synthetic crystals can readily be cleaved into plates and laser cut [48] to produce suitable shapes in a broad range of sizes, up to around 8 mm as standard [47,50], with crystallographically orientated sides and cutting edges. Figure 2.6 show some kinds of single crystal diamond tools.

2.5.3. *Bonded Diamond Grits and Powders*

This is by far the largest group of diamond tools used in a variety of workpiece machining applications. They consist of diamond particles, either mono or polycrystalline, which are embedded in diverse metallic or non-metallic matrices by various fabrication routes. This kind of diamond tools classifies in four categories of electro plated, vitrified bond, resin bonded, and metal bonded diamond tools [16].

Nowadays diamond electroplated tools (Figure 2.7) are used on a broader scale for sawing, grinding, boring, profiling, brushing, and surface-finishing of glass, porcelain, cemented carbides, refractory metals, plastics, and other materials. Both natural and synthetic

diamond grits, and powders, are used for electroplating. Synthetic crystals often require purification prior to electro-deposition since metallic inclusions, originating from the metal solvents used during diamond synthesis, may promote harmful over plating of the abrasive particles [51]. Natural diamonds, being inherently free from metallic inclusions, do not require any chemical or thermo-chemical pre-treatments and are perfectly suited for the tool fabrication by electroplating.

Figure 2.6 Samples of single crystal diamond tools

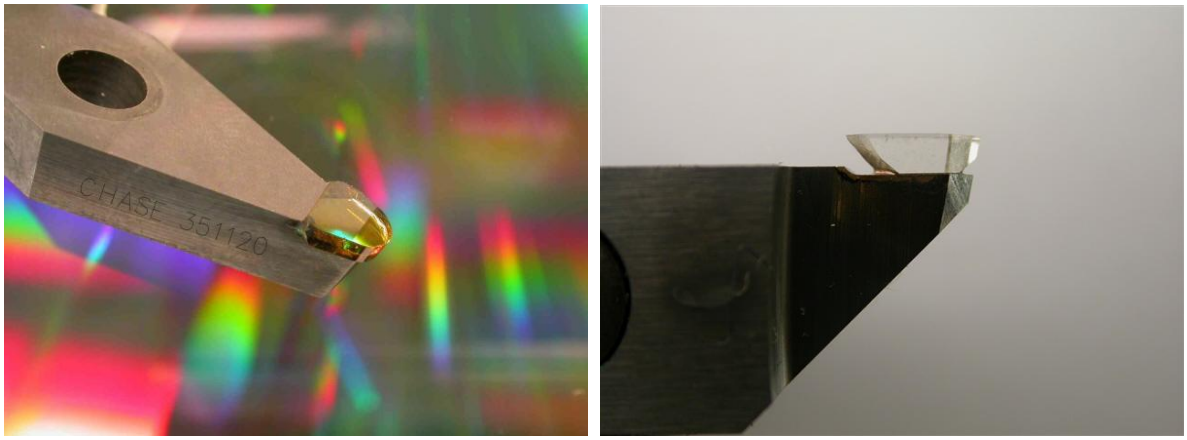

Source: www.chasediamond.com.

Figure 2.7 Electro plated diamond wheels.

Source: Balaji Abrasives Tools Pvt. Ltd.

The main compounds used to produce vitrified bonds are SiO_2, Na_2O and CaO that comprise the basic glass [52]. Some other constituents, such as SiC, $A1_2O_3$, B_2O_3, ZnO, K_2O, as well as feldspar, clays and other natural minerals, are also added in varying proportion to

modify the characteristics of the material [52, 53]. The powdered bond-diamond abrasive mix, with diamond concentration typically between 18 and 37 vol% [54], is either cold pressed and sintered in a furnace at 900-950°C [55] in an inert atmosphere or, preferably, hot pressed at around 730°C [52]. The advantage of the latter route is markedly shorter processing time at lower temperature. Such a procedure yields tools with lower porosity and is less detrimental to the diamond toughness if a synthetic abrasive has been chosen (Figure 2.8).

Figure 2.8 Vitrified bond diamond wheel.

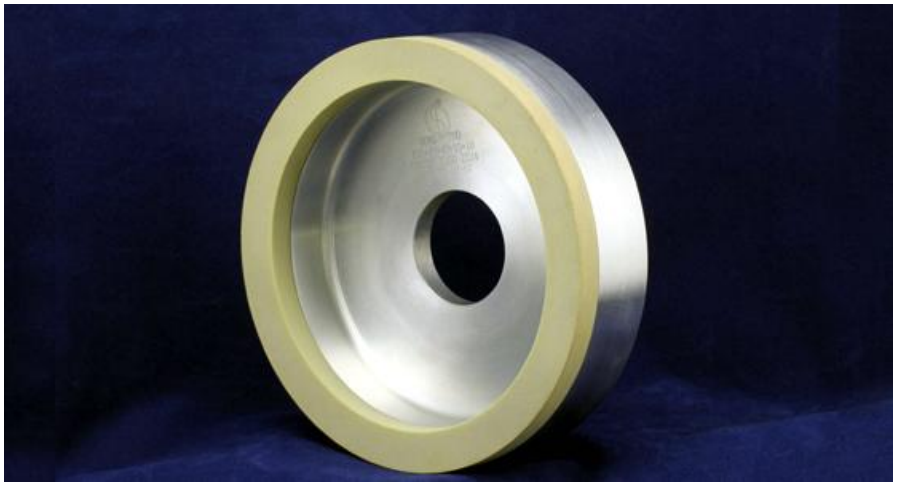

Source: www.superabrasives-tools.com.

In the vast majority of cases resin bonds are based on either phenolic resins or, more thermally stable, phenol-aralkyl resins [56]. They are used in the form of a very fine powder which accounts from around 30 to 40 wt% of the bond in dry and wet grinding wheels, respectively. To impart strength to the bond, the resins are mixed with SiC filler [53]. The bond components are carefully mixed with a suitable amount of natural or friable synthetic diamond grit. The mix is poured into a mould and hot pressed to shape the abrasive rim which is subsequently attached to the tool body by using a suitable adhesive [56].

Resin-bonded diamond tools (Figure 2.9) offer cost-effective grinding where close dimensional tolerances and good surface finish are critical. For that reason they have found application in grinding of cemented carbides [53, 57], oxide and non-oxide ceramics, glass [58, 59], as well as in fine grinding and polishing of natural stones [60].

In the production volume terms, metal-bonded tools account for around two-thirds of the whole bonded-grit diamond tool market [61]. In the metallurgical sense, the term 'metal bond' should be applied to electroplated products rather than to metallic matrix diamond

composites which, after all, most frequently occur in the colloquial technical language as 'metal-bonded' or 'sintered' tools. As characterized by the latter synonym, the distinctive feature of what has been classified as metal-bonded diamond tools (Figure 2.10) is an application of different powder metallurgy (PM) techniques to the manufacture of the diamond-impregnated working layer.

Figure 2.9 Resin bonded diamond wheel.

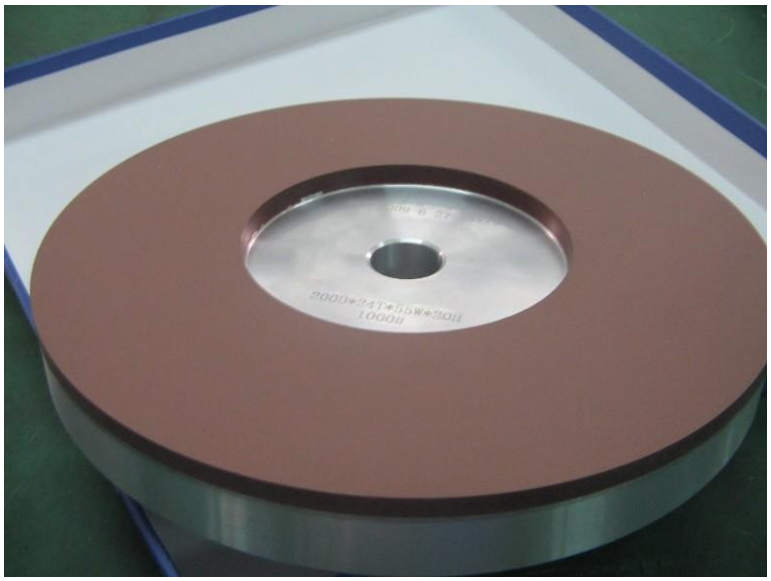

Source: www.bjkshs.com.

Figure 2.10 Metal bonded diamond tools with copper alloy matrix.

Source: www.cdtusa.net.

2.5.4. *CVD diamond tools*

An alternative route to synthesis diamond is by various chemical vapor deposition (CVD) techniques, which consist in deposition of metastable polycrystalline diamond film from a gaseous phase onto a suitable substrate maintained at between 700 and 1000°C [47,

62, 63]. In general, a mixture of carbon carrier gas, typically 1% methane, and hydrogen is introduced into a CVD reactor where the gases are decomposed, below atmospheric pressure, by utilizing various energy sources, such as the electric arc, hot filament, microwaves, combustion flame, etc. The use of hydrogen facilitates removal of non-diamond deposits, whereas the diamond film is allowed to nucleate on the substrate and grow. As no metal catalysts are used in the synthesis process, the CVD diamond is free from metallic inclusions and therefore it is thermally stable.

Thus far CVD diamond coated drills (Figure 2.11) and turning inserts have not made significant progress in industrial application mainly due to problematic preparation of the cutting edge and the ease of delaminating of the diamond layer [47].

Figure 2.11 Carbide CVD diamond coated drills.

Source: www.apacheaerospace.com.

2.5.5. *Polycrystalline Diamond (PCD)*

Since the early 1970s, PCD has become established as a high-performance and cost effective alternative to conventional tools in the most demanding industrial applications, such as high-temperature drawing of wire [64], machining of metal matrix composites [65], fiber reinforced plastics, high Al-Si alloys [47], and abrasive wood composites [66], drilling in various rock formations [67], etc.

PCD is produced by consolidating together accurately sized, high-quality diamond powder in the presence of either metallic or non-metallic binding phase at temperatures between 1200 and 1700°C and at high pressures of the order of 6-7 GPa [68]. When Cobalt is used as the solvent/catalyst metal, it promotes the conversion of graphite, which has formed at exposed grain surfaces, into diamond through a dissolution/reprecipitation process under

conditions of diamond thermodynamic stability. This leads to a marked amount of intergrowth between the randomly orientated diamond grains. The final grain size depends on the average grain size of the diamond starting powder which, in commercially available grades, varies from 2 to 50 μm [68]. As would be expected, fine-grained PCD grades are tougher and enable better surface finish to be achieved, whereas the coarse-grained grades are more resistant to wear.

The presence of around 8 vol% Cobalt in the commercial grades of PCD impairs the mechanical properties of the material after its prolonged exposure to temperature in excess of 700°C. There are two reasons for this. First, the presence of Cobalt promotes diamond graphitization and, second, the large difference between the thermal expansion coefficients of diamond and Cobalt leads to high internal stresses at elevated temperature [64, 69].

In order to impart better thermal stability to the material it is necessary to either leach out the residual Cobalt from the PCD composite or to replace the metallic phase with a suitable metallic or non-metallic binder [70, 71]. For example, when silicon is used, instead of Cobalt, a catalytically inactive SiC binder is created by the reaction between silicon and diamond. Since the thermal expansion coefficient of SiC is very close to that of diamond, the PCD grades which contain SiC, typically around 19 vol% [68], can withstand processing at temperatures up to around 1200 °C in an inert or reducing atmosphere [68, 70]. PCD wire drawing dies (Figure 2.12) are an example of PCD tools.

PCD can classify in a category of diamond tools called polycrystalline diamond composite. Polycrystalline diamond composite also includes PDC that is the main objective of this project. In the next section, this kind of diamond tool is specially described.

Figure 2.12 PCD wire-drawing dies.

Source: www.anchwiredie.com.

2.6 Diamond composite

Diamond composites have a wide range of compositions and applications. They have been variously referred to as PCD (polycrystalline diamond), PDC (polycrystalline diamond compact/cutter) and TSP (thermally stable polycrystalline diamond composite, sometimes represented as TSDC). Although not commonly referenced as diamond composite material, diamond impregnated metal matrix composites (MMC) are an integral part of the industrial diamond industry. The common parameters to be considered for this wide range of diamond composites are: the quality of the diamond itself, the strength of the bonding between the diamond grain and the matrix, the diamond concentration in the composite and the wear rates of the diamond and matrix as a function of the abrasivity of the material being drilled, machined and sawn [72].

The quality of individual diamond grains used in the production of these composites will depend on the source material. Synthetic diamonds, the most commonly used variety, are produced under HPHT conditions and their quality will depend on the solvent-catalyst system used in production of the diamonds. The usual catalysts are Ni, Fe, Co, Mn and Ti [23]. These elements can be incorporated into the diamond structure to produce a wide range of point defects that have been extensively studied [18]. While such point defects are not expected to significantly influence the mechanical and wear properties of diamond, if their concentration is too high, they can aggregate into fine-scale nano precipitates. The coefficient of thermal expansion of these nano precipitates will be different from that of diamond itself so thermally induced residual stresses will be generated in these diamond grains by thermal cycling events during cutting. These stresses may well be sufficient to initiate microcracks which will have a detrimental effect on the strength, wear resistance and fatigue properties of the diamond grains. One outstanding exception to the apparent neutral role of point defects has recently been reported with boron-doped diamond crystals [73]. Thermal stability, compressive strength and impact toughness all showed significant increases in the doped crystals compared with the normal diamonds. The solvent/catalyst was based on Fe-Ni alloy and the HPHT conditions were given as 1300–1400°C and 5.4–5.7 GPa.

In addition to their being several manufacturing processes, the form and shape of the product grains from these manufacturing processes can vary widely. In the case of PCD and PDC, the actual diamond composite is normally molded onto a substrate during sintering and, in most applications; the substrate is cemented Tungsten carbide (WC). The major advantages of this product format are (a) the binder phase in both components is Cobalt and (b) in this

hybrid form, the PCD element can be easily brazed onto any shaped tool. The obvious disadvantage is that such tooling components are limited to low-temperature conditions as the Cobalt is a catalyst for the back transformation of diamond to graphite [74, 75].

The major diamond composite type used in mining and manufacturing operations is PCD/PDC. An excellent history of the development of these diamond composites is given by Scott in [76]. These cutters have been shown to perform well in both civil construction and mining/exploration industries [77–79].

The physical properties of these composites are markedly dependent on both grain size and grain shape. In ceramic-type materials, the relationship between strength and grain size is complex. The relationship between fracture toughness and grain size is less clearly defined but the normal trend, within the same grain size range, is an inverse relationship.

2.7 Polycrystalline diamond compact (PDC) tools

Polycrystalline diamond compact (PDC) cutting tools are widely used in a variety of cutting applications including cutting tools for non-ferrous materials machining (Figure 2.13), drawing dies (Figure 2.12) and drill bits for oil and gas drilling. They consist of a polycrystalline diamond layer in-situ bonded onto a Tungsten carbide substrate as shown in Figure 2.14 via a high temperature and high pressure sintering route. PDC tools can present in different shapes and formats. For oil and gas drilling, they are usually cylindrical shaped with a Tungsten carbide to polycrystalline diamond layer thickness ratio ranging from 4 to 6 that are attached to a bit with different design and arrangement according to application. Figure 2.15 shows a sample of PDC drills bit.

The high abrasion resistance of PDC cutting tools has been recognized as the key contributor to the increased economy of oil and gas drilling. On the other hand, these tools still present a high susceptibility to fractures due to low fracture toughness. This is especially the case when drilling through highly interbedded hard rock formations and during dynamically unstable drilling [80].

The process of manufacturing polycrystalline diamond compact cutters is accomplished by sintering diamond powder on a cemented carbide substrate with Cobalt as a binder by applying high pressure and high temperature to the components [18]. The combination of the high pressure and the heat allows the catalytic material (usually Cobalt) to flow from the substrate to the diamond enabling the diamond-to-diamond sintering process and the substrate to diamond bonding [81].

Figure 2.13 PDC cutting tools for machining.

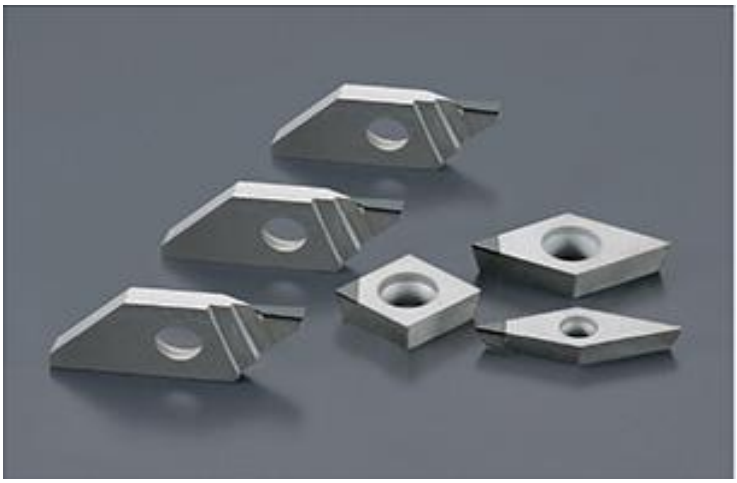

Source: www.ntkcuttingtools.com.

Figure 2.14 Geometry of a typical PDC cutting tool used in oil & gas drilling.

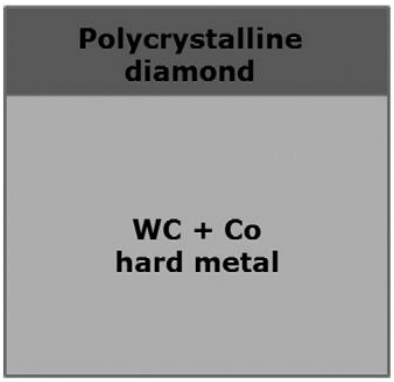

Source: [80].

Figure 2.15 Rotary PDC drill bit.

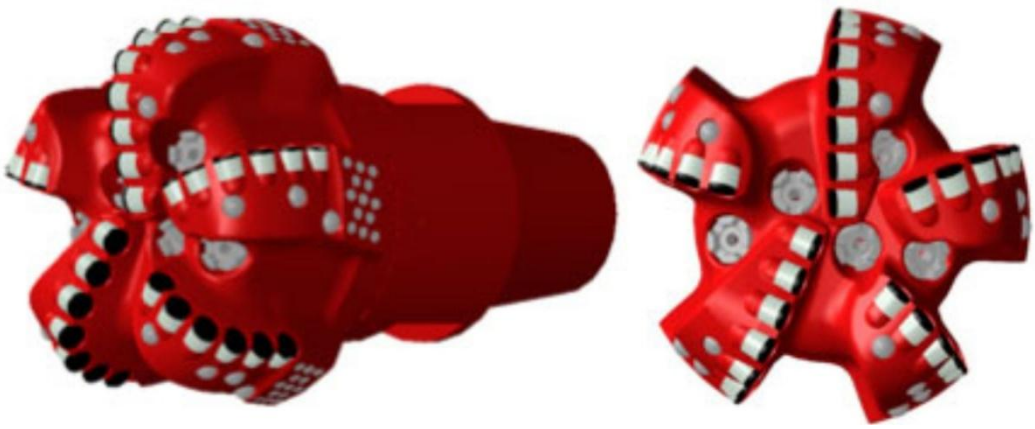

Source: www.constructionequipmentguide.com.

In Figure 2.16 a Polycrystalline Diamond Compact insert (a) can be observed where the sintered diamond layer (b) is bonded to the Tungsten carbide substrate (c). We can also observe in Figure 2.16 (b) the synthesized diamond crystals denoted as the darker areas. The brighter areas are remaining Cobalt. In Figure 2.16 (c) the Cobalt binder is indicated in the darker areas between the Tungsten carbide crystals.

Figure 2.16 (a) PDC insert, showing (b) the sintered diamond layer bonded to (c) the Tungsten carbide substrate and their pertinent microstructure pictures.

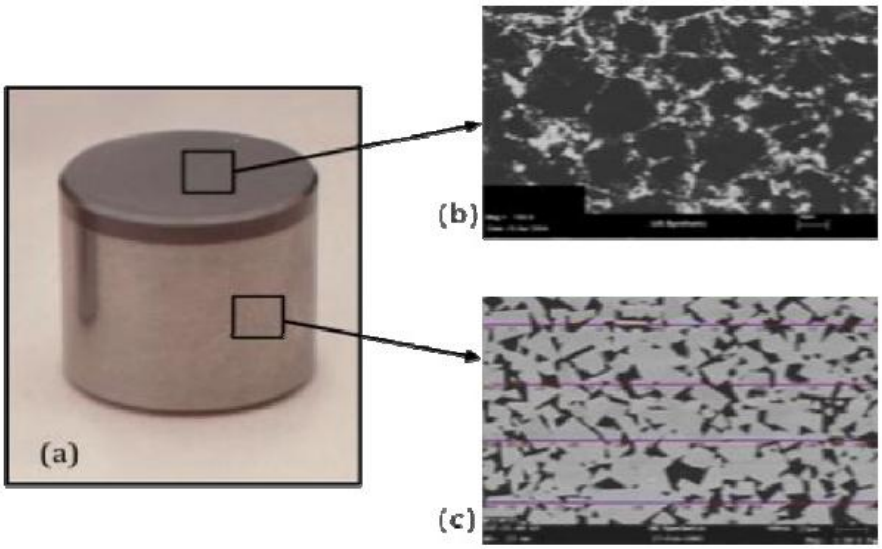

Source: [82].

A high pressure high temperature apparatus is utilized to exert the pressure and conduct an electric current to a cube-cell assembly. The cube-cell assembly is the combination of many components responsible for transferring the pressure, heating, and containing the samples to be sintered.

Since the early days of the manufacturing of PDCs or Polycrystalline Cubic Boron Nitride inserts, the size of the cube cell assembly has been limited by the size of the HPHT apparatus chamber. The chamber, as shown in Figure 2.17, is composed of anvils with a specific face surface area limiting the size of the cube assembly. The difference in size between the anvil faces and the cube cell assembly faces is a ratio that has been optimized in order to provide the material necessary to create the gasket between the anvils. This gasket is a key component to support the press anvils, distribute pressure, and confine the sample being pressed [27].

Figure 2.17 Schematic of cubic press assembly showing the six opposite anvils and the cube assembly in the middle.

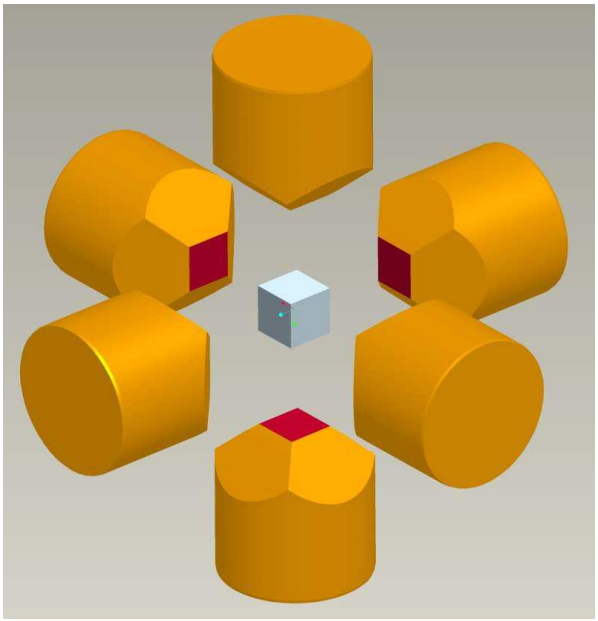

Source: [82].

After being pressed, the cube assembly dimensions remain slightly larger than the anvil face dimensions. This anvil-to-cube ratio has been utilized and optimized by US Synthetic through the last 30 years. US Synthetic is a polycrystalline diamond insert manufacturer founded by Dr. Bill Pope and Louis Pope in 1978. It is located in Orem, Utah. US Synthetic is one of the current leaders in the manufacture of polycrystalline diamond cutters, which are utilized by most of the oil and gas bit manufacturers [82].

To produce PDC, the assembled compact including hardmetal substrate and diamond top layer is placed in suitable position on the bottom anvil of high pressure high temperature apparatus. Then the operator starts the press, causing the cylinder rams to advance the anvils simultaneously to guarantee a proper alignment of the press components and the cube assembly. This will prolong the life of the press and provide a consistent pressure to the cell. Once the pressure in the cell is at appropriate pressure, the current is turned on, and it is allowed to flow from the top and bottom anvils to the cell assembly. Once the temperature in the cell is in the correct region, the current is stabilized and the samples soak for a predetermined period of time to ensure a uniform heat distribution through the sample. Then the current gets gradually turned off, and when the temperature is low enough so the diamond will not convert back to graphite, the pressure is released and the sample assembly is pulled from the apparatus and the sintered material is removed [82].

Sintering of PDC materials can be divided into 3 stages: cold compaction, hot compaction and liquid phase sintering (LPS) [83]. These stages will be discussed in more detail below.

2.7.1. Cold and Hot Compaction

The initial stage of PDC sintering occurs when pressure is applied to the PCD material during sintering; this is the cold compaction stage. Three processes occur within this stage; particle rearrangement, crushing of diamond and filling of voids by crushed particles. Once heat is applied with the pressure the stage changes to the hot compaction stage. During the hot compaction stage the temperatures are not high enough for infiltration to occur and therefore liquid phase sintering to occur. The processes which take place during this stage are graphitization of the diamond particles facing the voids, plastic deformation of the diamond grains and densification of the compact. Figure 2.18 shows the processes occurring during cold and hot compaction stages.

Figure 2.18 Schematic of the processes during Cold and Hot Compaction; (a) particle crushing, rearrangement and void filling during Cold compaction and (b) graphitization of diamond facing the voids during hot compaction.

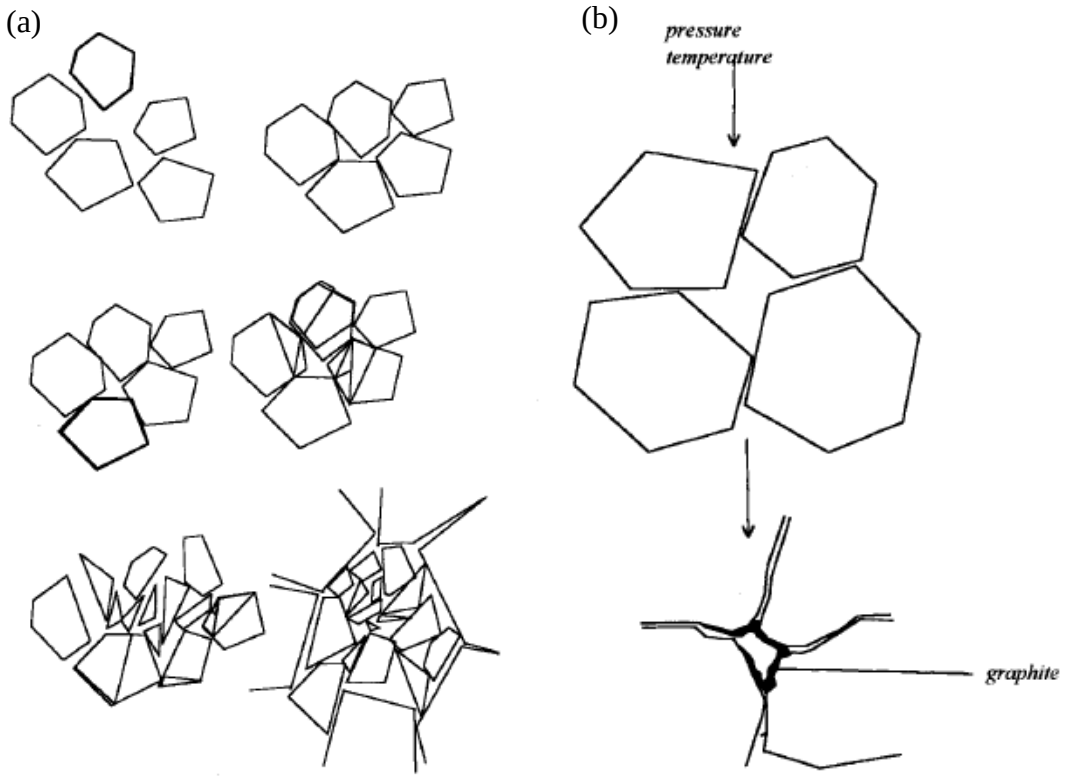

Source: [83].

2.7.2. Liquid phase sintering of PDC materials

The general sintering mechanism involves the partial dissolution and recrystallization of the diamond to bond the diamond particles via "intergrowth". The liquid phase sintering of the PCD material requires a molten metal infiltration source (Co, Ni, Fe, Mn) [83]. This metal infiltration source can be introduced to the hot pressed diamond bed by admixing and/or infiltration. Admixing involves combining the metal directly with the diamond powder before hot pressing. This can occur through various methods, such as milling metal and diamond powders together, milling precursor and diamond powders together to form a metal base or coating the diamond with a metal precursor.

Infiltration can occur in conjunction with admixing; the metal infiltration source is the substrate thus being separate from the diamond bed. The substrate is a Tungsten carbide/Cobalt (WC-Co) hardmetal, where the Cobalt is the source of molten metal.

Utilization of a binder for sintering of diamond compacts has two major benefits: decreasing sintering temperatures and pressures, cleaning diamond particle surfaces of graphite [83]. The binder (Co) in PDC makes the PCD material electrically conductive which allows the material to be cut into intricate shapes which is virtually impossible with traditional machining techniques due to its high hardness.

There are four main stages in the infiltration of a diamond compact [84]:

(1) In the first stage, the temperature is high enough to cause melting of the Cobalt with dissolved W and C at the interface; excessive amounts of carbon cause a lowering of the eutectic temperature. The melted metal immediately infiltrates into the diamond due to the high pressure gradients between the porous diamond body and the solid interface.

(2) In the second stage, the binder in the bulk substrate starts to melt. As the temperature increases and the metal in the bulk substrate melts it starts infiltrating into the diamond compact similarly due to pressure gradients.

(3) In the third stage, mass transfer of the metal decreases as the pressure gradient decreases. Once there is no pressure gradient the pores are filled completely.

(4) In the fourth stage, a change in the direction of the flow of the liquid phase occurs. The quantity of liquid phase in the diamond layer decreases, and it increases in the substrate. This is caused by a change in the pressure gradient between diamond and substrate.

The process of liquid phase sintering using conventional carbide substrate (WC-Co) materials occurs by the molten infiltration metal becoming a Cobalt alloy with dissolved Tungsten and carbon. Initially the Cobalt alloy is saturated with C corresponding to the carbon activity of the WC. This activity is much lower than that of fine carbon. This results in dissolving most of the first layer of diamond in contact with the interface. Once the infiltrant is saturated with carbon it can then operate as a liquid sintering aid. The Tungsten in the molten Cobalt react with some of the extra carbon and precipitate as Tungsten carbide (WC) crystals at the interface of the substrate and PCD layer. This results in a large depletion of diamond at the substrate interface and a thick Co layer. This causes the formation of plumes (Co and WC rich regions, several mm in dimension). If fine grained diamond powder is used, the fine diamond particles at the interface dissolve, the larger ones remain, albeit somewhat reduced in size as residual crystal seeds. These particles now have a lower solubility than the bulk of the fine diamond bed. Therefore, the chemical potential of carbon is much higher in the vicinity of the diamond bed than in the vicinity of the large diamond particles. The result is that carbon will migrate to these large diamond particles and preferentially precipitate on them, causing them to grow abnormally. The formation of plumes and coarse grained diamond are disastrous for the properties of the PDC material. Figure 2.19 shows a schematic diagram of what occurs during sintering of the PDC material [85].

Figure 2.19 Schematic diagram of the sintering of PCD materials.

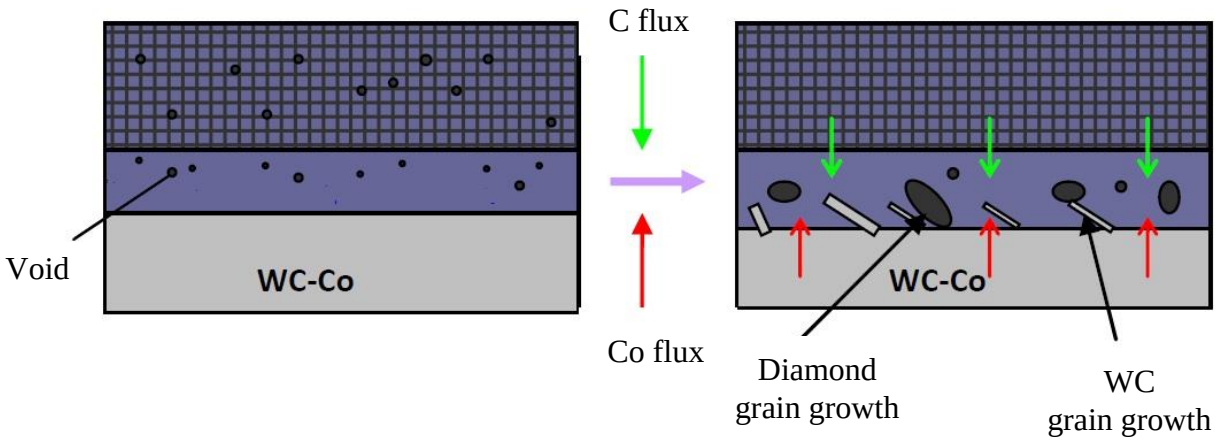

Source: [85].

A well-known problem in sintered PCD materials is the residual amount of Co. This has a negative effect on the performance of the material at high temperatures. The thermal degradation is a result of two different reasons; the first is thermal expansion differences

between the Co catalyst and the diamond particles. At temperatures above 400°C the expansion of Co is much greater than that of the intergrown diamond particles, but due to the constraints of the diamond skeleton micro-fractures are generated in the diamond material. The strength of the bonded diamond is reduced. The second problem is caused by the facilitation of the Co to catalyse the transition of diamond to graphite at temperatures above 700°C. This therefore suggested that for optimum performance the PDC materials should be kept at temperatures below 700°C, thus limiting industrial application and fabrication routes [86, 87].

After sintering, PDC inserts need a finishing process to be prepared for using as a tool. The finishing process of PDC sample is divided in several operations [82]:

(a) Outer diameter pre-sizing: Once the inserts have been lapped to the specified diamond thickness, the outer diameter gets ground to a dimension approximately 0.010" larger than that specified by the customer finish size.

(b) Pre-bonding height grind: The bottom side of the insert gets surface ground to remove the excess material and to prepare the surface for the bonding operation.

(c) Cleaning cycle: The inserts are submerged in a solution in an ultrasonic bath to remove all the residues from the previous processes.

(d) Bonding: A secondary Tungsten-carbide substrate is bonded to the insert utilizing a special high-temperature brazing alloy. This process is done to achieve the customer's required height. Steps (a) though (d) would not be necessary if the insert could be originally sintered in a mold to the customer's required height.

(e) Outer diameter second pre-size grinding: After the insert gets its extension bonded, its outer diameter is ground to a dimension 0.001" larger than the finish requirement.

(f) Finish outer diameter grinding: The insert is ground to finish outer diameter as per customer requirement.

(g) Second height grind: The bottom of the insert gets surface ground to the finish height.

(h) Diamond Radius/Chamfer: The diamond outer edge gets ground to a specified radius or chamfer as per customer requirements.

(i) Blasting and inspecting: The insert gets bead blasted to clean its surfaces and a full inspection is performed to ensure all the dimensions match customer's expectations.

2.8 Failure of PDC tools and proposed solutions

PDCs formed in the above-described manner may be subject to a number of shortcomings. For example, the coefficients of thermal expansion and elastic constants of cemented carbide and diamond are different. Thus, during heating or cooling of the diamond compact, thermally induced stresses occur at the interface between the diamond layer and the cemented carbide substrate. The magnitude of these stresses is dependent on the applied pressure, the temperature of zero stress and the disparity in thermal expansion coefficients and elastic constants [88].

Another potential shortcoming which should be considered relates to the creation of internal stresses within the diamond layer which can result in a fracturing of that layer. Such stresses also result from the presence of the cemented carbide substrate and are distributed according to the size, geometry and physical properties of the cemented carbide substrate and the polycrystalline diamond layer. Figures 2.20 to 2.22 show failures in PDC insert.

Figure 2.20 A failure in PDC. Diamond layer separated from hardmetal substrate.

Source: www.netwasgroup.us/directional/chipped-cutter.html.

Figure 2.21 A failure in PDC. Fracture inside diamond layer.

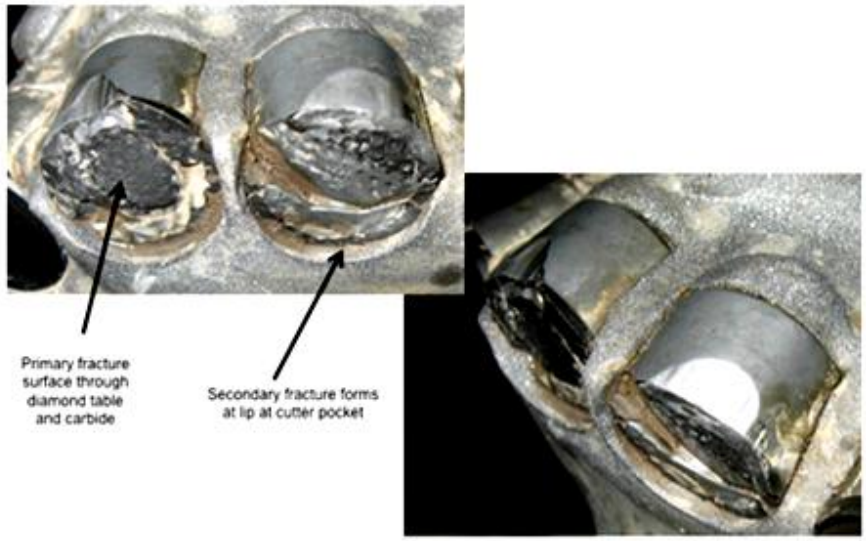

Source: www.qualitydigest.com.

Figure 2.22 A failure in PDC. Fracture inside diamond layer and in hardmetal substrate.

Source: www.perfob.blogspot.com.br.

It has already been recognized that in a cemented material comprising a hard component and a binder metal, the binder metal found in a boundary zone close to the surface of the substrate is responsible for the poor adhesion properties. It is therefore not surprising that many processes have already been proposed for reducing the interfering influence of the binder metal at the surface.

Those shortcomings were greatly alleviated by a cutting element disclosed by Malhon in U. S. Patent No. 4784023 [89]. That cutting element comprises a cemented carbide

substrate having a surface formed with alternating ridges and grooves. When the diamond layer is formed on the surface of the substrate, diamond particles will fill the grooves, whereby the final diamond layer will contain alternating ridges and grooves interlocked with the grooves and ridges of the substrate (Figure 2.23 and 2.24).

Figure 2.23 Different hardmetal substrate design for PDC.

Source: Jinan Xinyu Cemented Carbide Co.,ltd.

For another solution, Richard [90] suggests polycrystalline diamond compact in which the polycrystalline diamond body is completely free of metal binders and is to be mounted directly on a metal support. However, the mounting of a diamond body directly on metal presents significant problems relating to the inability of the metal to provide sufficient support for the diamond body. This patent further suggests the use of spaced ribs on the bottom surface of the diamond layer which are to be embedded in the metal support.

In summary, he proposes to eliminate the problems associated with the presence of a cemented carbide substrate and the presence of metal binder in the diamond layer by completely eliminating the cemented carbide substrate and the metal binder. However, even though the absence of metal binder renders the diamond layer more thermally stable, it also renders the diamond layer less impact resistant. That is, the diamond layer is more likely to be chipped by hard impacts, a characteristic which presents serious problems during the drilling of hard substances such as rock [90].

It will also be appreciated that the direct mounting of a diamond body on a metal support will not, in itself, alleviate the previously noted problem involving the creation of stresses at the interface between the diamond and metal, which problem results from the very large disparity in the coefficients of thermal expansion between diamond and metal. For example, the thermal expansion coefficient of diamond is about $1x10^{-6}$ °K^{-1} as compared to a coefficient of $12x10^{-6}$ °K^{-1} for Iron. Thus, very substantial thermally induced stresses occur in the cutter.

Wentrof and Rocco in US Patent No. Re 32380 E [91] describe a super abrasive composite tools comprising a polycrystalline diamond layer wherein substantially all of the diamond grains are bonded directly to adjacent grains and a typically Cobalt bonded Tungsten carbide substrate. This substrate is substantially larger in volume compared to the volume of the diamond layer. This patent also teaches that the Cobalt in the cemented carbide substrate is made available in the HPHT process as both a binder for the Tungsten carbide and as a solvent/catalyst necessary for conversion of graphite to diamond. Although tools made according to the teaching of the above patent are suitable for some applications, the uncontrolled infiltration of Cobalt from the WC/Co substrate into the diamond surface leaves excessive Cobalt between the diamond particles, which results in less than optimum abrasion resistance of the diamond layer. The physical and mechanical properties of the cemented carbide substrate at the diamond/carbide interface are also seriously reduced due to Cobalt depletion from the carbide.

Ishizuka [92] describes a method to overcome the above problems by placing a thin metallic material having a melting temperature lower than the eutectic point of the Tungsten carbide/Cobalt composition between the diamond powder and hardmetal interface. The assembly is heated to the melting temperature of the metallic material, but lower than the melting temperature of the Cobalt/Tungsten carbide composition. This allows a somewhat controlled infiltration of the diamond particles with catalyst/solvent material without undue

depletion of the Cobalt from the carbide substrate. This method can also supply an excessive amount of Cobalt to the diamond layer, thereby reducing its abrasion resistance.

Another means of controlling the amount of metallic infiltrant into the diamond layer is described in US. Patent No. 4440573 [93] in which a mass of diamond particles and a mass of infiltrant metal are separated by a higher melting point metallic barrier layer, whereby the infiltrant metal is regulated to flow around the barrier metal layer into the diamond particle layer under HPHT conditions. Although this method does somewhat improve the flow of metal into the diamond table, abnormal diamond grain growth is still a problem. This condition creates a large mismatch of thermal expansion causing very high stresses with subsequent internal cracks in the sintered diamond layer.

Chapter 3:

Materials and methods

3. Materials and methods

In this project, obtaining triple layer polycrystalline diamond compact, as schematically shown in Figure 3.1, was done in three different stages. The first stage was finding a proper binder for sintering diamond powder under HTHP conditions and reaching to appropriate sintering parameters (temperature, pressure and holding time).

The second stage was studying the hardmetal substrate at different HPHT sintering conditions to find the behavior of this layer during sintering. During this stage, it was decided to conduct a more comprehensive study on WC 10 wt% Co hardmetal.

In the third and last stage, according to the results achieved in the previous stages a triple layer PDC was obtained. To avoid the problem explained in the previous chapter, a thin layer of WC 20 wt% Nb/Ni was used between diamond and substrate hardmetal layers. The emphasis was on interfaces between layers to study infiltration of binders in layers, adhesion of layers and cracks in microstructure especially at interfaces.

The flowchart of different stages of project is shown in Figure 3.2 and detailed materials and method is explained in this chapter.

Figure 3.1 schematic of PDC obtained in this project.

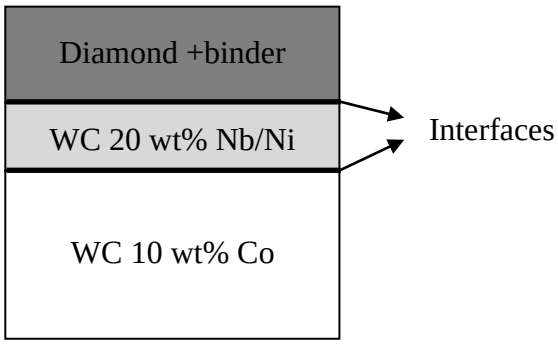

Source: Author.

3.1 First stage – Sintering of diamond powders

Ni, Fe and Co are strong catalysts for transforming graphite to diamond and the usually use for sintering PCD [23]. These elements also can act as a catalyst in reverse transformation (diamond to graphite). An important parameter for choosing the element is the difference between thermal expansion coefficients with diamond. As it is necessary to have a catalyst during sintering and in order to reduce the negative effect of huge different between

thermal expansions coefficient using Nb, it was decided to try different mixture of element as binder. Table 3.1 shows thermal expansion for element used in project.

Figure 3.2 Flowchart of experimental procedure.

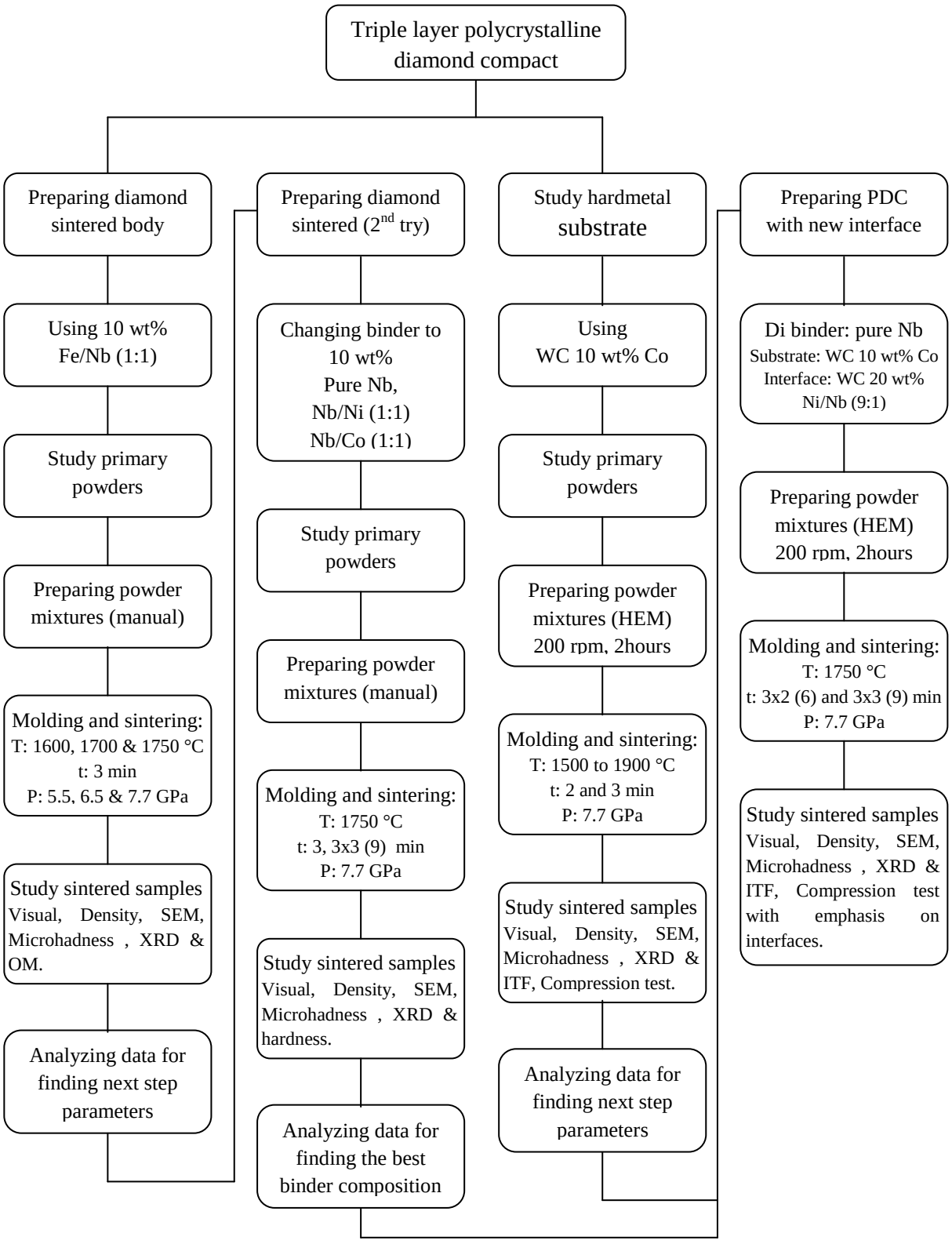

Source: Author.

Table 3.1 Thermal expansion coefficients of diamond and other elements.

Elements	*Diamond*	*Fe*	*Co*	*Ni*	*Nb*
Thermal Expansion Coefficient ($°K^{-1}$) x 10^{-6}	1	11.8	13	13.4	7.3

Source: [94].

3.1.1. First attempt by Fe/Nb binder

For first attempt to sinter diamond powders, a mixture of pure Iron and pure Niobium in weight ratio of 1:1 was used. 10 wt% binder was used and powders were mixed manually in a mortar.

Iron, Nb and diamond powders were provided from Escola de Engenharia de Lorena da USP ‐ SP, and Element 6 Company respectively. Figure 3.3 shows SEM micrograph and relative dimensions of Fe, Nb and Diamond powders. Small particles of Nb and Fe are observed, in order of 1 μm, as well as large ones. The particles present the irregular shapes, which are typical of the process of obtaining. Diamond particles are more uniform in shape and size according to production process (CVD) and specific sieving process used by the factory.

Particle size of powders also measured using particle meter (Cilas 920 L). Figure 3.4 to 3.6 show histograms obtained by laser diffraction with dimensions of the powders particles in bimodal form for these three primary powders.

According to the results, Diamond average particle size was 26.50 μm. For Nb and Fe this average particle sizes were 14.93 and 20.82 μm respectively. Smaller particle sizes were chosen for binders in order to better distribution between diamond particles.

As can be seen in Figure 3.4, particle size distribution of diamond particles is perfectly uniform with little amount of small particles. Particle meter analysis shows that only 10 percent of diamond particles have an average particle size less than 20.26 μm, very close to its average particle size of 26.50 μm.

For Nb, Particle meter analysis shows that 10 percent of particles have an average particle size of 4.67 μm that is almost far from average particle size and is in agreement with SEM micrograph showed in figure 3.3 b. This analysis also showed that Niobium powder has large particle size up to around 32.00 μm indicated that particle distribution is not as uniform as diamond.

Figure 3.3 SEM micrograph of Diamond (a), Niobium (b) and Iron (c) powders.

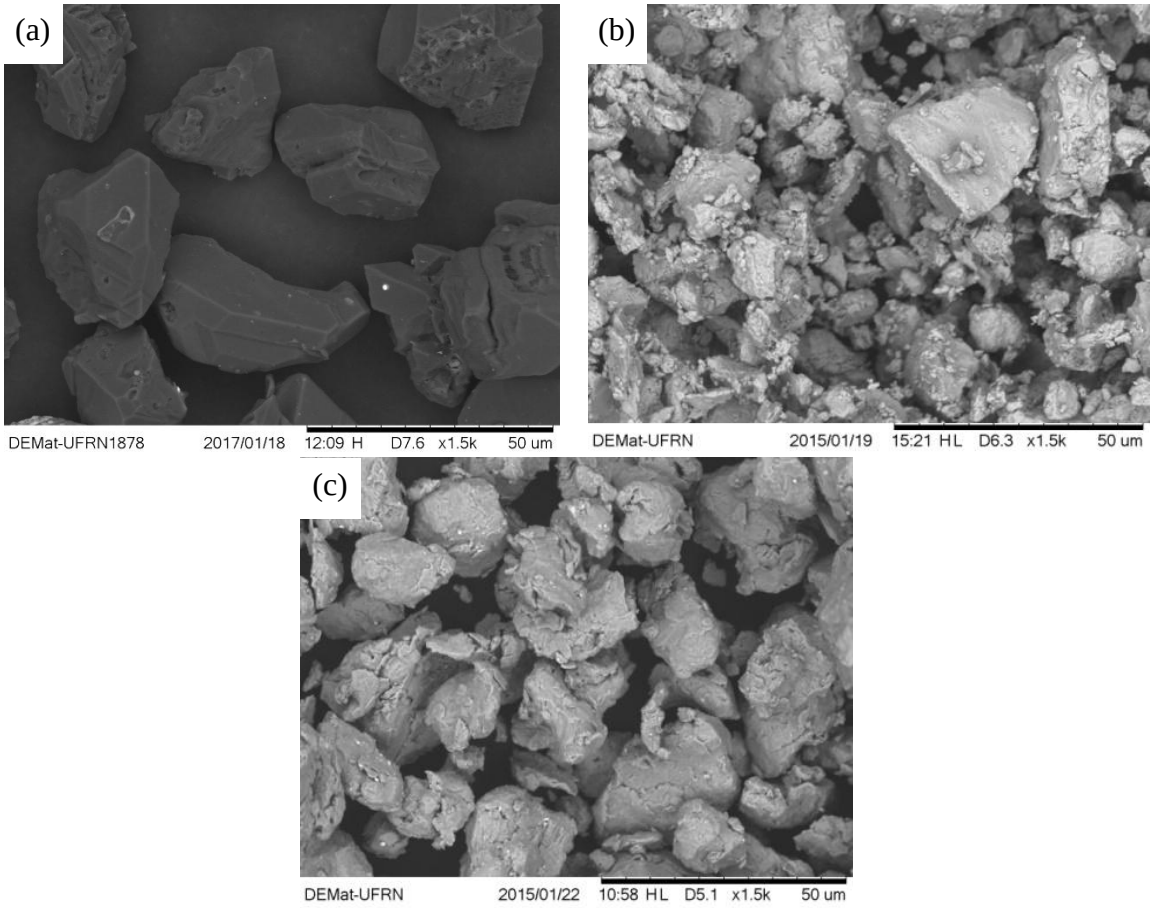

Source: Author.

Figure 3.4 Particle size distribution of Diamond powders.

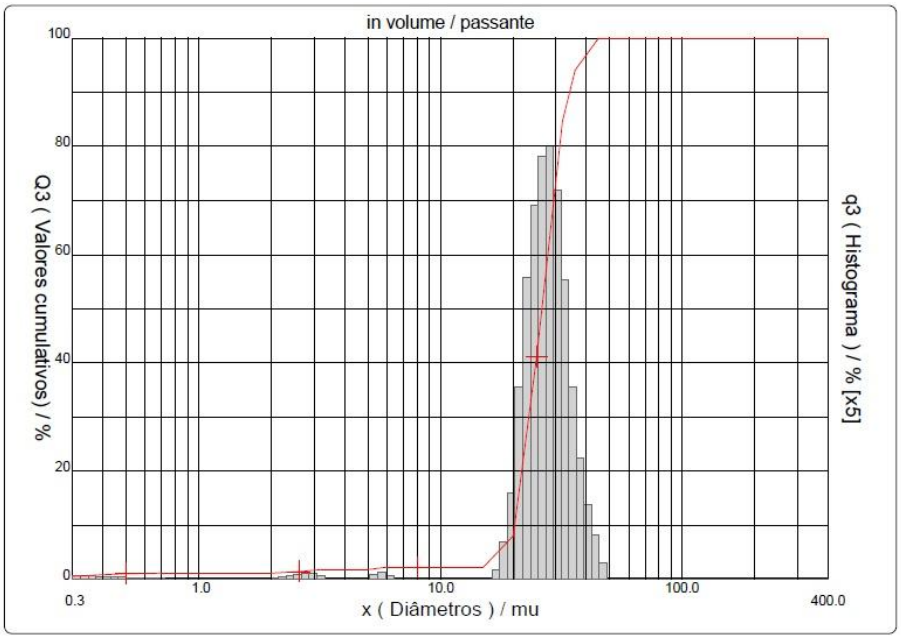

Source: Author.

Figure 3.5 Particle size distribution of Niobium powders.

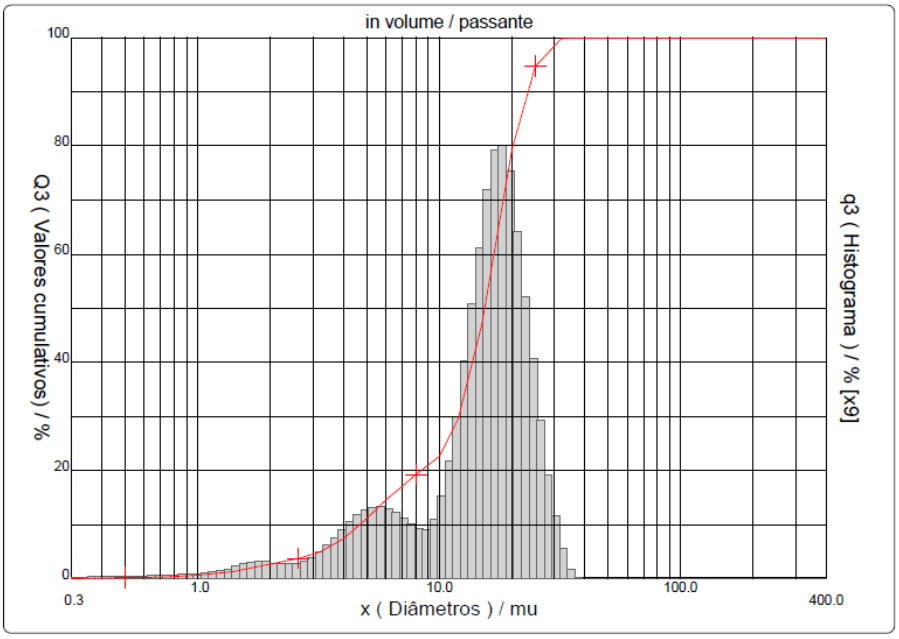

Source: Author.

Figure 3.6 Particle size distribution of Iron powders.

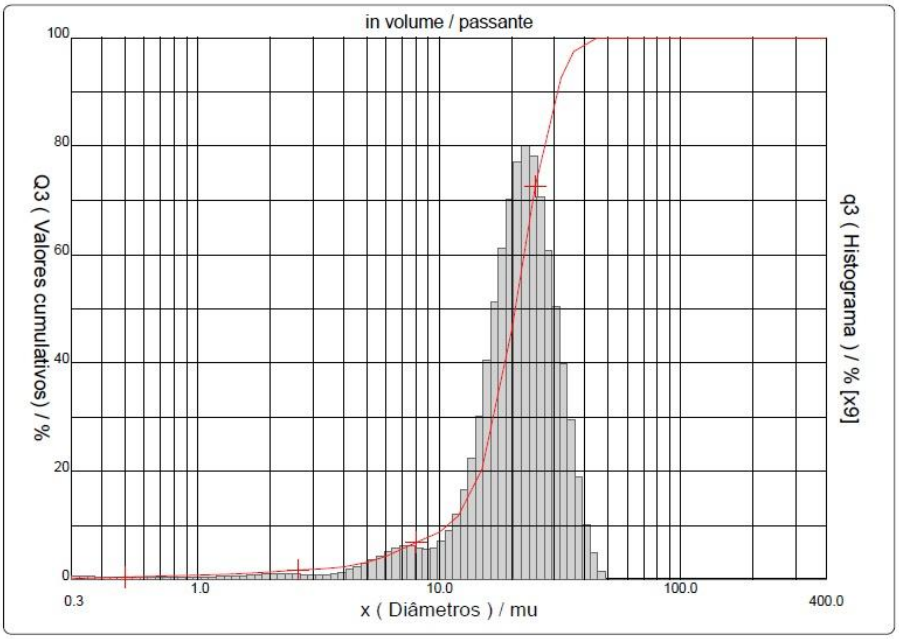

Source: Author.

For Fe, Particle meter analysis shows that 10 percent of particles have an average particle size of 10.74 µm and largest particles had a particle size around 36.00 µm. Wider diagram in Figure 3.6 shows a bigger variety of particle sizes in Fe powders in compared with

Diamond and Nb, however the particle size distribution is more uniform than Niobium powder but not as uniform as Diamond.

After mixing, prepared powders were encapsulated in a cylindrical graphite capsule of 5 mm diameter with graphite cap and a holder made of $CaCo_3$ (Figure 3.7) was used to concentrate the heat during sintering. Sintering was performed using an industrial HPHT machine Razianse Pressmach with 630 tons capacity (Figure 3.8).

Figure 3.7 Mold, Caps and support used for encapsulating the powder (a) and prepared capsule ready for HPHT sintering.

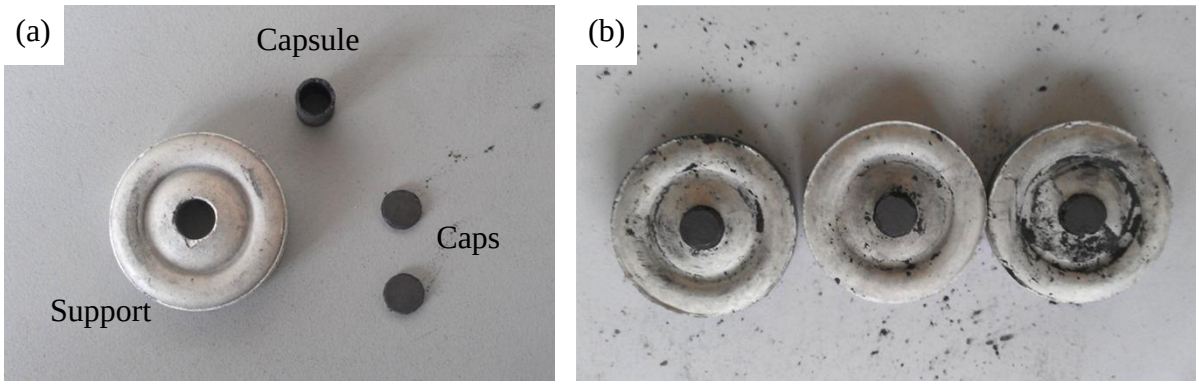

Source: Author.

In order to study the effects of sintering parameters and possibility of sintering diamond with selected binder, compacted capsules were subjected to different temperatures of 1600, 1700 and 1750 °C. Pressures were 5.5, 6.5 and 7.7 GPa. These temperature and pressures was chosen according to diamond-graphite stability diagram showed in Figure 2.3 and generally in diamond stable region however three samples (samples at low pressure of 5.5 GPa) sintered at graphite stable region to study the effect of binder.

Holding time for all samples was equal to 3 minutes. Samples were coded as A_1 to A_9 with sintering parameters listed in Table 3.2. Sintering machine parameters lined up to apply pressure followed by heating for 3 minutes when the pressure reached to selected amount. After applying heat, the pressure was kept until the sample reached to lower temperature to avoid transformation of diamond to graphite at high temperature and low pressure (Figure 2.3).

After sintering the sintered samples were dispatched from graphite capsule and cleaned ultrasonically in alcohol for 1 hour. Cleaned samples were visually inspected to find

any surface fracture. Then Archimedes principle according to ASTM B962-13 [95] was used to determine the density.

Figure 3.8 HPHT machine used for sintering (a) and a capsule after sintering (b).

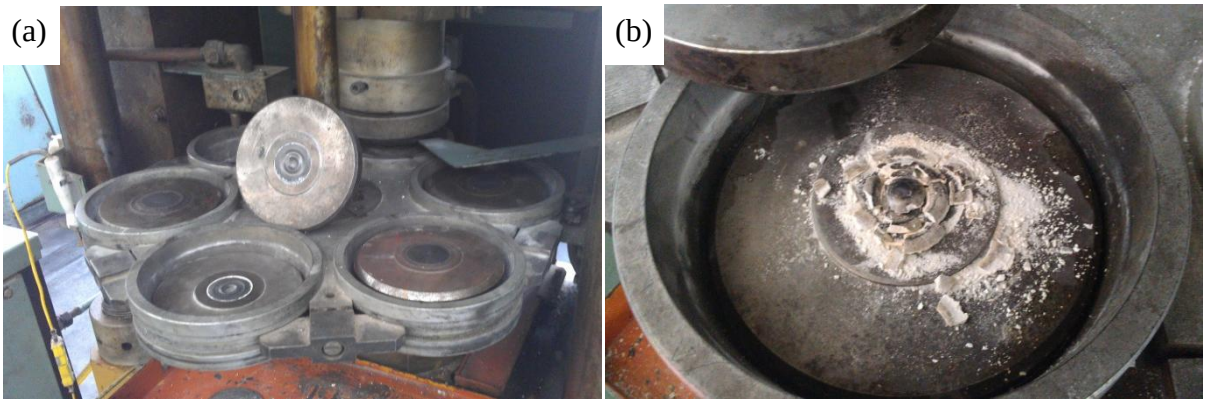

Source: Author.

Table 3.2 Sintering parameters for sample with Nb/Fe binder.

Sample code	*Sintering parameters*		
	Temperature (°C)	*Pressure (GPa)*	*Holding time (min)*
A_1	1600	5.5	3
A_2		6.5	
A_3		7.7	
A_4	1700	5.5	
A_5		6.5	
A_6		7.7	
A_7	1750	5.5	
A_8		6.5	
A_9		7.7	

Source: Author.

The measurements performed through this principle have a smaller variation range than the measurements obtained by the direct relationship between mass and volume. A standard analytical balance with precision of ± 0,0001g was used to perform the measurements of the dry (m_d) and immersed (m_i) sample bodies. By using water as immersing media with density equal to d_0 (can change according to temperature), the density of samples can be calculated according to Equation 3.

$$d = \frac{m_s}{m_s - m_i} d_0 \qquad \text{(Equation 3.1)}$$

All the values of densities in this work are presented in percentage of relative density to theoretical calculated through Equation 3.2. This is the relation between the density calculated by the Archimedes principle and the theoretical density samples.

$$d_r = \frac{\mathrm{d}}{\mathrm{d_t}} . 100\,\% \qquad \text{(Equation 3.2)}$$

Where: d_t is the theoretical density of the prepared samples. In this case, d_t is the weighted average of the theoretical densities of used elements, taking into account the percentage contents of each ones by mass for each composition. Theoretical densities for all elements used in this project are listed in table 3.3.

Table 3.3 Theoretical density of elements used in this project.

Elements	*Diamond*	*Fe*	*Co*	*Ni*	*Nb*	*WC*
Theoretical Density (g/cm^3)	3.51	7.78	8.9	8.9	8.57	15.63

Source: www.en.wikipedia.org.

Samples then crosscut, mounted and metallographically prepared for SEM and OM analysis. For preparing the samples, silicon carbide abrasive paper with standard grit number of 80, 120, 240, 360, 400, 600, 800, 1000 and 1200 were used. Polishing was also done using diamond pate of 9, 6, 3 and 1 µm grit size.

Optical microscopy analysis was done using a MV5000 Novel Optic microscope. SEM analysis in backscattered mode (BSE) with EDS (Hitachi Desktop TM 3000) was also done in order to study the microstructure and interactions between binder (Nb and Fe) and diamond particles. The emphasis at this study was checking the microstructure for available cracks, porosities and any sign of graphitization. Point-wise, linear and map analysis by EDS were performed to find any microstructural changes and inter-particles diffusion.

Microhardness was measured with 500 gf load and 15 s dwell time according to ISO 3878 [96] using a Shimadzu MV-G 20ST microhardness tester. An inverted pyramid-shaped diamond penetrator was used to carry out the measurements and to view and record the prints, an objective lens with a magnification of 40X and a digital camera were used. Since the hardness measurement values generate dispersion, at least five impressions were required for each sample, and then the mean value was determined.

X-ray diffraction analysis (Bruker D2 PHASER) was also performed using Cu-Kα radiation and Ni filter with scanning step of 0.02° in the 10–90° (2θ) range to acquire complete spectra to study the structured feature and any structural change specially graphite forming during the sintering.

3.1.2. Second attempt by Nb/Co and Nb/Ni binders

According to achieved results from previous tests (see next chapter), It was found that Fe/Nb binder cannot be used for sintering diamond under selected sintering parameters because of internal cracks and graphitization during sintering. Then it was decided to try another kind of binder. For this reason, Niobium was kept as an element in binder (because of lower thermal expansion coefficient and better results at previous tests) and Iron was substituted with two other catalyst for diamond Co and Ni.

Figure 3.9 shows SEM micrograph of used Co and Ni. As can be seen Cobalt has small particles size in compared with Nickel and both powder have irregular particle shape with a mixture of small and large particles.

Figure 3.9 SEM micrograph of Cobalt (a) and Nickel (b) powders.

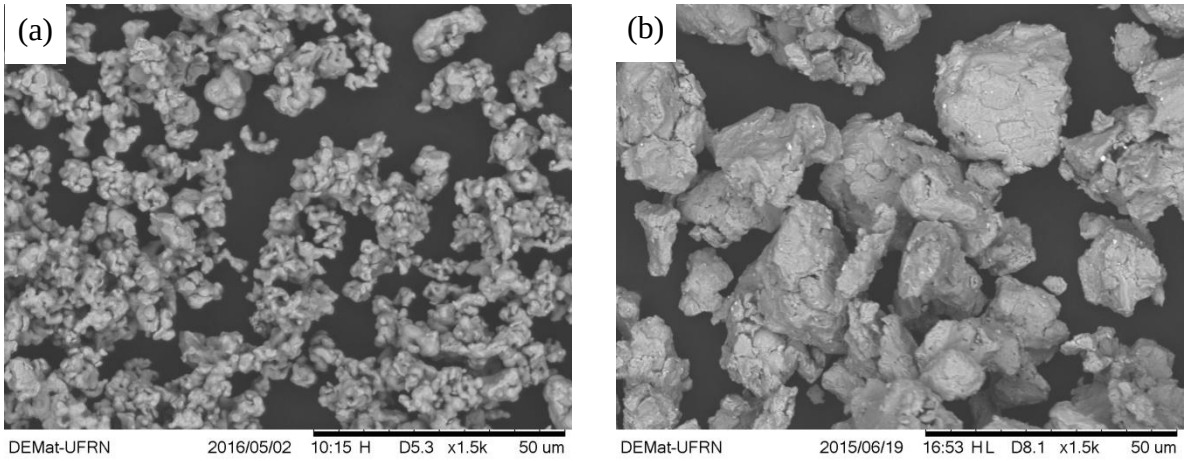

Source: Author.

Average particle size for Ni, as measured by laser particle meter (Cilas 920 L), was 35.22 µm and it was 11.12 µm for Cobalt. Figures 3.10 and 3.11 show histograms obtained by laser diffraction with dimensions of the powders particles in bimodal form for these two primary powders. Diamond and Niobium powders were the same used in previous test.

Particle size distribution of Co and Nickel shows that Nickel has a wider variety of particle size from 10 to around 90 µm however its distribution is perfectly uniform. On the

other hand, Cobalt powder includes small particles in order of 3.00 µm and the biggest particles have a size around 20.00 µm.

Figure 3.10 Particle size distribution of Nickel powders.

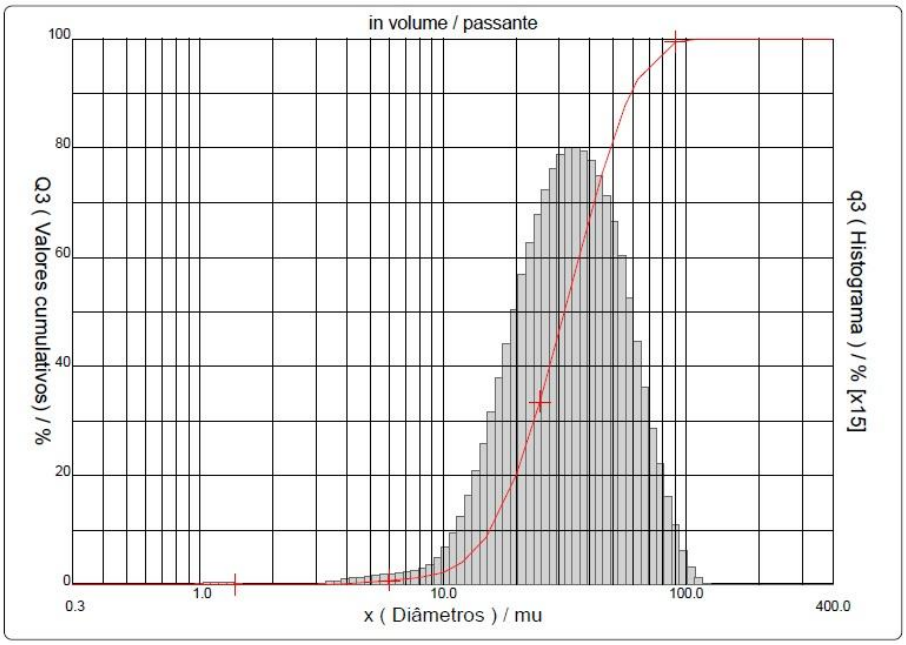

Source: Author.

Figure 3.11 Particle size distribution of Cobalt powders.

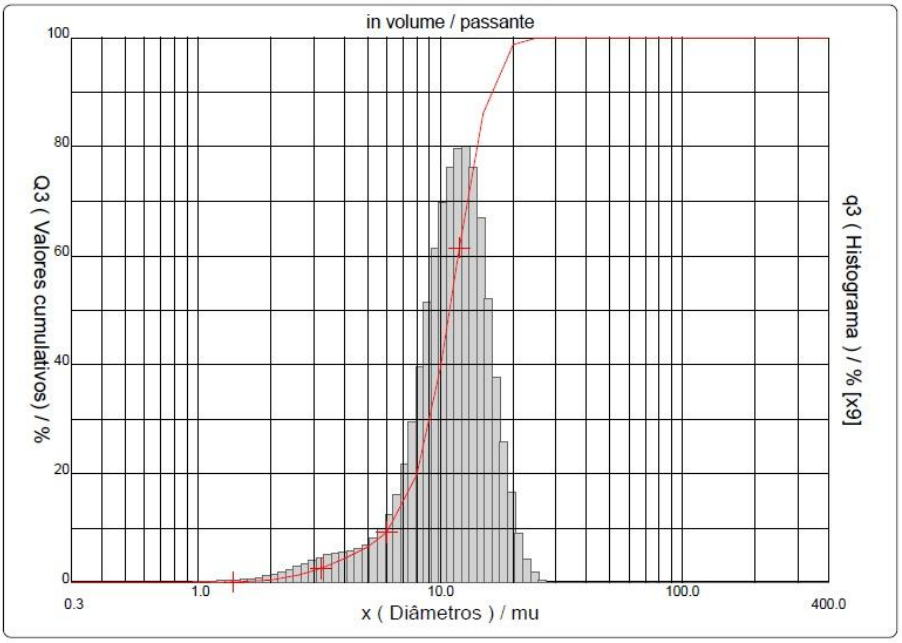

Source: Author.

Like previous test 10 wt% binder was used in diamond mixture but this time Fe was replaced with Ni and Co. Ratio of Ni to Nb and Co to Nb in both binders was 1:1. Mixing was performed manually in a mortar along with 90 wt% diamond powders.

As it was found in first attempt to sinter diamond powders with Fe/Nb binder, sintering at low temperature did not result in a proper sintering even at high pressure. According to these results, sintering temperature was selected to be 1750 °C and with higher possible pressure according to the capacity of machine equal to 7.7 GPa.

It was suggested that longer holding time is necessary to better sintering then two different holding times of 3 and 9 minutes were selected. Regarding to limitation with HPHT sintering machine, it is impossible to apply heat and force for a period of time longer than 3 minutes then 9 minutes holding time was applied in three successive cycles of three minutes each. Table 3.4 lists the sintering parameters for samples with Nb/Co and Nb/Ni binders.

Table 3.4 Sintering parameters for sample with Nb/Co and Nb/Ni binders.

Binder	*Sintering parameters*		
	Temperature (°C)	*Pressure (GPa)*	*Holding time (min)*
Nb/Co	1750	7.7	3
Nb/Co			9 (3x3)
Nb/Ni			3
Nb/Ni			9 (3x3)

Source: Author.

After mixing, prepared powders were encapsulated and sintered in the selected conditions. The procedure and sintering method were the same as explained at previous section. Sintered samples were cleaned, cross-cut, prepared and subjected to SEM and XRD analysis. Microhardness and density measurements were also performed. All equipments, standards and procedures explained at previous section, were also used for these series of tests. Besides, hardness was measured with a 15 kgf load and 15 seconds dwell time according to ISO 3878 [95] to have better understanding of overall hardness.

3.1.3. Third attempt by pure Niobium binder

Second attempt also did not result in suitable sintering of diamond powders (see next chapter) but during microstructure study, it was found that microstructure near Niobium particles is more uniform and no graphitization was found near those particles. Then it was

suggested that pure Niobium as a binder can have better results. For the third attempt, 10 wt% pure Niobium, the same powder as previous tests, was used as binder for sintering the diamond. The sintering temperature and pressure were 1700 °C and 7.7 GPa respectively. Two different holding time of 3 and 9 (three cycles of here minutes each) as second attempt were selected.

Mixture preparation, encapsulating and sintering procedure were the same as previous tests. The same procedure of cleaning, cross cutting, preparing were performed and microstructure and structure were investigated by SEM and XRD with the same equipments and procedures. Density, hardness and microhardness measurement were also done.

3.2 Second stage - Study WC 10wt% Co substrate

Study WC/Co substrate was the second stage of the project. Microstructure and properties of this substrate has an important role in overall properties of PDC tools. As explained before, it was decided to conduct a comprehensive study to understand effect of HPHT sintering method on microstructure and properties of WC 10wt% Co hardmetal.

Commercial WC with average particle size of 12.55 µm and the same Co explained in section 3.1 were used. Figure 3.12 shows SEM micrograph of WC powder particles and Figure 3.13 shows histograms obtained by laser diffraction with dimensions of the powders particles in bimodal form. Particles size distribution of WC is uniform and includes particle size in 1.00 to 25.00 µm however 90 percent of particles are smaller than 19 µm.

Figure 3.12 SEM micrograph of WC powders.

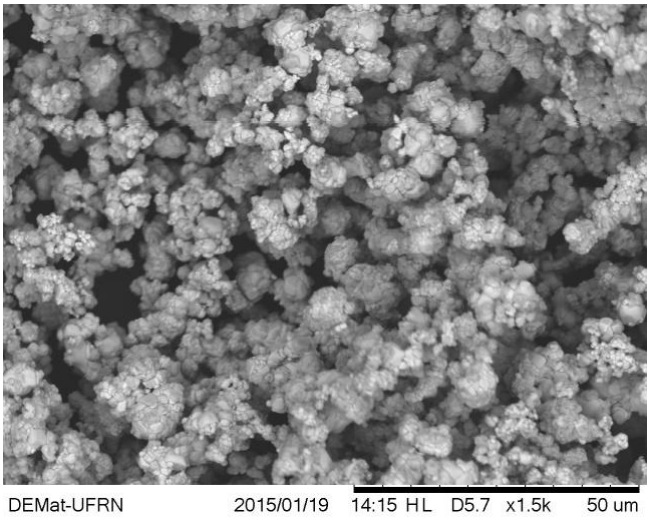

Source: Author.

Figure 3.13 Particle size distribution of WC powders.

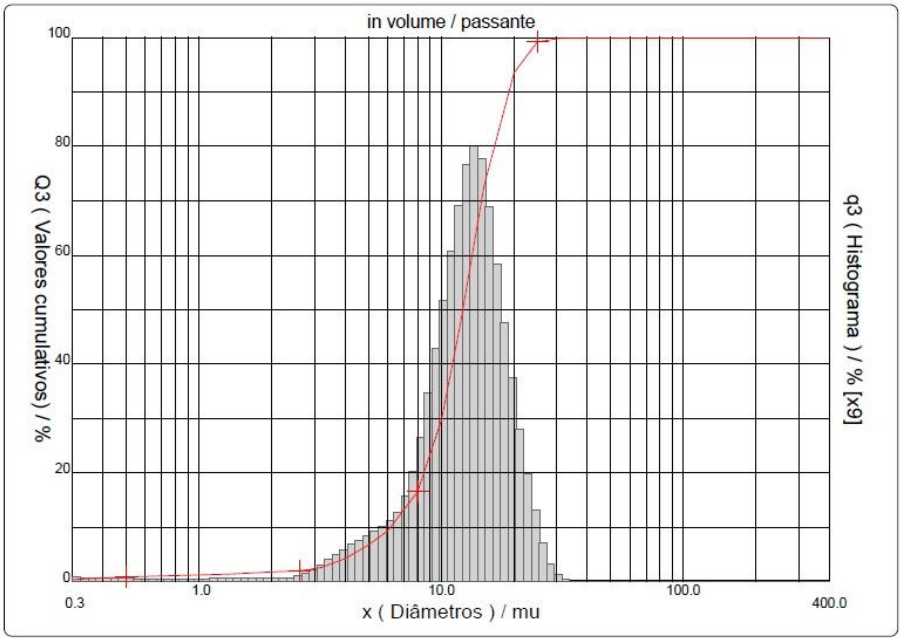

Source: Author.

Powders were weighted with the nominal composition of WC–10 wt% Co and were mixed via ball milling (Fritsch, Pulverisette 7) in cyclohexane media. Milling speed and time were 200 rpm and 1 h, respectively, with ball to powder ratio of 10 to 1 by weight. Hardmetal balls and vessel were used to prepare the powders. Finally, WC–10 wt% Co powder mixture was obtained after drying in controlled atmosphere to avoid any contamination. Figure 3.14 shows charged vessels with balls and powders prepared for milling. The high energy milling used in this project is also shown in the Figure.

Figure 3.14 Prepared vessel (without cyclohegzane) for high energy (a) and Fritsch, Pulverisette 7 milling machine (b).

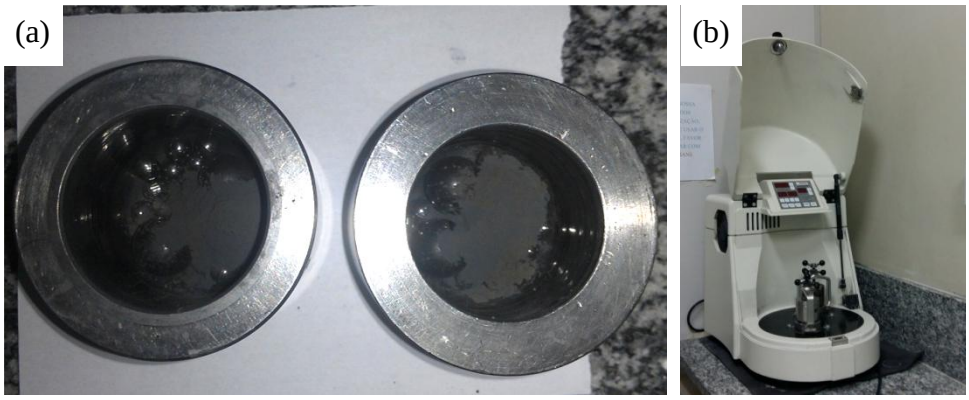

Source: Author.

Mixed powders were encapsulated in cylindrical graphite as explained before and sintering was performed using an industrial HPHT machine (see 3.1.1). In order to study the effects of sintering temperature and morphology evaluation, compacted capsules were subjected to five different temperatures of 1500, 1600, 1700, 1800 and 1900°C under a constant pressure of 7.7 GPa and 2 and 3 min of holding time. All procedures for sintering were exactly the same as discussed before.

XRD (Bruker, D2 PHASER) was performed using Cu-Kα radiation and Ni filter with scanning step of 0.02° in the 20–90° (2θ) range to acquire complete spectra of the mixed powders, in order to find the available phases in mixture.

The morphologies of WC, Co and WC–10Co powders and sintered samples were discerned by a scanning electron microscope (Hitachi Tm3000 desktop SEM) equipped with EDS. X-ray diffraction analysis (Shimadzu PDA 7000) of sintered samples was also done. The samples were ultrasonically cleaned for 1 hour and then were cross cut, ground, and polished to mirror finished using diamond paste up to grit size of 1 μm (complete explanation in section 3.1.1).

Microstructures were observed in the mode of backscattered electron and XRD for sintered samples was performed using Cu Kα radiation and Ni filter with scanning step of 0.02° in the 20–90° (2θ) range for acquisition of complete spectra. The densities of sintered composites were measured by the Archimedes' principle according to ASTM B962 [95]. Compression test was also done according to ISO 4506 [97] in order to find the yield and compression strength.

The Hardness was measured with 15 and 30 kgf load and 15 s dwell time according to ISO 3878 [96]. Palmqvist indentation toughness was determined on cemented carbide specimens and the indentations for each load were carried out on diamond polished surfaces. The lengths (l) of cracks, starting at the corners of indentation, were measured by light optical microscopy at 500× magnification. Figure 3.15 shows a photograph of Vickers indentation and cracks around it. The length progression of cracks was observed with increase of the applied load. Palmqvist fracture toughness was assessed from Shetty et al.'s equation [98], according to

$$K_{IC} = \beta \left(\frac{PH}{\sum l}\right)^{\frac{1}{2}} \qquad \text{(Equation 3.3)}$$

Where H is the hardness, P is the applied load, Σl is the sum of crack lengths, β is a constant with value of 0.0988, and KIc is fracture toughness given as MPa/m1/2. For HV15 and HV30 values expressed in (kgf/mm2), Palmqvist fracture toughness can be calculated as:

$$K_{IC} = 0.383 \left(\frac{HV_{15}}{\sum l}\right)^{\frac{1}{2}} \quad \text{(Equation 3.4)}$$

$$K_{IC} = 0.541 \left(\frac{HV_{30}}{\sum l}\right)^{\frac{1}{2}} \quad \text{(Equation 3.5)}$$

Figure 3.15 Photograph of Vickers (30 kgf) indentation of the typical sample sintered at 7.7 GPa/1900°C/2 min.

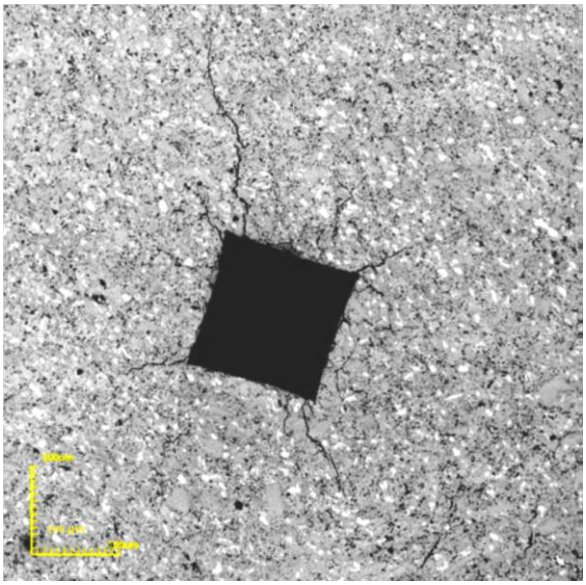

Source: Author.

3.3 Third stage - Triple layer PDC

For last stage a triple layer PDC was obtained via HPHT methods. Powder mixture for each layer was prepared separately as listed below using high energy ball milling:

- First layer (substrate): WC 10 wt% Co.

- Second layer (interface): WC 18 wt% Ni and 2 wt% Nb.

- Second layer (top layer): Diamond 10 wt% Nb.

Powders were weighted with the nominal compositions and were mixed via ball milling (Fritsch, Pulverisette 7) in cyclohexane media. Milling speed and time were 200 rpm and 1 h, respectively, with ball to powder ratio of 10 to 1 by weight. Hardmetal balls and vessel were

used to prepare the powders. Finally, powder mixtures were obtained after drying in controlled atmosphere to avoid any contamination.

For encapsulating the powders (see section 3.1.1) to obtain triple layer sample, around 1/2 of height of internal volume of capsule was filled by substrate powder mixture. Approximately interface with 0.5 mm thickness of powder mixture was used and the remaining was diamond powder mixture.

It was almost difficult to control the thickness of each layer because the process was manual but for more precision, powder mixture of each layer was weighted according to the related thickness using theoretical density of powder mixture. Each layer pressed weakly using a mandrel before pouring the next layer. According to high pressure during sintering, it is not necessary to compact powders before sintering and manual pressing was only used to have more powder in the capsule and bigger sample after sintering.

Prepared capsules were put in HPHT machine in a way diamond layer being the top layer. It was to avoid any infiltration of elements from substrate and interface layers to diamond layer. As it discussed before, Nickel and Cobalt are catalyst for graphite to diamond transformation (and vice versa), then avoiding infiltration of these element can reduce the diamond graphitization during sintering. Figure 3.16 shows a set of prepared capsule with top surface mark.

Figure 3.16 Prepared capsule for sintering with mark to show top diamond layer.

Source: Author.

Sintering parameters for sintering the triple layer samples was chosen according to the results achieved from previous tests as follows:

- Temperature: 1750 °C.

- Pressure: 7.7 GPa.

- Holding time1: 6 minutes (3 cycles of two minutes each).

- Holding time1: 9 minutes (3 cycles of three minutes each).

The procedure for sintering was the same as explained in section 3.1.1 and sintered samples were cleaned, cross cut, mounted, and prepared like the other samples discussed before. Preparing a triple layer sample needs more attention and time because in this kind of samples at least to layer with different hardness are available then, the process must be done carefully to avoid making an even finishing surface.

Besides, during grinding, separated diamond from diamond layer can penetrate into hardmetal surface and make the further analysis difficult. Thus grinding was done with very slow speed and during a long period of time and after each step of grinding, samples ultrasonically cleaned for next grinding step.

Microstructure analysis at this stage was generally to study the properties of interface lines (Figure 3.1) and founding any mismatching, lack of adhesion and availability of cracks. The diffusion of elements between layers was also investigated via EDS.

Microhardness measurement was also done from a point far from the interfaces. The measurement repeated in a decreasing distance toward interfaces to fine hardness changes according to diffusion or any other reasons.

Density of sintered bodies was not measured because according to impossibility of measuring theoretical density of triple layered samples, relative density cannot be calculated and a number for density does not have any sense.

All equipments and procedures using to study the samples at this stage were the same used for previous stages and explained earlier in this chapter.

Chapter 4:

Results and Discussions

4. Results and Discussions

In this chapter the results obtained at each stage are presented and discussed. The order of results is as same as chapter 2 in which, the results of sintering diamond will be discussed followed by study of WC 10 wt% Co substrate. At the end achieved data from investigating the triple layer PDC will be considered.

4.1 First stage – Sintering of diamond powder

4.1.1. Nb/Fe binder

a) Visual analyses

After cleaning samples were visually inspected to find any superficial cracks and study the surface quality. The samples were not in a fair cylindrical shape and there were deformation in both base and side surfaces. Samples were in different height according to HPHT process and manual capsule. 5 mm. Figure 4.1 shows the shape and surface condition of two different samples sintered at different condition.

Figure 4.1 Deformation near base surface in sample sintered at 1700 °C/6.5 GPa/ 3min (a) and fracture in side surface in sample sintered at 1600 °C/7.7 GPa/ 3min (b).

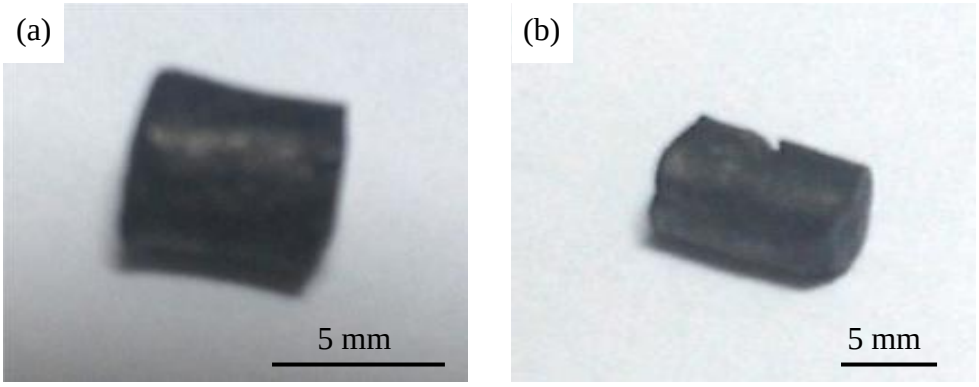

Source: Author.

During ultrasonically cleaning, the sample A_1 that had been sintered at 1600 ºC with 5.5 GPa of pressure, was broken when it was in ultrasonic bath (Figure 4.2). I seems that the vibrations along with ultrasonic caused it. This sample had the lowest sintering temperature and pressure that has high risk of graphitization. Then breaking this sample can be related to internal phase changes during sintering that made the samples too brittle that can fracture even at ultrasonic vibration. Fractured surfaces were clean with any contaminations that show the fracture had been occurred during ultrasonic process not during sintering.

Figure 4.2 Broken sample A_1 sintered at 1600 °C/5.5 GPa/ 3min.

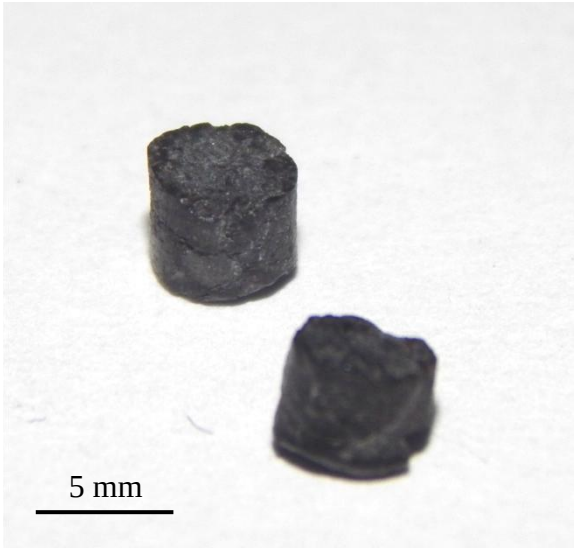

Source: Author.

b) Density results

Average density and relative density of samples are listed in table 4.1. Relative densities were calculated using theoretical density of sintered mixture equal to 3.72 g/cm^3.

Table 4.1 Density and relative density of samples with Nb/Fe binder at different sintering conditions (holding time of 3 minutes)

Sample code	*Sintering parameters*		*Density (g/cm^3)*	*Relative density (%)*
	Temperature (°C)	*Pressure (GPa)*		
A_1	1600	5.5	3.22	86.61
A_2		6.5	3.52	94.59
A_3		7.5	3.63	97.44
A_4	1700	5.5	3.16	84.90
A_5		6.5	3.35	90.03
A_6		7.5	3.60	96.77
A_7	1750	5.5	3.08	82.91
A_8		6.5	3.59	96.58
A_9		7.5	3.66	98.29

Source: Author.

It was expected to have high density (near 100%) at high pressure, but as can be seen in table 4.1 none of the sample achieve to full density. Lower densities found at samples sintered at lower pressure (A_1, A_4 and A_7) that according to Figure 2.3 were sintered at

graphite stable region even at high temperature. Density of graphite is 2.56 g/cm^3 that is lower compared with the density of diamond (3.51 g/cm^3), then if there graphitization occur, density can decrease.

Relative density for samples sintered at higher pressure is closer to 100% showing that possibility of graphitization is less even when sintering takes place at high temperature up to 1750 °C. Better understanding can achieve by microstructure study that is explained later in this chapter.

c) Microstructure study

SEM micrograph of samples with Nb/Fe binder showed some quantity of graphitization in all samples sintered at different temperatures and pressures (Figure 4.3). Fewer graphitizations found in samples sintered at higher pressure and all graphitization were taken place close to Iron particles. Microstructure near Niobium particles was almost perfect without any trace of graphitization.

As can be seen in figure 4.3 (a) to (i), almost all Iron particles were collapsed during sintering and their shapes completely changed. Figures 4.3 (b), (e) and (h) clearly show the changes in Iron particles. On the other hand, Niobium particles kept their shape without any changes. Niobium particles can be seen in Figures 4.3 (a), (d) and (g).

In Figure 4.3 (g) a Nb particle is located very close to an Iron particle. It clear that situation during the sintering (temperature and pressure) at this region is the same for both Nb and Fe particles, but as can be seen the Fe completely changed and Nb is without any change. It can be related to catalyst ability of Fe for diamond that accelerates graphitization.

Diamond is a metastable allotropic of carbon, then graphitization of diamond particles in diamond composite can occur. It is believed that the beginning temperature of graphitization would be associated with the catalyst of diamond powders. The catalysts such as some metallic elements reduce the beginning temperature of diamond graphitization [99]. It is understandable that both for the graphitization and its reverse reactions, their activation energies can be decreased by catalytic agents.

The graphitization of diamond has been found to be facilitated in the presence of a small amount of residual oxygen in the atmosphere surrounding diamond powders [100]. When diamond reacts with oxygen or oxides, CO or CO_2 is produced, leading to the formation of small pits on the surface of diamond particles. These small pits cause an increase of the specific surface of diamond particles, which results in an acceleration of graphitization.

Figure 4.3 SEM micrograph of samples sintered with Nb/Fe binder at different sintering conditions. (a) to (i) are related to samples A_1 to A_9 listed in table 3.2, respectively.

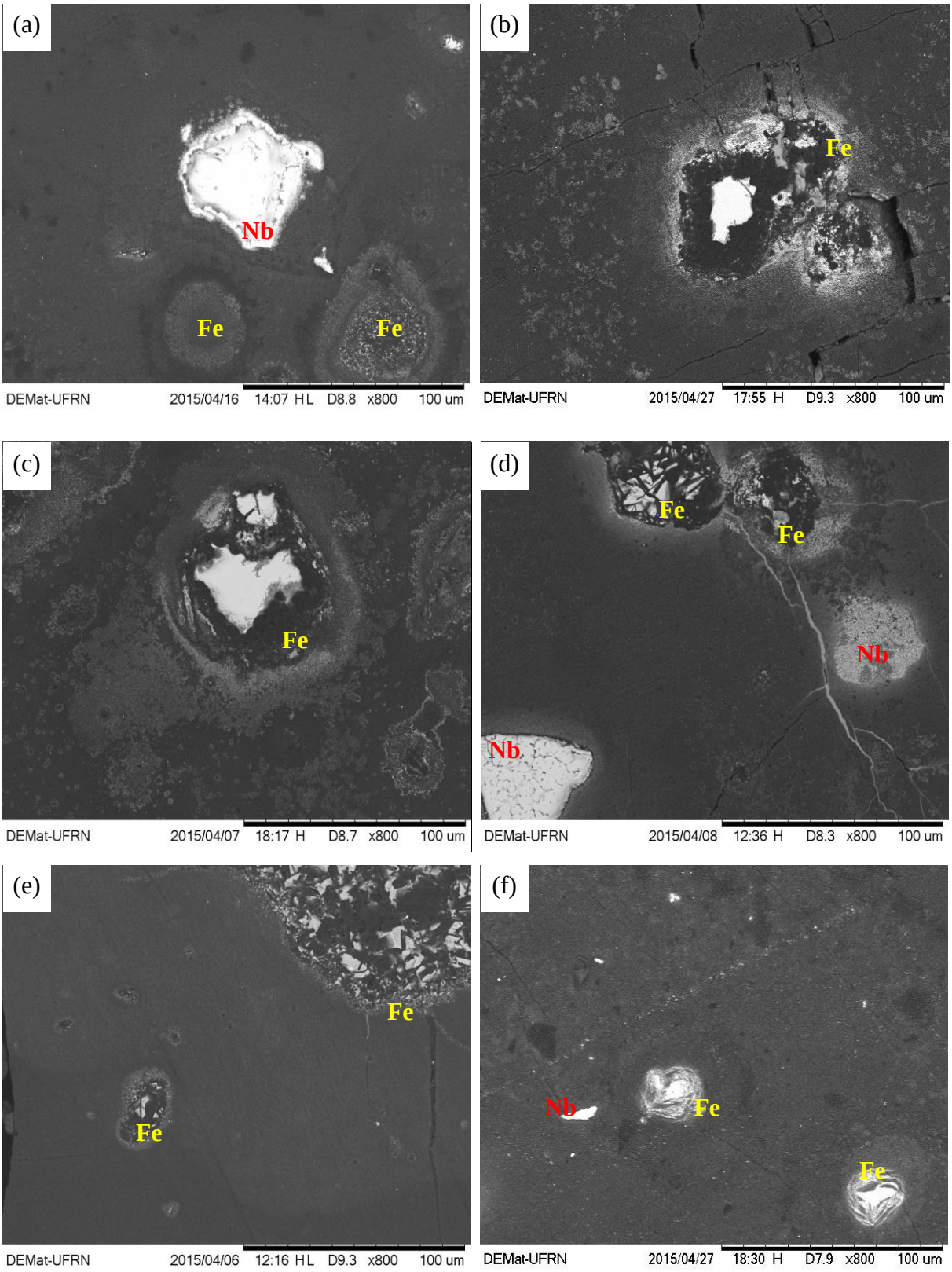

Figure 4.3 (continue).

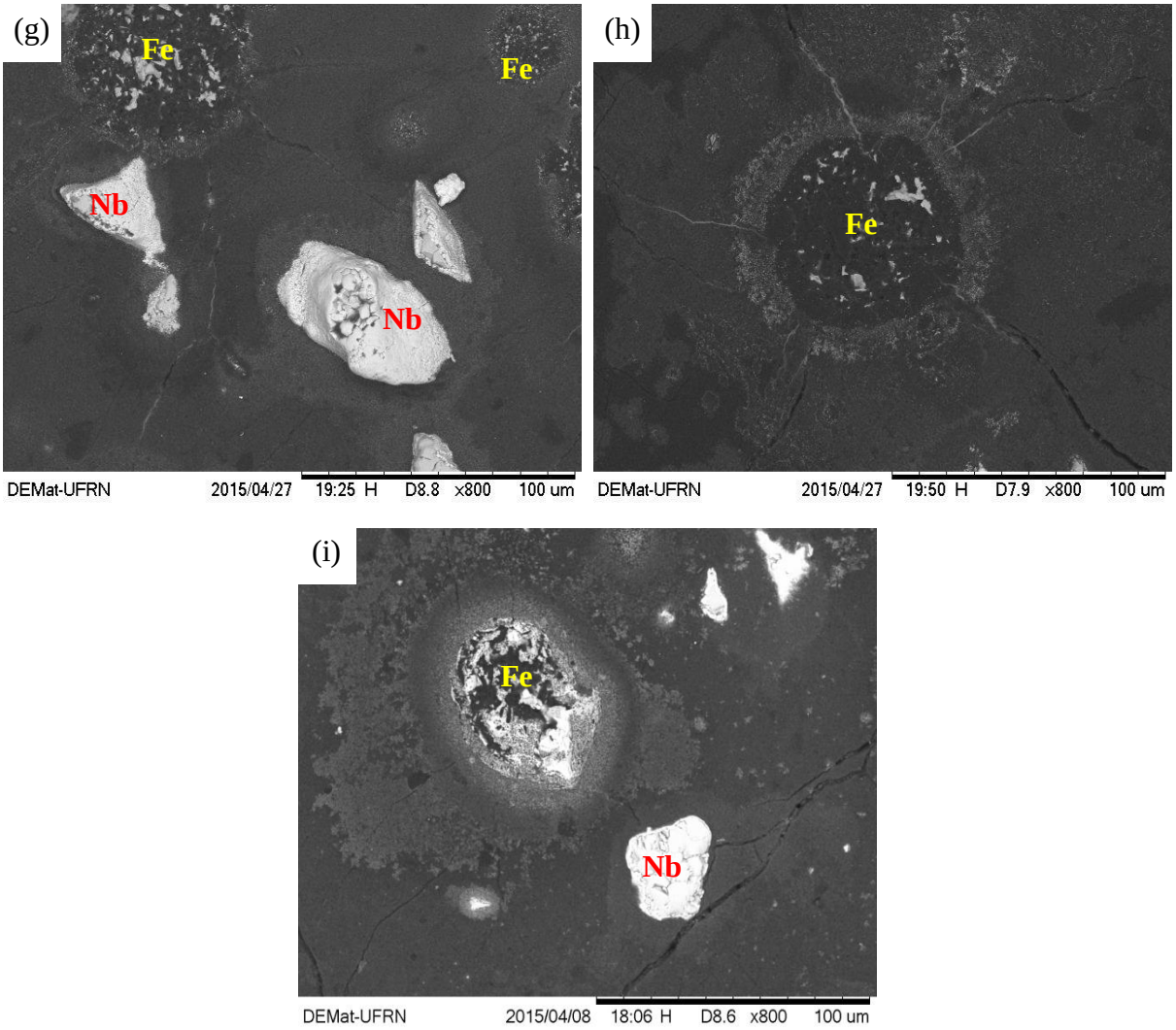

Source: Author.

The microstructures also showed a lot of cracks at different regions between diamond and binders particles. Again almost all cracks were observed inter diamond particle or near Iron particles. In Figure 4.3 (h) can be seen that a collapsed Fe particle is origin for cracks but Nb particle in Figure 4.3 (g) acts as a barrier for the cracks started from Fe particle.

These cracks can have two origins, first, the difference between thermal expansion coefficient between diamond and Iron as explained before (see chapter 3) and second, the volume change from transforming diamond to graphite. Transforming diamond to graphite accompanies an increase in volume around 37%. Difference between thermal expansion coefficients and increasing the volume from transforming diamond to graphite makes an internal stress in samples which can result in internal cracks especially in brittle microstructure of diamond.

Micrograph obtained from optical microscope showed cracks in the microstructure of samples more clear. Figure 4.4 shows optical micrographs of some sample with Nb/Fe at different sintering conditions.

Figure 4.4 Optical micrograph with Nb/Fe sintered for 3 minutes at 1600 °C/5.5GPa (a), 1600 °C/6.5GPa (b), 1700 °C/5.5GPa (c) 1750 °C/5.5GPa (d).

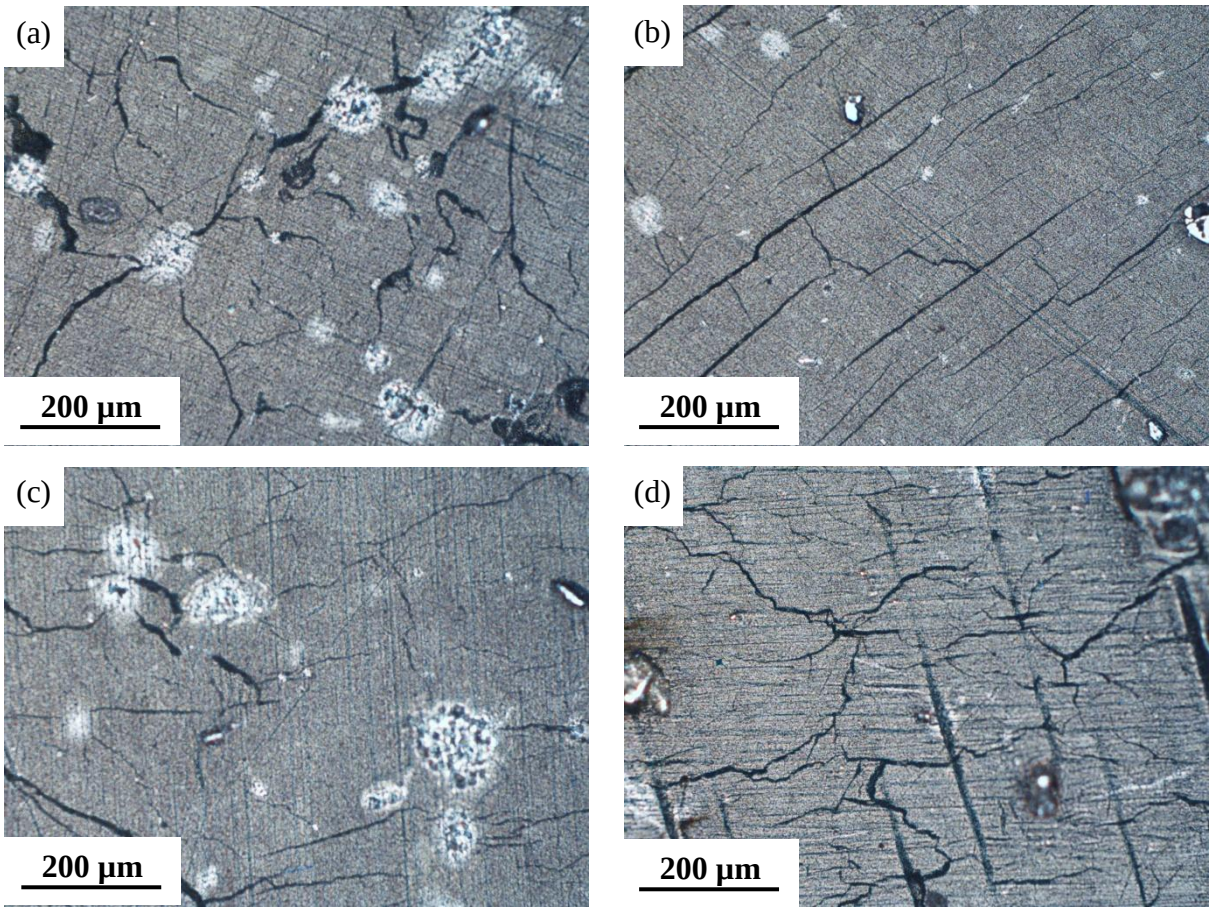

Source: Author.

Despite internal cracks, no porosity was found in samples or it was too small to find (Figures 4.3 and 4.4). Then as explained before about density, it seems that low relative density is related to graphitization.

Figure 4.5 is a SEM micrograph of fractured surface of the broken sample during cleaning (see part a section 4.1.1). Separation of binder particle from diamond matrix can be observed in this micrograph. It shows that sintering at this situation (1600 °C/5.5 GPa/3 min) could not provide good adhesion between matrix and particle, then crack propagation separated the particle that can result in fracture as it happened for this sample by vibration during ultrasonically cleaning.

This separation can also happen during cooling after sintering be because of difference between thermal expansion coefficient of diamond matrix and presented particle which can be Nb or Fe.

Figure 4.5 Separation of particle and diamond matrix by crack propagation.

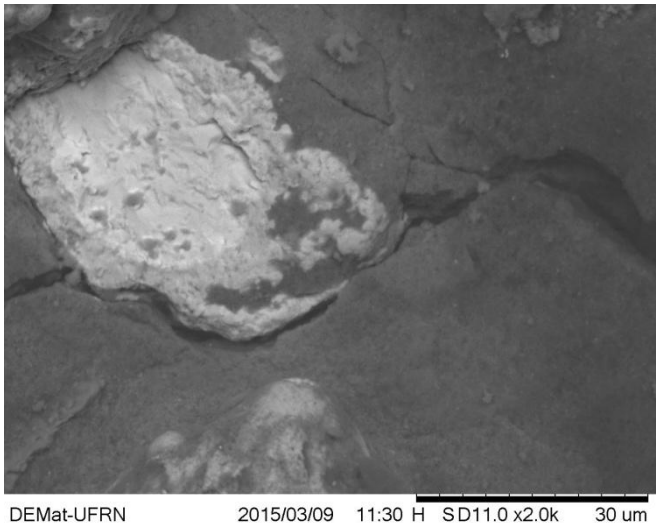

Source: Author.

EDS was used to distinguish Nb and Fe particles. Figure 4.6 shows a map analysis of the sample sintered at 1600 °C/5.5 GPa. This Figure also shows diffusion of Iron in the diamond matrix around it and also diffusion of carbon into the iron particle. The analysis also shows carbon (graphite) in the center of Iron particle that can prove graphitization of diamond in contact with Iron. Diffusion of metallic binder between diamond particles helps diamond sintering by achieving to more diamond particle surfaces.

Figure 4.7 shows chemical analysis performed via EDS at an area near a Fe particle in the sample sintered at 1750 °C/5.5 GPa/3 min. Results listed in the figure show that around 10 wt% Iron is available at diamond matrix in a distance approximately 30 μm from particle surface.

Figure 4.8 show the same analysis in figure 4.6 but for a Niobium particle in the sample sintered at 1600 °C/5.5 GPa/3 min. In this Figure, diffusion of Niobium into diamond matrix in a distance approximately 50 μm can be observed, but despite Figure 4.6, there is no trace of carbon inside Niobium particle and any graphitization as it was also observed earlier in Figure 4.3. It shows that Niobium can also diffuse easily into diamond matrix especially at high temperatures and in might also help diamond sintering.

Figure 4.6 Map analysis by EDS. Mixed (a), Diamond (b), Niobium (c) and Iron (d).

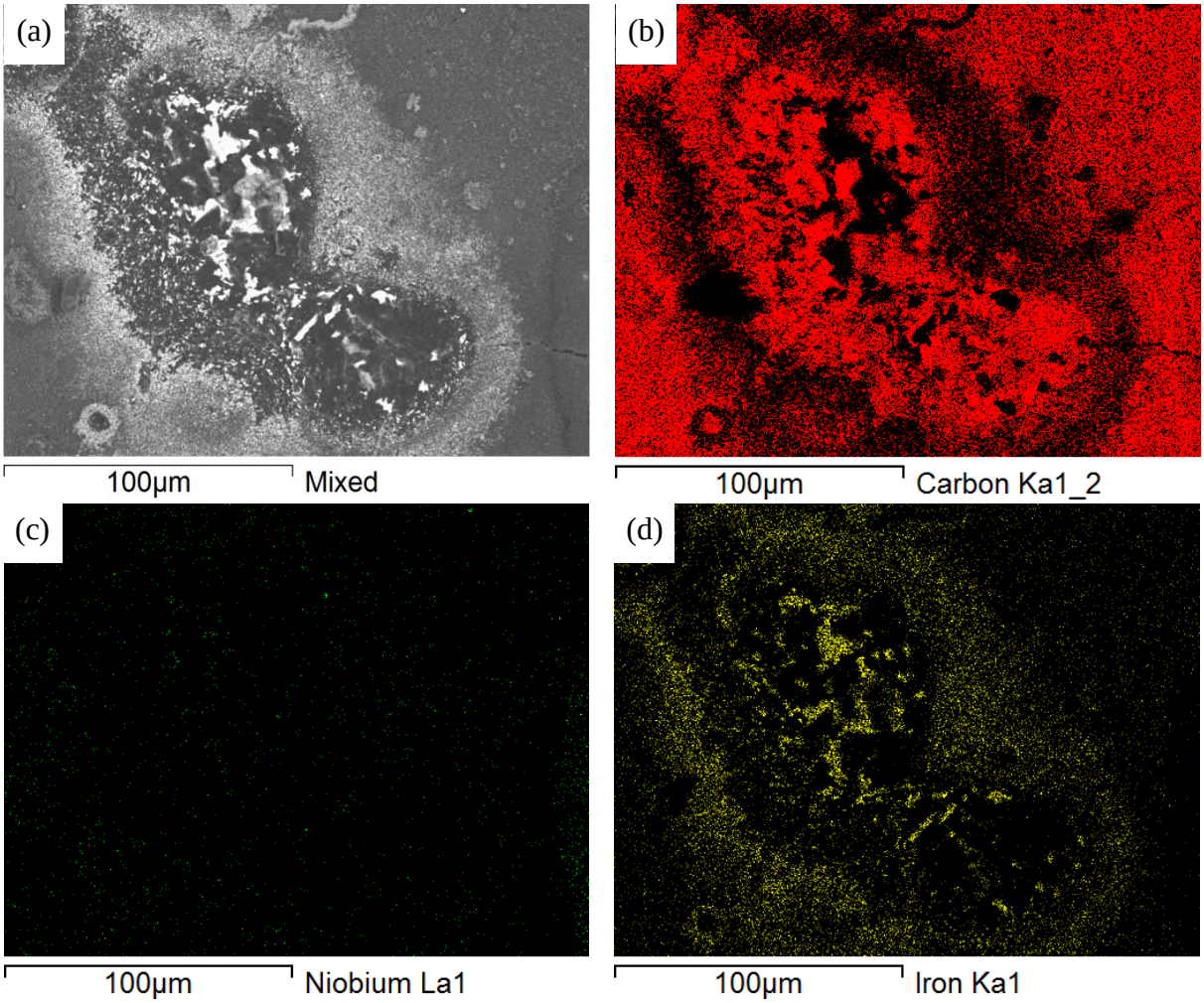

Source: Author.

Figure 4.7 Chemical analysis by EDS at an area near Iron particle.

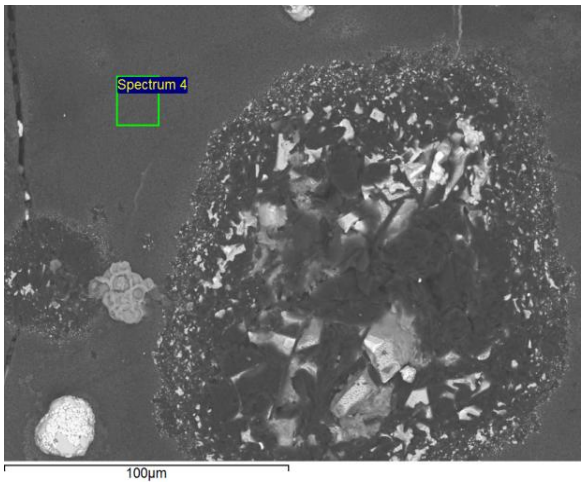

Element	*Weight %*
Carbon	89.346
Iron	9.896
Niobium	0.758

Source: Author.

Figure 4.8 Map analysis by EDS. Mixed (a), Diamond (b), Niobium (c) and Iron (d).

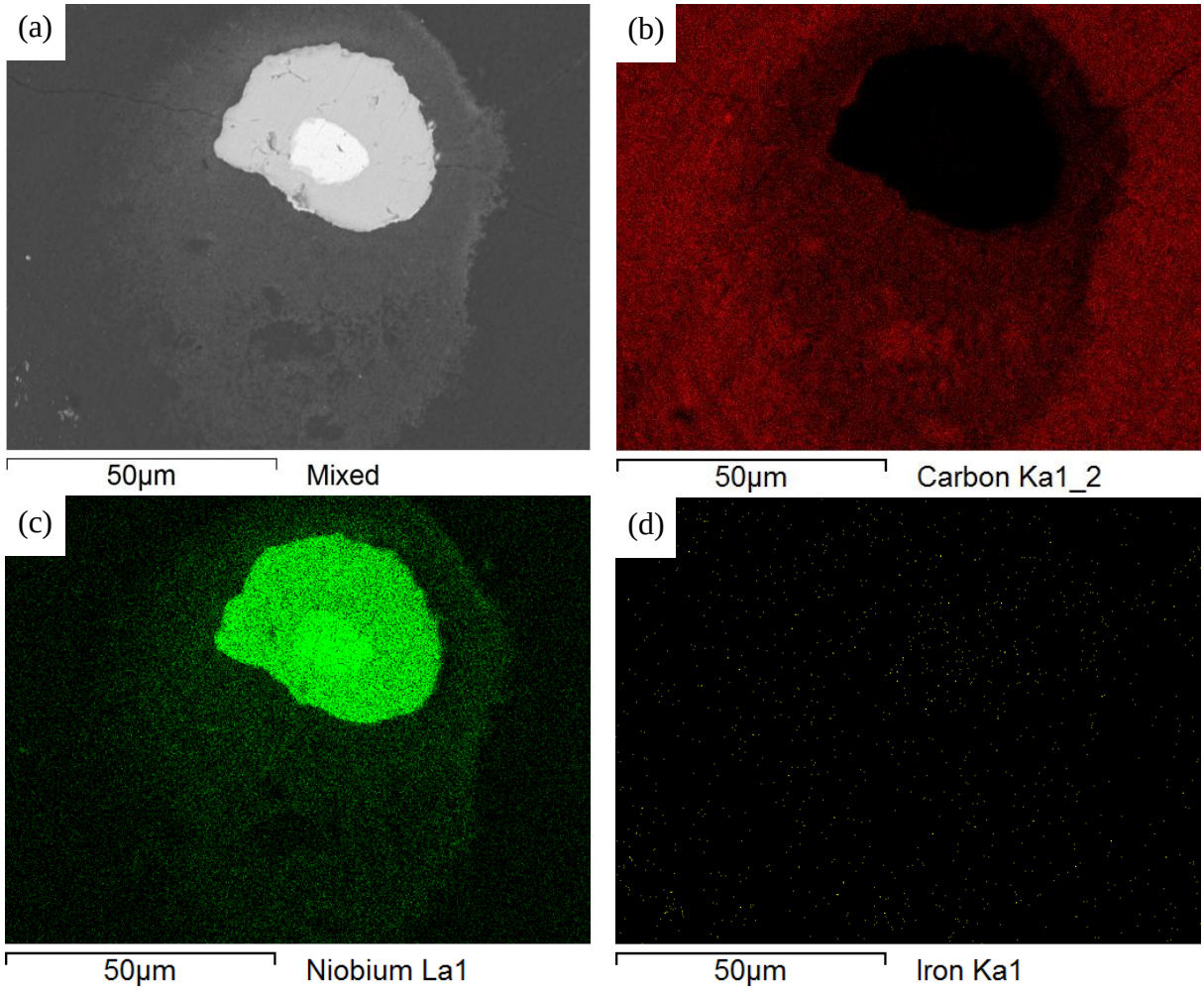

Source: Author.

Figure 4.9 shows an Iron particle surrounded by a Niobium particle in diamond matrix of the sample sintered at 1700 °C/5.5 GPa/3 min along with the linear chemical analysis performed via EDS.

As can be seen in this picture, only Niobium diffused into diamond matrix (blue line in the diagram) and Iron could not diffuse long distance up to diamond, however it diffused into surrounded Nb (green line in the diagram). The graph also shows that carbon from diamond matrix diffused into both Nb and Fe (red line in the graph) however; there is more carbon in Niobium than Iron. Carbon did not diffuse (or less diffused) in the center part of Fe (white area in the center).

According to this Figure, it seems that absence of Fe in diamond matrix prevented graphitization around the particle but at there is some trace of graphitization especially at top

and right interface of diamond and particle where the Fe is closer to the diamond and probably could diffuse into it.

Figure 4.9 A Fe particle surrounded by Nb in Diamond matrix with a linear chemical analysis by EDS.

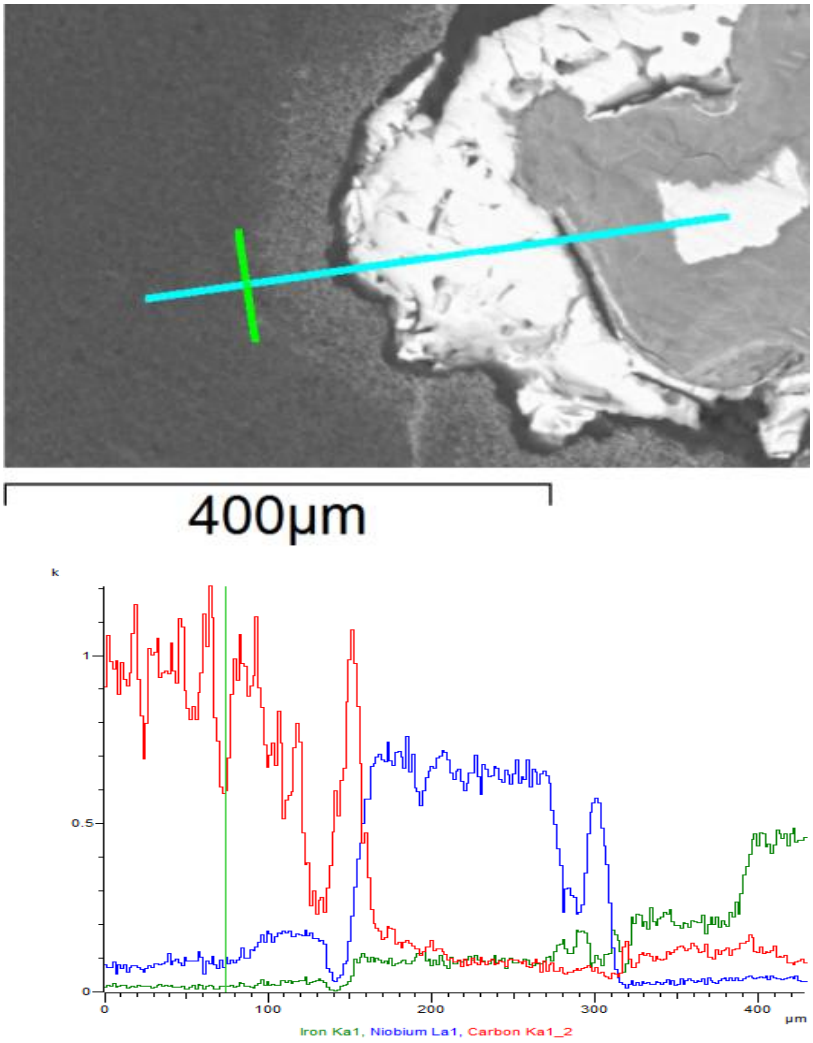

Source: Author.

d) XRD analyses

Figure 4.10 shows XRD patterns in 2θ range of 10° to 90° for three primary powders of Diamond, Niobium and Iron performed separately before mixing and sintering. In this range, Diamond has two distinct peaks at 2θ ≈ 43.9° and 75.4°, Niobium has a big peak located at 2θ ≈ 38.7° and two other small peaks at 2θ ≈ 55.8° and 69.8°. Iron powder only showed a small peak at 2θ ≈ 44.6°.

Figure 4.10 XRD pattern of Diamond, Niobium and Iron powders.

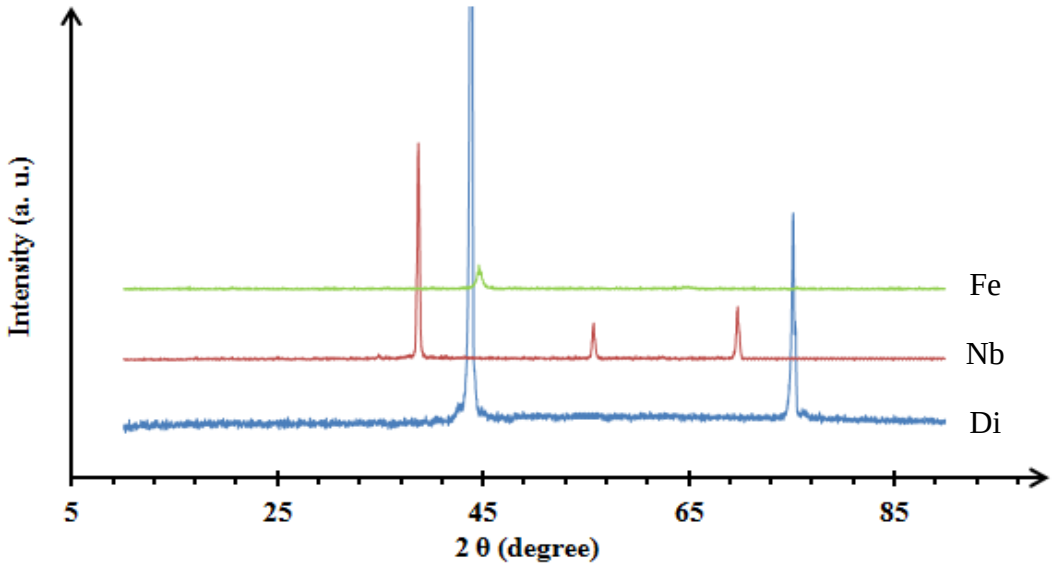

Source: Author.

In Figure 4.11 shows XRD patterns for samples sintered at 1600 ° for 3 minutes and with different pressures are presented. There is a peak located at 2θ ≈ 26.6° related to graphite (002) peak in all three samples that shows graphitization occurred. It is the only graphite peak observed in these samples, because of strong anisotropic nature, graphite grows preferentially along the (002) plane [101].

The peaks of Diamond are located at 2θ ≈ 43.9° and 75.4° as they observed in diamond powder (Figure 4.10), but the intensity of the peak at 2θ ≈ 75.4° decreases by decreasing the sintering pressure showing more diamond transformation. In the other hand, graphite peaks becomes stronger by decreasing sintering pressure demonstrating more graphite formation. These two changes in diamond and graphite peaks can prove more graphitization in sample sintered at 1600 °C/3 min under lower pressure.

According to diamond graphite stability diagram (Figure 2.3), 1600 °C/5.5 GPa is in graphite region and probability of diamond to graphite transformation is high, it can be the reason for more intense graphite peak at sample sintered at this situation. For two other samples sintering was in diamond stable region, however, in these sample graphitization also occurred. It can be explained by high catalyst ability of Iron for transforming diamond to graphite as it was seen in SEM micrographs of Figure 4.3. It seems that Iron could not act as a catalyst in reverse transformation (graphite to diamond) or reverse transformation was not completely done.

Figure 4.11 XRD patterns of samples sintered at 1600 °C/3 min with different sintering pressures.

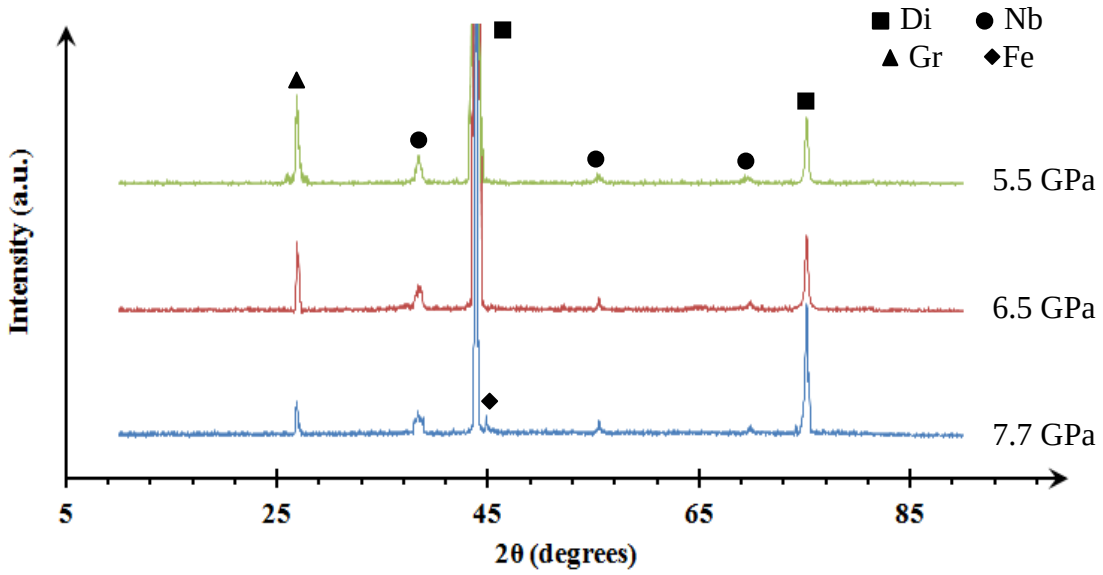

Source: Author.

All three Nb peaks available in XRD pattern of Nb powder (Figure 4.10) are still observed in XRD patterns sintered samples even the intensity is low compared with diamond which can be explained by lower amount of Nb in mixture (only 5 wt%). Peaks of Nb in Figure 4.11 are slightly shifted in compared with peaks in XRD patterns of Nb powders that can be related to deformation of Nb crystallite and changing lattice parameter under high pressure used for sintering or carbon diffusion into Niobium structure [102].

Iron has only a peak near the principal diamond peak (Figure 4.10), but this peaks is not available in XRD pattern of sintered sample except the sample sintered at 1600 °C/7.7 GPa/3 min in which, a small peak can be observed at $2\theta \approx 45.0°$. Two reasons can be offered for absence of Iron peak in sintered samples.

First of all, the peak of Fe is with low intensity and very close to intensive peak of diamond and with a little shifting according to change in crystallite shape due to high pressure sintering, they can be overlapped and it is only possible to see the diamond peak.

The next reason can be explained as low amount of Fe in the mixture, despite Nb, Iron particle were almost collapsed during sintering and graphite was formed around and inside them, then the possibility of having a peak of Fe reduced. As can be seen in Figure 4.3, some Fe particles completely destroyed or covered by graphite around them.

Figure 4.12 show XRD patterns for samples with Fe/Nb binder sintered under 5.5 GPa of pressure for 3 min at different temperatures. In the face of the Figure 4.11, in which the effect of sintering pressures was shown, in this Figure the effect of sintering temperatures can be seen.

Figure 4.12 XRD patterns of samples sintered under pressure of 5.5 GPa °C for 3 min at different temperatures.

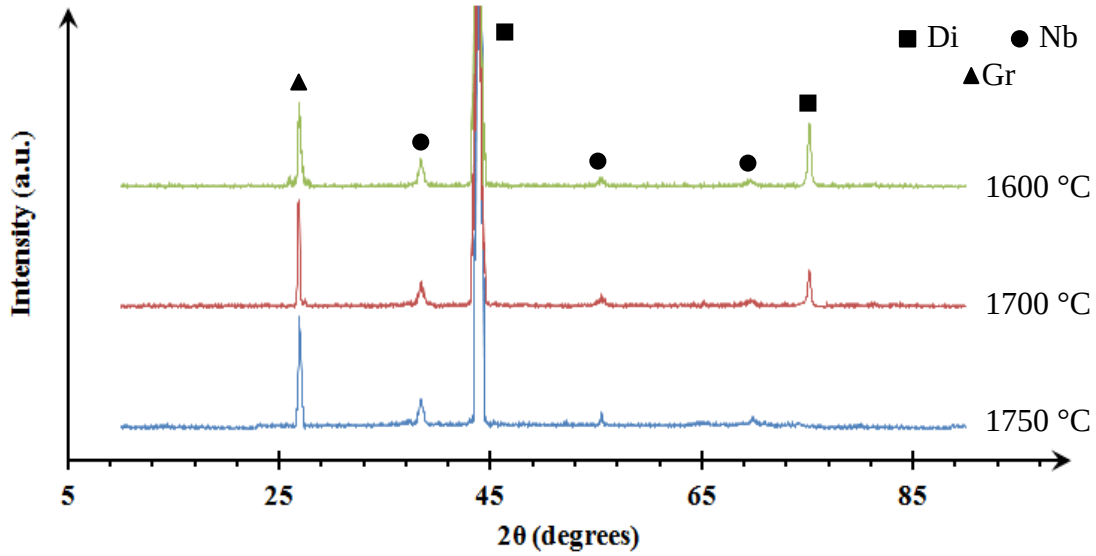

Source: Author.

All these three samples sintered in graphite stable region in diamond-graphite stability diagram (Figure 2.3) and among them, the sample sintered at 1600 °C/7.5 GPa/3 min has the worst condition with higher risk of diamond to graphite transformation. As can be seen, the diamond peak at $2\theta \approx 75.4°$ completely disappeared for this sample and also graphite peaks is stronger than all other presented in Figures 4.11 and 4.12. It shows more graphitization that means more diamond to graphite transformation under these sintering conditions.

By decreasing sintering temperature at 5.5 GPa of pressure (being close to the diamond stability region in diamond-graphite stability graph of Figure 2.3), the intensity of diamond peak at $2\theta \approx 75.4°$, that disappeared for sample sintered 1750 °C, increases and the intensity of graphite peak decreases. It shows that at a constant sintering pressure, graphitization and transformation of diamond to graphite is easier at higher temperature especially where a strong catalyst like Fe is available.

Again, all three Nb peaks can be observed in the patterns of sintered samples with a little shifting with the same reason explained before. No Iron peak observed in the three patterns that can be explained as proximity of this peak to diamond peak and higher amount of graphite formed during sintering.

e) Hardness and microhardness measurements

Vickers microhardness measurement results are listed in Table 4.2 as microhardness range and maximum microhardness measured for each sample. During the test, various hardness results were found at different part of microstructure demonstrating anisotropy of hardness in the samples thus; the microhardness result was shown as a hardness range. The maximum hardness can show if sintering process for this composition is appropriate and it achieved to the hardness necessary for cutting tools or not.

Table 4.2 Vickers microhardness results of samples with Nb/Fe binder sintered at different conditions (holding time of 3 minutes).

Sample code	*Sintering parameters*		*Microhardness range (HV)*
	Temperature (°C)	*Pressure (GPa)*	
A_1	1600	5.5	469-1156
A_2		6.5	313-1789
A_3		7.5	520-1943
A_4	1700	5.5	436-1691
A_5		6.5	560-1446
A_6		7.5	485-3109
A_7	1750	5.5	223-850
A_8		6.5	398-1420
A_9		7.5	940-3285

Source: Author.

As can be seen in the Table 4.2, even the maximum hardness is not in a range of diamond sintered body that is generally more than 4500 HV. There is a broad variation of hardness in all samples but with attention to the maximum amount, it can be resulted that the samples sintered at higher pressure are harder than those sintered at low pressure at constant temperature. For example, sample A_9 that was sintered at 1750 °C/7.7 GPa has the highest Vickers hardness value than other sample equal to 3285 HV. It can be explained according to stability of diamond at higher pressure even at high temperature and lower graphite formation. Up to now, it can be said that sintering under higher pressure, results in higher hardness.

The samples sintered under the lowest pressure of 5.5 GPa (A_1, A_4 and A_7) have the lowest hardness. They are the sample that their XRD patterns are shown in Figure 4.12 with intensive graphite peaks. The lowest hardness belongs to the samples sintered at 1750 °C/5.5 GPa (A_7) that was sintered in a situation with high possibility of diamond to graphite transformation. According to this explanation, lower pressure is not a proper situation for sintering diamond especially at high temperature. These results are in a good agreement with XRD results presented in previous section.

In Table 4.2, it can also be seen that increasing sintering temperature at higher pressure results in higher hardness. It seems that at lower temperature, sintering process is not complete and resulting to lower hardness. At high sintering temperature, hardness is higher, but as mentioned before, this hardness is not in the range for diamond tools, then it can be concluded that holding time (3 min) is not sufficient for sintering these set of samples.

It is also important to notice that lower microhardness measured near the Fe binder that can be another sign of graphitization and negative effect of this binder during sintering of diamond at selected sintering parameters.

To have a better view of hardness, macro Vickers hardness test was also performed and the obtained result listed in Table 4.3. The trend is the same as observed in Table 4.2 with higher hardness for samples sintered under higher pressure vice versa.

Table 4.3 Vickers hardness results of samples with Nb/Fe binder sintered at different conditions listed in Table 3.1.

Sample code	A_1	A_2	A_3	A_4	A_5	A_6	A_7	A_8	A_9
Sintering temperature (°C)	*1600*			*1700*			*1750*		
Sintering Pressure (GPa)	*5.5*	*6.5*	*7.5*	*5.5*	*6.5*	*7.5*	*5.5*	*6.5*	*7.5*
Average hardness (HV)	442	635	980	765	637	1342	368	748	1672

Source: Author.

This table gives a better understanding how low the hardness of samples is. However, there are some points with high hardness in microstructure; macro hardness results showed that the hardness in general is quite low. These points can be points with better sintered diamond microstructure and low graphite. As discussed before, this low hardness results can be related to graphite formation in microstructure (see section 4.1.1 c and 4.1.1 d) and incomplete sintering at selected sintering conditions (see section 4.11 e).

All figures, tables and discussions in this section showed that sintering diamond powder with Nb/Fe as binder at different temperatures and under different pressures (listed in Table 3.1) for 3 minutes, has not resulted in a good quality sintered diamond body. Then, it was decided to change binder and use Ni and Co instead of Fe. Also, as sintering under low pressure resulted in lower hardness and more graphite formation; new tests were only done under 7.7 GPa of pressure. Besides, sintering was done at 1750 °C with two different holding times of 3 and 9 minutes (see section 3.1.2) to prevent incomplete sintering by giving time to diamond and binder powder for better diffusing at high temperature.

4.1.2. Nb/Co and Nb/Ni binders

a) Visual analyses

Visual inspection of samples sintered with Nb/Co and Nb/Ni binder showed that despite the previous samples with Nb/Fe binder, they have better surface quality without any distinct superficial cracks and fractures. Like before, samples did not have fair cylindrical shape and were in different sizes.

Sample were ultrasonically cleaned without happening any fracture but one of the samples with Nb/Co binder sintered at 1750 °C under 7.7 GPa of pressure for 3 minutes fell down during handling after cleaning and broke (Figure 4.13). The falling height was around 50 cm and breaking the sample shows a high degree of brittleness in this sample. Brittleness is a characteristic of diamond sintered body but it seems that the impact caused by falling was not too high to break a fair sintered diamond. Then, this breaking can be a result of internal problem such as graphitization. Microstructure and XRD analyses along with hardness result in next sections can prove this claim.

Figure 4.13 Broken sample with Co/Nb binder sintered at 1750 °C / 7.7 GPa/ 3min.

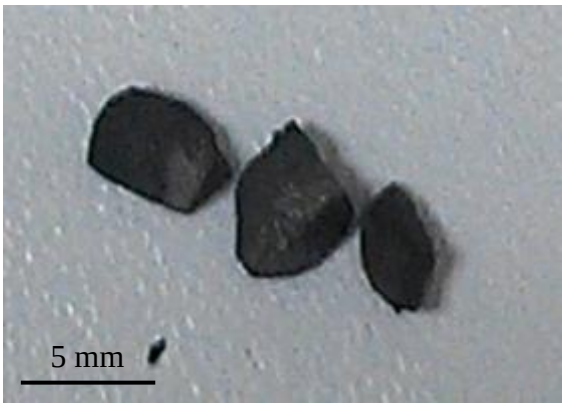

Source: Author.

b) Density results

Average density and relative density of samples are listed in table 4.1. Relative densities were calculated using theoretical density of mixture equal to 3.73 g/cm^3 for both used binders.

Table 4.4 Density and relative density of samples with Nb/Co and Nb/Ni binders sintered at 1750 °C/7.7 GPa with different holding time.

Binder	*Holding time (min)*	*Density (g/cm^3)*	*Relative density (%)*
Nb/Co	3	3.45	92.43
Nb/Co	9 (3x3)	3.56	95.44
Nb/Ni	3	3.50	93.83
Nb/Ni	9 (3x3)	3.66	98.12

Source: Author.

In general, the relative density is higher than those achieved for samples with Nb/Fe binder listed in Table 4.1 but like before, it was expected to have high density (near 100%) at high pressure and none of the samples achieved to full density. However, the relative density of sample with Nb/Ni sintered for 9 minutes are very close to 100%.

Selected temperature and pressure for sintering of this set of samples fell at diamond stable region in diamond-graphite stability diagram to avoid any graphitization but the density results and a broken sample show that graphite might be formed during sintering.

c) Microstructure study

The focus of this study was on finding any trace of graphitization, internal cracks and effect of binder particles on diamond matrix.

Figure 4.14 and 4.15 show micrograph obtained by confocal microscope for samples with Nb/Co and Nb/Ni, respectively. These figures show a sintered diamond matrix with dispersed binder sand binder particles can also be seen as bright points. No cracks observed in these set of samples that is a sign for better sintering and less or no graphitization.

Figure 4.14 and 4.15 show SEM micrograph of samples with Nb/Co and Nb/Ni, respectively. SEM micrographs for all samples also did not show any cracks in microstructure. Besides, no collapsed particles, changed matrix around particle or graphite formation, like what observed in samples with Nb/Fe binder (Figure 4.3 and 4.4), were considered in these samples.

Figure 4.14 Confocal micrograph of samples with Nb/Co binder sintered at 1750 °C/7.7 GPa for 3 min (a) and 9 (3x3) min (b).

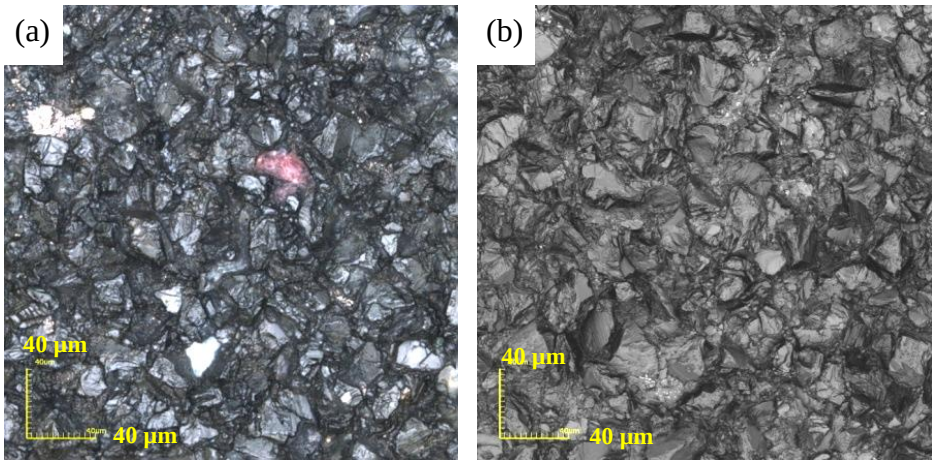

Source: Author.

Figure 4.15 Confocal micrograph of samples with Nb/Ni binder sintered at 1750 °C/7.7 GPa for m min (a) and 9 (3x3) min (b).

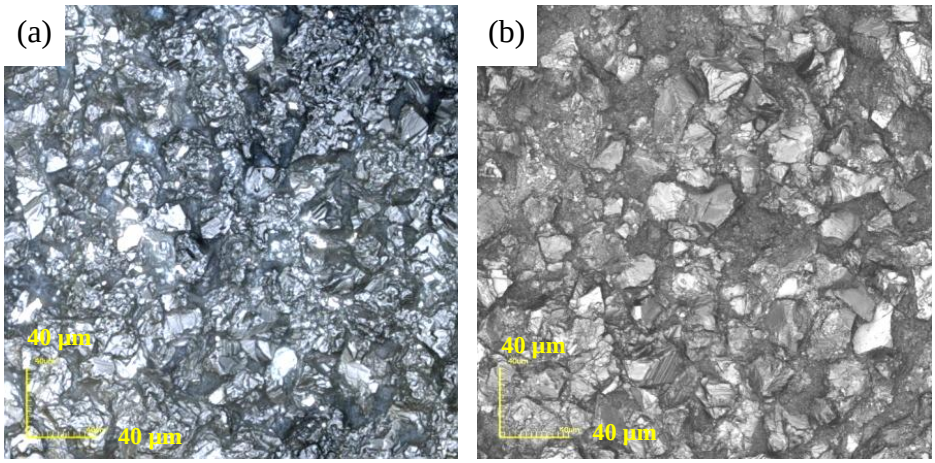

Source: Author.

As can be seen in Figure 4.16 b and 4.17 b, samples sintered for longer time (9 min) have better binder distribution in diamond matrix. It seems that high temperature along with long holding time made a good situation of diffusion of binder between diamond particles during liquid phase sintering.

Better binder distribution results in homogenous properties for sintered samples by providing the same sintering situation for any diamond particle in the mixture during the sintering. By diffusion, binder can reach to diamond particle surface and make the proper situation for sintering the particles. To show the binder distribution, SEM micrograph of a

sample with Nb/Co binder and sintered at 1750 °C/7.7 GPa/9 min is presented at low magnification in Figure 4.18.

Figure 4.16 SEM micrograph of samples with Nb/Co binder sintered at 1750 °C/7.7 GPa for 3 min (a) and 9 (3x3) min (b).

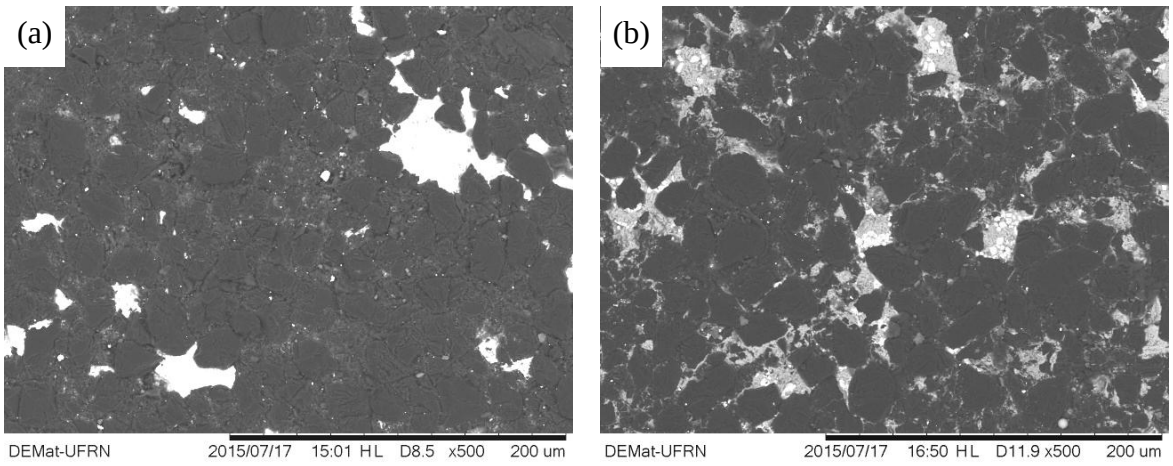

Source: Author.

Figure 4.17 SEM micrograph of samples with Nb/Ni binder sintered at 1750 °C/7.7 GPa for 3 min (a) and 9 (3x3) min (b).

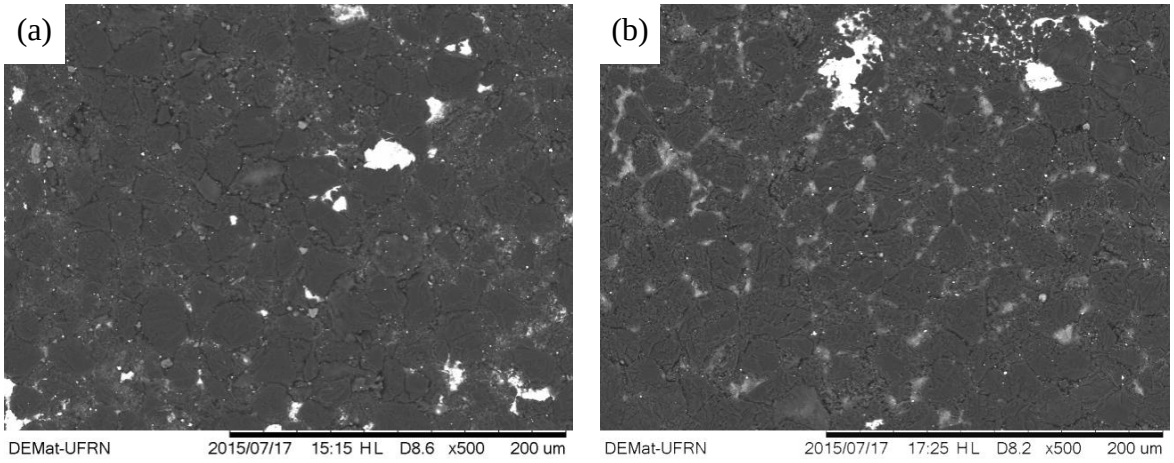

Source: Author.

In the microstructure presented in Figure 4.16 and 4.17 there are some regions around diamond particle that are like porosities but, according to high pressure used for sintering it is less probable. Then, they seem to be the distributed binder that removed during preparation. These empty regions can be seen more in samples sintered for shorter time because of insufficient time to distribution and subsequent sintering.

Figure 4.18 Micrograph of sample with Nb/Co binder sintered at 1750 °C/7.7 GPa/9 min.

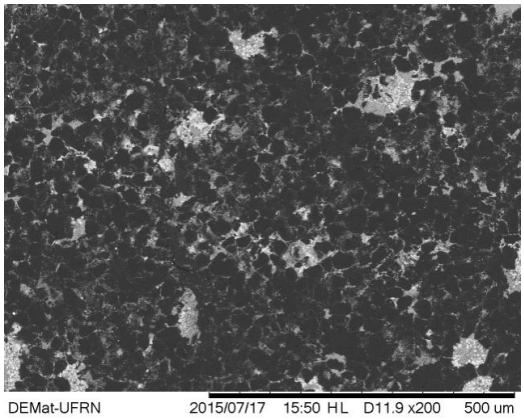

Source: Author.

Figures 4.19 and 4.20 show map analyses performed by EDS in samples with Nb/Co and Nb/Ni binder, respectively. The binder distribution in matrix can also be seen in these figures.

Figure 4.19 Map Analysis for sample with Nb/Co binder sintered at 1750 °C/7.7 GPa/9 min. Mixed (a), Diamond (b), Niobium (c) and Cobalt (d).

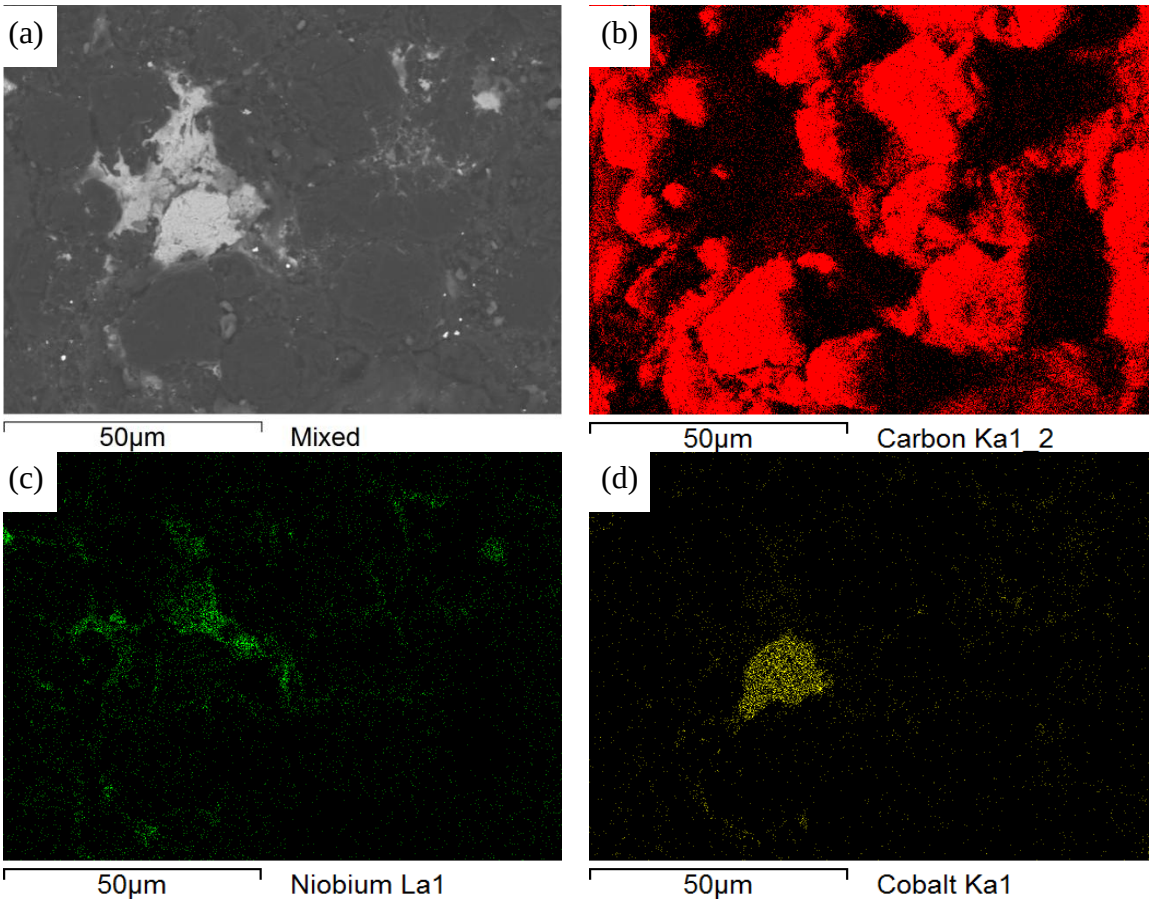

Source: Author.

Figure 4.20 Map Analysis for sample with Nb/Ni binder sintered at 1750 °C/7.7 GPa/9 min. Mixed (a), Diamond (b), Niobium (c) and Nickel (d).

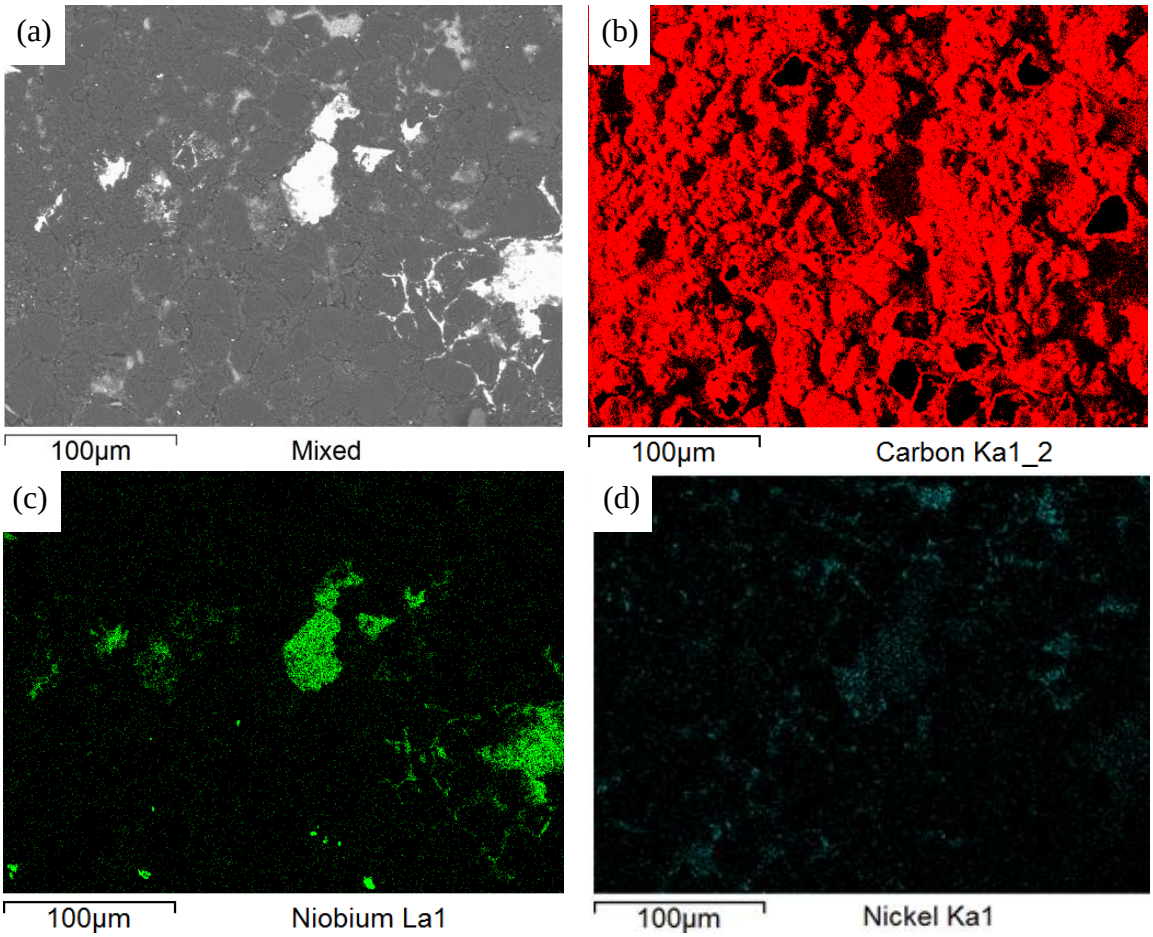

Source: Author.

d) XRD analyses

Figure 4.21 shows XRD patterns for two other primary powders of Cobalt and Nickel in 2θ range of 10° to 90°. In this range, Cobalt has three small peaks at 2θ ≈ 43.7°, 49.6° and 46.6°. Nickel also has three peaks located at 2θ ≈ 37.3°, 44.4° and 51.9°. These peaks are small in compare with Diamond and Niobium (Figure 4.10), and then it is probably difficult to find these peaks in the sintered samples considering that there is only 5 wt% of these elements in the sintered samples.

XRD patterns at different holding times for samples with Nb/Co and Nb/Ni binder sintered at 1750 °C/7.7 GPa are shown in Figures 4.22 and 4.23, respectively. As can be seen in Figure 4.22, the Graphite peak at 2θ ≈ 26.6° can be observed only for sample sintered for 3 minutes showing the transformation of diamond to graphite at this sintering situation. XRD pattern of sample sintered for longer time up to 9 minutes does not have this graphite peak

demonstrating that using Nb/Co binder and sintering at high temperature under high pressure and giving time for sintering can prevent graphitization.

Figure 4.21 XRD pattern of Cobalt and Nickel powders.

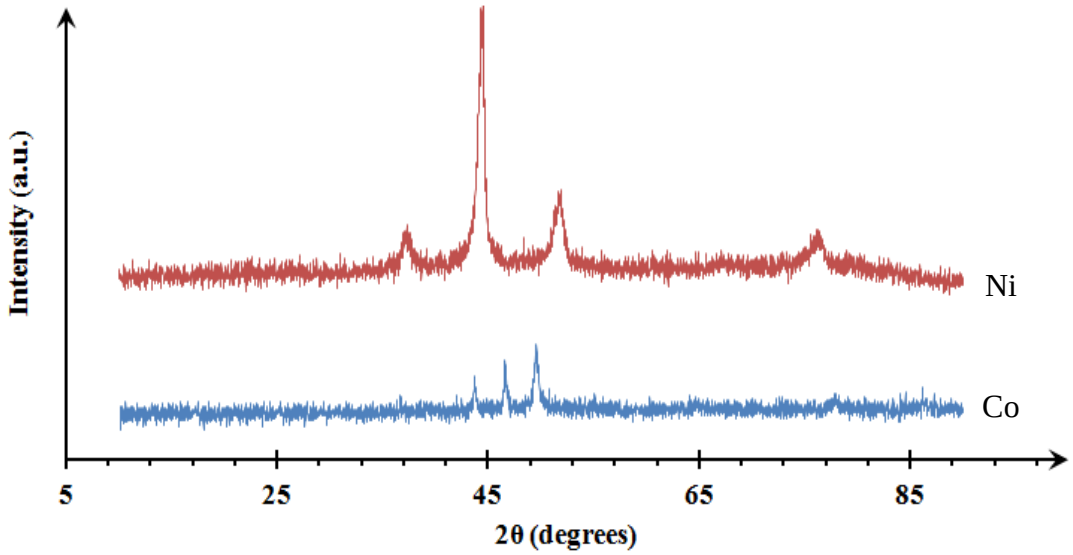

Source: Author.

Figure 4.22 XRD patterns of samples with Nb/Co binder sintered at 1750 °C/7.7 GPa with different holding times.

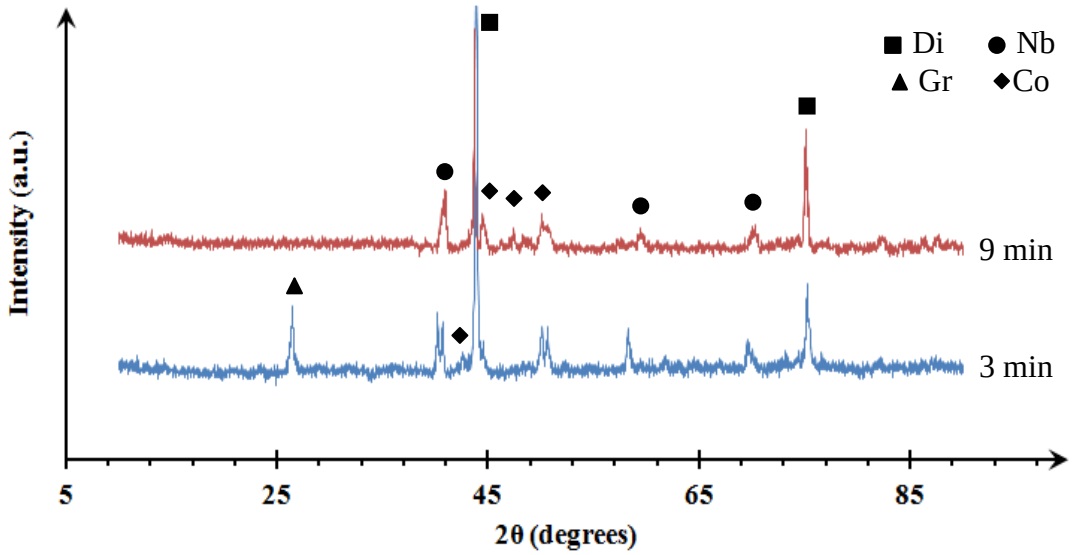

Source: Author.

It seems that 3 minutes of holding time is not enough for sintering of diamond powders with Nb/Co binder even at high temperature of 1750 ºC. In shorter holding time,

binder has not sufficient time to spread in the microstructure, act as binder for sintering, and then act as a catalyst to transform formed graphite to diamond.

Figure 4.22 also shows that sample sintered for 3 minutes has weaker diamond peak at 2θ ≈75.4º which can be the result of graphitization. Peaks of other elements are also observed however, almost all of them shifted to different 2θ compared with their peaks in the XRD patterns of used raw materials (Figures 4.10 and 4.22) that as explained before can be because of crystallite deformation and changing lattice parameter under high pressure sintering.

Cobalt peaks are visible in the XRD sample sintered for 9 minutes even they also shifted and as two of them are close to strong peak of diamond at 2θ ≈ 43.9º, they merged with diamond peak in pattern of sample sintered for 3 minutes.

Figure 4.23 shows the XRD patterns of sample with Nb/Ni. Sintering parameters is explained before for sample with this binder and two patterns related to samples sintered for 3 and 9 minutes are presented. No peak related to Graphite is available neither in samples sintered for 3 minutes nor in samples sintered for 9 minutes. Diamond peaks in both patterns are well strong showing that no transformation of diamond to graphite happened or at least it has not detected in presented patterns. None or low graphitization is in agreement with microstructure studies presented in previous section.

Figure 4.23 XRD patterns of samples with Nb/Ni binder sintered at 1750 °C/7.7 GPa with different holding times.

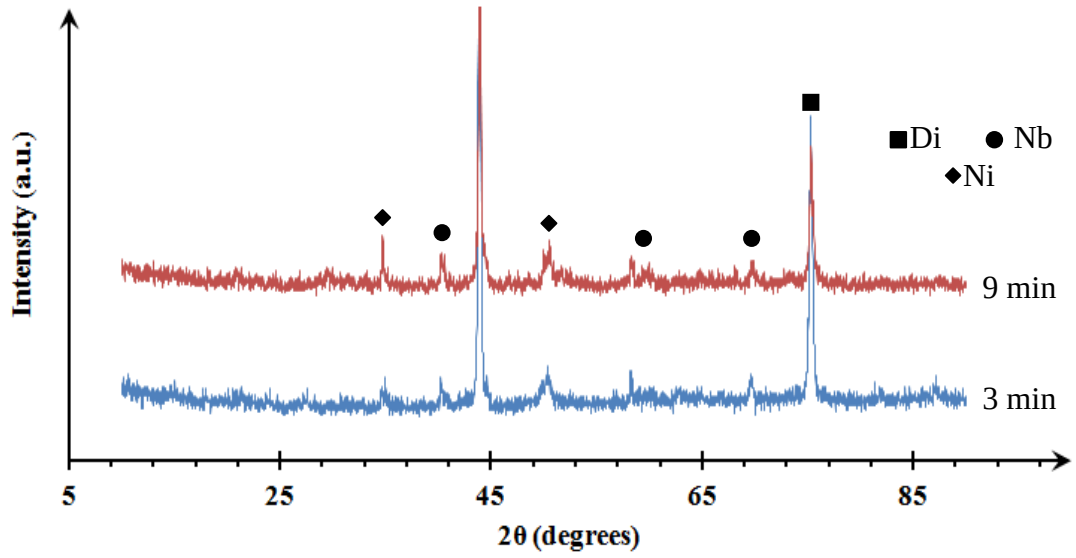

Source: Author.

One of the Ni peaks is located almost at the same angle that Diamond peak located (43.9 and 43.7 for Diamond and Nickel, respectively), then except this peak then can be merged with diamond peak, two other can be observed in both patterns presented in Figure 4.23 however these two peaks also shifted to different 2θ angle. All three peaks are Niobium are also observed in the XRD patterns.

XRD results shows that graphitization occurred only in the sample with Nb/Co binder sintered for short time but for having a conclusion about which one is the best binder microhardness and hardness result were also done.

e) Hardness and microhardness measurements

Table 4.5 shows the microhardness results of sample with Nb/Co and Nb/Ni binder at different sintering condition. Like Table 4.2, results presented as microhardness range because of the variation of microhardness in the microstructure.

Table 4.5 Vickers microhardness results of samples with Nb/Co and Nb/Ni binder sintered at different conditions.

Binder	*Holding time (min)*	*Microhardness range (HV)*
Nb/Co	3	1139-2145
Nb/Co	9 (3x3)	1453-3048
Nb/Ni	3	1713-2845
Nb/Ni	9 (3x3)	1865-3351

Source: Author.

Hardness of these samples is by far higher than those for samples with Nb/Fe. In both binders, samples sintered for longer time have higher maximum hardness than can be related to sufficient time for complete sintering. Between different binders, the results show that Nb/Ni binder has a little higher hardness in both sintering time investigated. The lowest hardness was measured in sample with Nb/Co binder sintered for 3 minutes with trace of graphitization according to its XRD pattern showed in Figure 4.22. It must be considered that the sample that broke after falling during handling (Figure 4.13) was also among this set of samples.

Even hardness higher than 3000 HV was achieved but it was expected to higher harness for sintered diamond body.

Like before, to have a better overall view of hardness, Macro hardness test was also done and the obtained results are listed in Table 4.6. Result is in agreement with microhardness result listed in table 4.5 in which higher hardness is for sample with Nb/Ni binder sintered for longer time and the lowest one in sample with Nb/Co binder sintered for shorter time.

Table 4.6 Vickers hardness results of samples with Nb/Co and Nb/Ni binder sintered at different conditions.

Binder	*Holding time (min)*	*Average hardness (HV)*
Nb/Co	3	1247
Nb/Co	9 (3x3)	2643
Nb/Ni	3	2355
Nb/Ni	9 (3x3)	3109

Source: Author.

Results at this stage showed that even the hardness increased and no graphitization observer in most samples, the achieved hardness is still low. It was also found that longer holding time results in better hardness and lower possibility of graphitization. According to Microstructure study at previous stage and this stage and obtained results, it was decided to use pure Niobium as binder for next attempt.

4.1.3. Pure Nb binder

a) Visual analyses

Visual inspection of samples sintered with pure Nb binder showed that like samples with Nb/Co and Nb/Ni binders, the surface quality is good without any distinct superficial cracks and fractures. These samples also did not have fair cylindrical shape with a little deformation near base surfaces and were in different sizes. These sample did not have any problem during cleaning and handling. Figure 4.24 shows a sintered diamond body with pure Nb binder and sintered at 1750 °C/7.7 GPa/9 min.

b) Density results

Table 4.7 shows the measured density and relative density of sintered samples with pure Nb binder. Relative density was calculated using mixture density equal to 3.73 g/cm^3. As can be seen for both holding time the relative density is almost the same and very close to 100% showing better results compare with other used binders explained before.

Figure 4.24 Sintered sample with pure Nb binder sintered at 1750 °C/7.7 GPa/9 min.

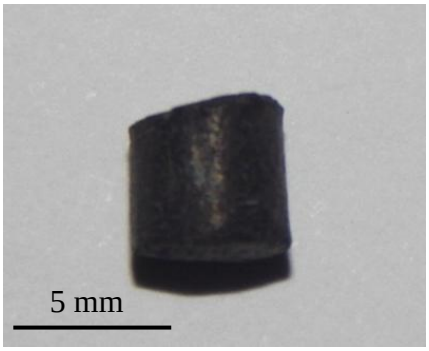

Source: Author.

Table 4.7 Density and relative density of samples with pure Nb binder sintered at 1750 °C/7.7 GPa with different holding time.

Holding time (min)	*Density (g/cm^3)*	*Relative density (%)*
3	3.67	98.39
9 (3x3)	3.66	98.12

Source: Author.

c) Microstructure study

SEM micrograph of samples with pure Niobium binder (Figure 4.25) did not show any graphitization or change in diamond matrix, the binder distribution was almost perfect and Niobium distributed between diamond particle however, distribution seems to be better for samples sintered for longer time (Figure 4.25 b).

Figure 4.25 SEM micrograph of samples with pure Niobium sintered at 1750 ºC/7.7 GPa for 3 min (a) and 9 min (b).

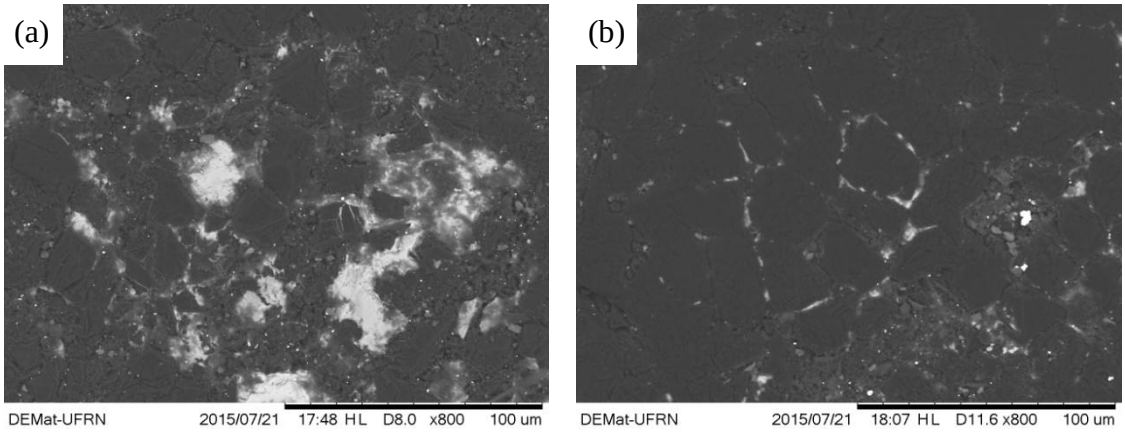

Source: Author.

As can be seen, when longer sintering time was used, the binder completely distributed between diamond particles. In Figure 4.25-b, there is no Nb particle in presented area but it is available between particle. This uniform distribution of binder can help to have better sintering resulting in uniform and better properties.

A map analysis via EDS of the same microstructure presented in Figure 4.25-b is shown in Figure 4.26 to better representing the Niobium distribution.

Figure 4.26 Map Analysis for sample with pure Nb binder sintered at 1750 °C/7.7 GPa/9 min. Mixed (a), Diamond (b), Niobium (c).

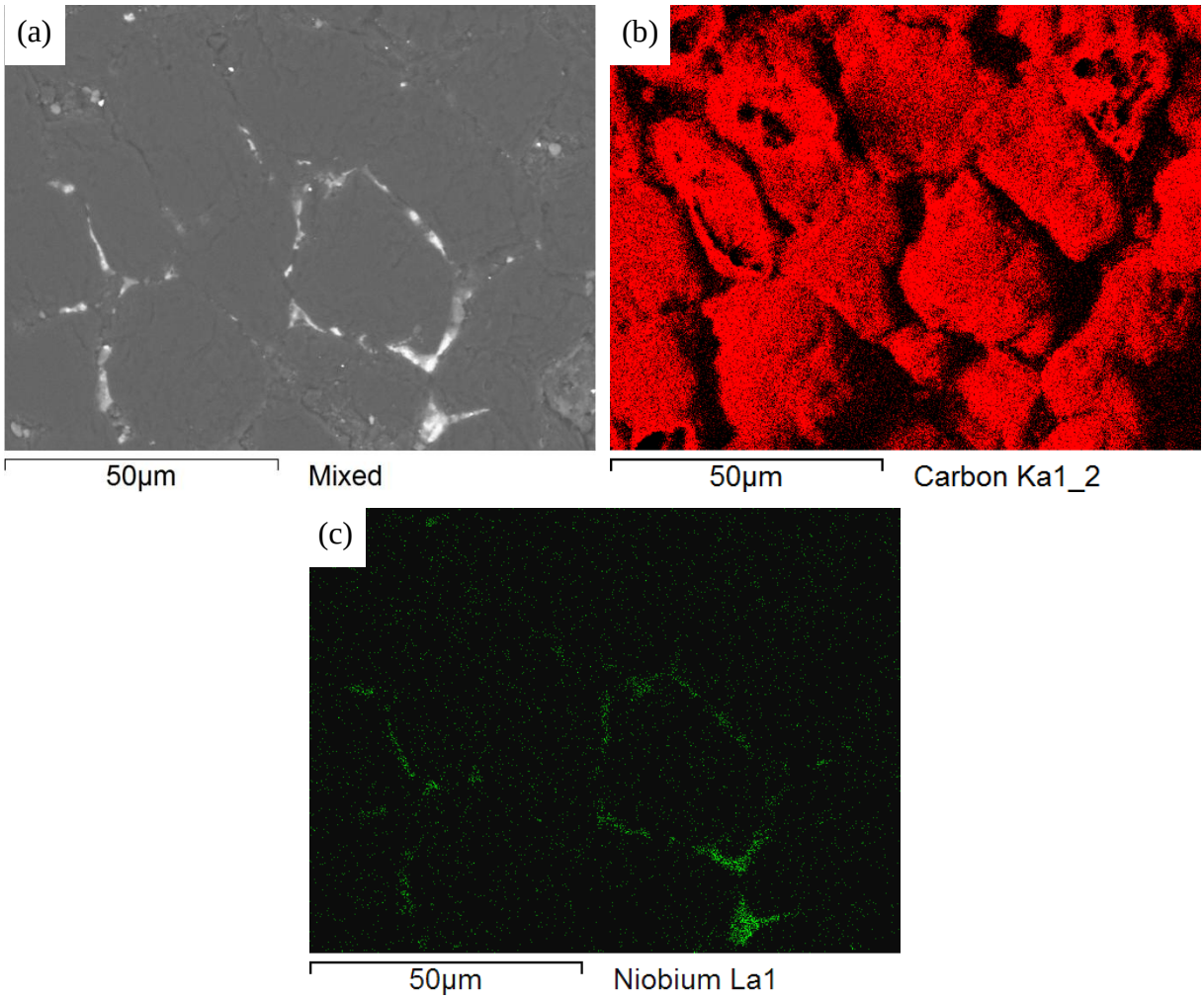

Source: Author.

d) XRD analyses

XRD patterns of samples sintered with pure Nb for different sintering time is presented in Figure 4.27. All peaks are related to elements of Diamond and Niobium and no peaks of Graphite can be seen in both patterns. Niobium peaks shifted like the previous

patterns explained before and as explained it is because crystalline deformation during sintering at higher pressure.

Figure 4.27 XRD patterns of samples with pure Nb binder sintered at 1750 °C/7.7 GPa with different holding times.

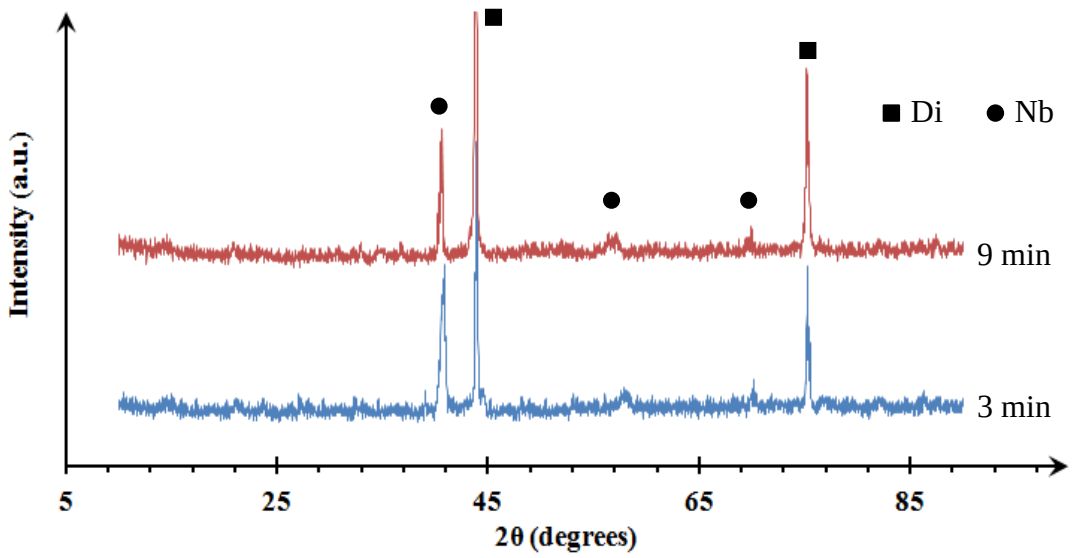

Source: Author.

e) Hardness and microhardness measurements

Microhardness ranges obtained for samples with pure Niobium are listed in Table 4.8.

Table 4.8 Microhardness ranges and maximum hardness for samples with pure Niobium.

Holding time (min)	*Microhardness range (HV)*
3	3637-4860
9 (3x3)	423-6217

Source: Author.

Results for these samples are interestingly higher than those with other binders. for both holding time, the hardness reached to more than 4500 HV that is proper hardness for diamond sintered body. These results also confirm that sintering for longer time has better results especially in hardness.

Macro hardness was also planned to perform for these samples, but, diamond indenter of hardness tester broke at first try that also shows the high hardness of samples.

According to the results obtained and explained in section 4.1, among all binder used for sintering the diamond, pure Niobium had the best results with no graphite formation and high hardness, and then it was decided to use this binder in producing triple layer polycrystalline diamond compact. It was also found that better mixing of powder can improve sintering process and results in better binder distribution, then for next stages high energy ball milling was used for mixing powders (see section 4.3).

4.2 Second stage - Study WC 10wt% Co substrate

In this section the results achieved from the tests performed on WC 10wt% Co are presented. Density, XRD and SEM analyses of powders and sintered samples, hardness, compression and indentation fracture toughness results will be explained.

Figure 4.28 shows SEM photograph of mixed powder, and XRD patterns of milled powders and initial powders of WC and Co are shown in Figure 4.29. Using high energy milling resulted in uniform mixing of WC and Co without any change as milling performed at low speed for short time.

Figure 4.28 SEM morphologies of WC 10 wt% Co powders.

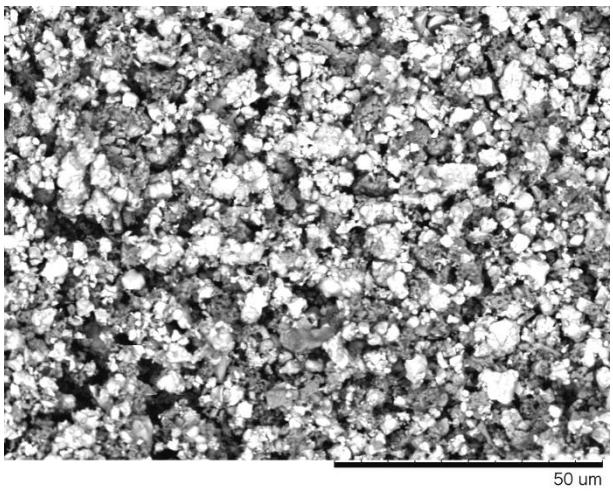

Source: Author.

Apparently, almost all of the peaks of starting materials were still observed in the XRD pattern of mixed powder after they had been milled and there are no peaks related to other phases, which shows the powder was only mixed during the ball milling and no intermediate phases formed. These results were expected because low milling speed and time were used. One of the Co peak at $2\theta \approx 41°$ disappeared in the mixed powder pattern, which can be related to lower intensity of Co peaks compared to WC peaks and also lower amounts

of Co in the powder mixture. Furthermore, it might be related to the Cu-Kα radiation used, which was probably absorbed by Cobalt [103]. Also there is another Co peak (at 2θ ≈ 76°) which is mixed with WC peak and cannot be identified in mixture pattern.

Figure 4.29 XRD patterns of the primary and mixed powders.

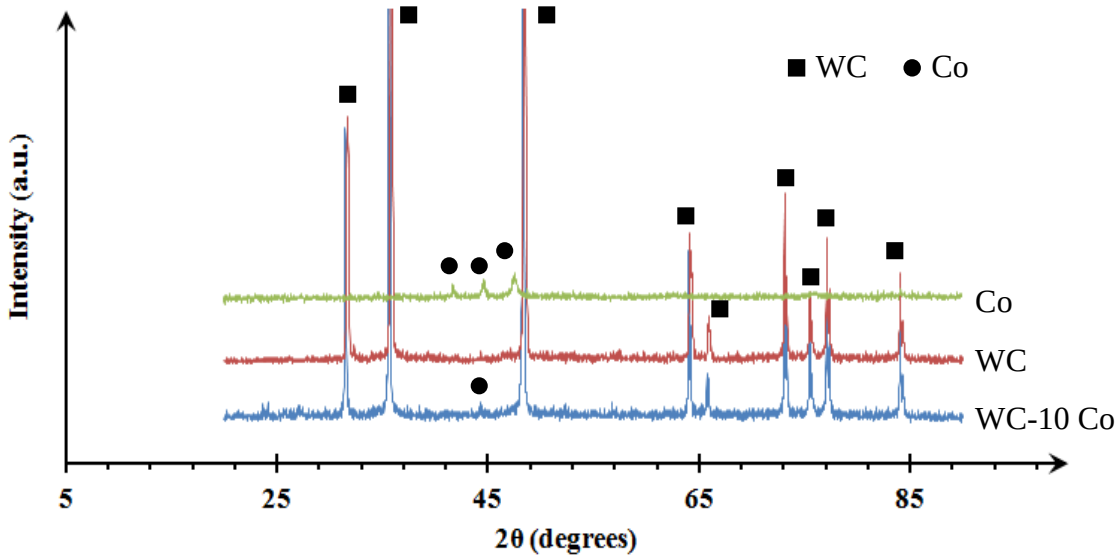

Source: Author.

Figures 4.30 and 4.31 show the micrographs of sintered samples at different temperatures for 2 and 3 minutes, respectively. As it was found in SEM images, the samples sintered at 1500 ºC had some porosities (see blue arrows in Figures 4.30-a and 4.31-a). Although some small porosity was found in the samples sintered at 1600 ºC, other samples were almost free of porosity (see blue arrows in Figures 4.30-b and 4.31-b).

It seems that short sintering time at lower temperature, even at high pressure, is not enough for rearrangement of the powder particles and diminishing of the free space between particles. The binder (Co) acts as a viscous mass spreading over WC surfaces, which leads to an increase in Laplace forces and rearrangements of the carbide particles into clusters. The first stage of WC–Co sintering is limited by the rate of binder spreading, which in turn is governed by intrinsic properties of the binder and the microscopic character of the carbide–binder composite [104].

At low temperature, spreading of liquid Co between WC particles is slower as compared to cases with higher temperature and the reason is lower viscosity. In addition, diffusion rate is higher at higher temperature, which leads to easier WC rearrangement and

porosity annihilation during sintering especially at very short times. Higher porosity in samples sintered at lower temperature can be explained with the latter two reasons.

Figure 4.30 SEM micrographs of sintered WC-10 Co at different temperature for 2 minutes. 1500 °C (a), 1600 °C (b), 1700 °C (c), 1800 °C (d), and 1900 °C (e).

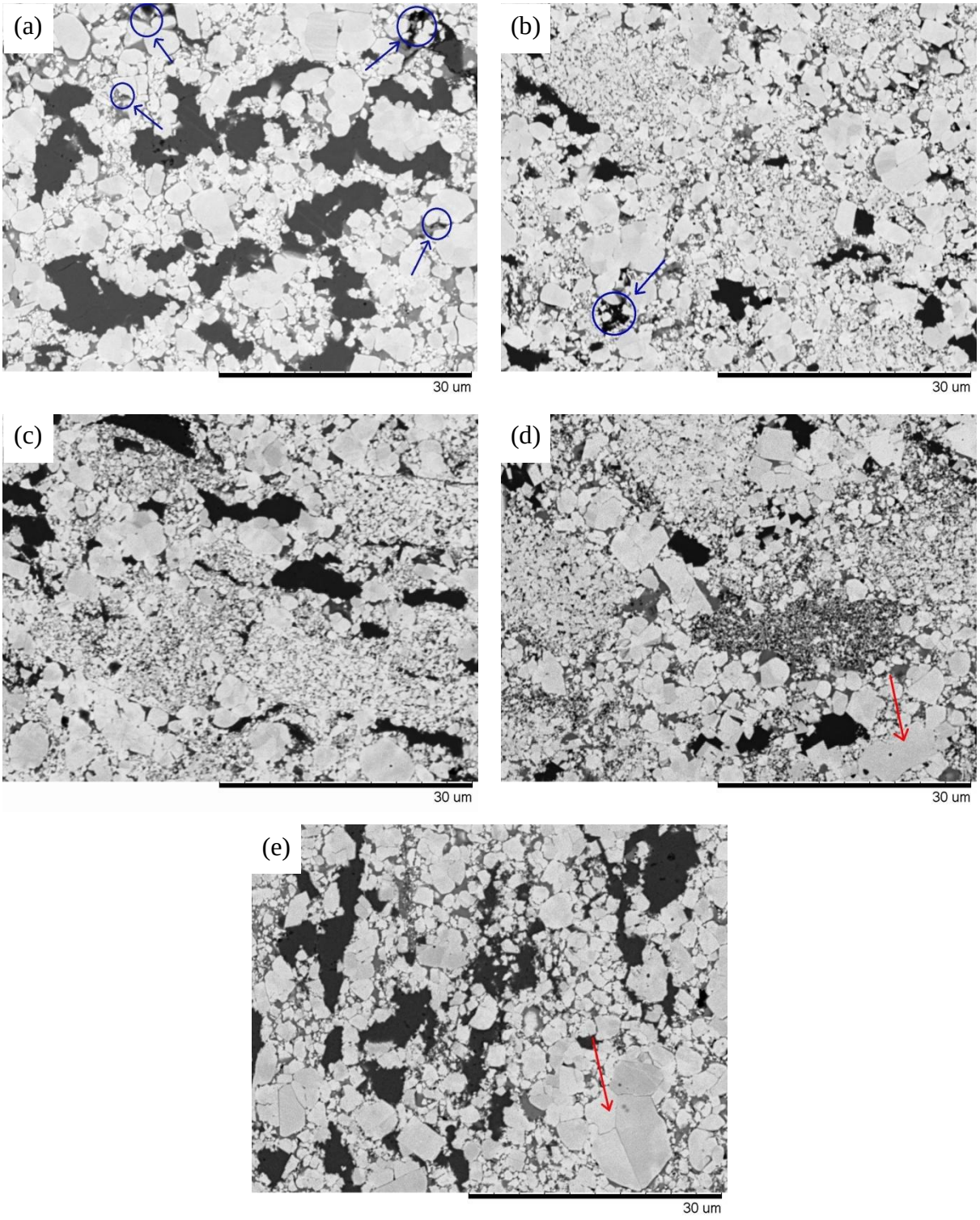

Source: Author.

Figure 4.31 SEM micrographs of sintered WC-10 Co at different temperature for 2 minutes. 1500 °C (a), 1600 °C (b), 1700 °C (c), 1800 °C (d), and 1900 °C (e).

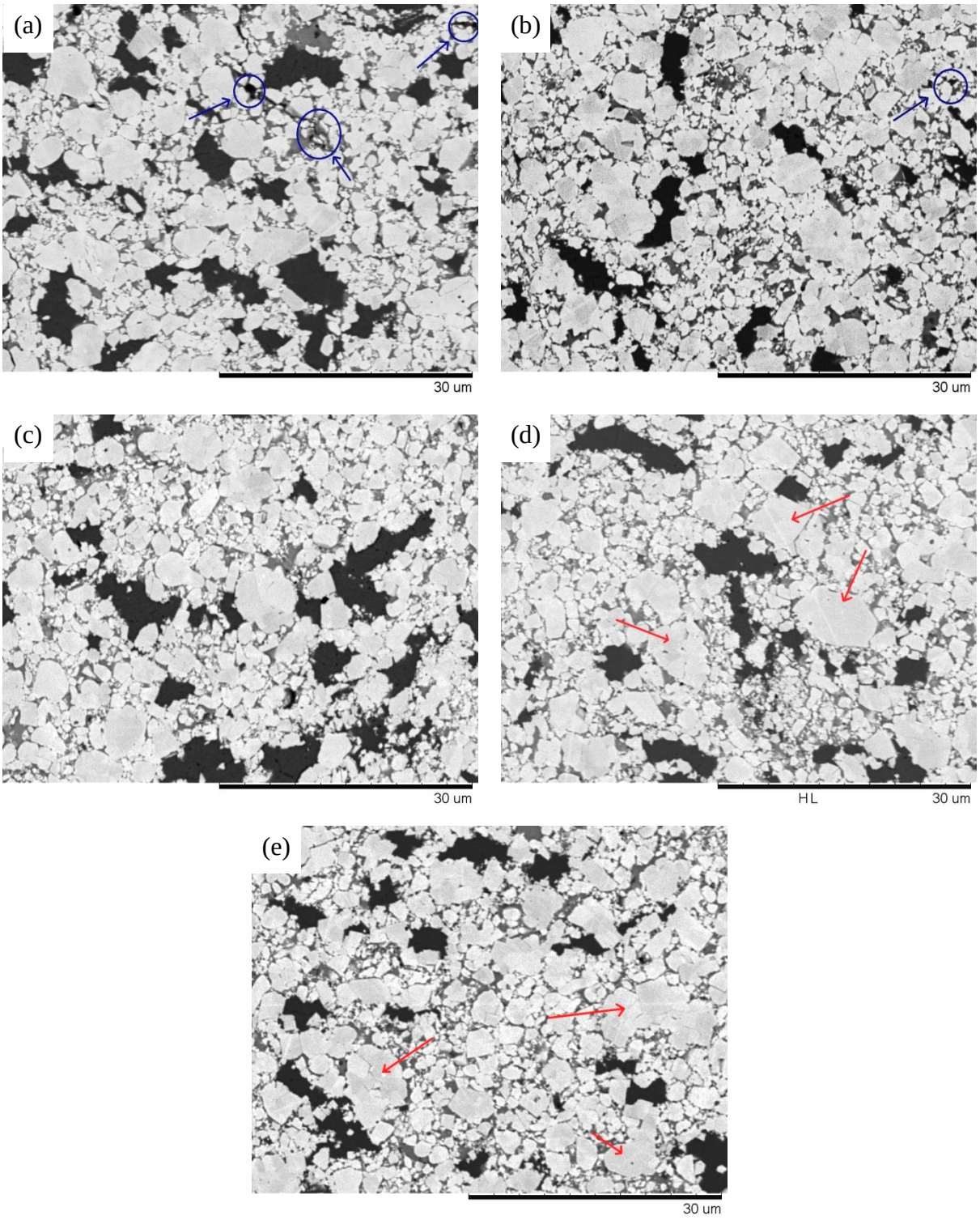

Source: Author.

Figures 4.30 and 4.31 also show that the WC particle size distribution in all samples are almost the same specially for samples sintered at 1500 to 1700 ºC (Figures 4.30-a to 4.30-

c and Figures 4.31-a to 4.31-c). As it observed in samples sintered at 1800 and 1900 ºC, there is abnormal grain growth in microstructure for both sintering time of 2 and 3 minutes. It is more obvious in samples sintered at 1900 ºC (see red arrows in Figures 4.30-e and 4.31-e). This can be explained by the effect of higher temperature on diffusion rate.

At higher temperature, due to higher diffusion rate, it is easier for bigger particles to dissolve the smaller particles and grow. Because of the short sintering time, these abnormal growths were found only in samples sintered at 1800 and 1900 ºC. However, some evidence of growth initiation in samples sintered at 1700 ºC was also found but it seems sintering time was not sufficient for severe growth.

Table 4.8 shows the relative density of sintered samples to the theoretical density of WC- 10wt% Co at different sintering time and temperatures. In samples which was sintered at 1500 ºC and 1600 ºC with some fine porosities (Figures 4.30-a, b and 4.31-a, b), full density could not be achieved but the other three samples with no evidence of porosity (Figures 4.30-c to e and 4.31-c to e), attained full density.

As discussed before, achieving to full density at higher temperatures can be related to higher diffusion rate at higher temperature. Also, as the temperature increases, porosities decrease due to the higher liquid phase flux during sintering and could be a reason for increasing relative density [105]. It seems that increasing sintering time from 2 to 3 minutes has no considerable effect on density. It can be explained according to this fact that increasing temperature is more effective than increasing the time in diffusion processes.

Table 4.9 Relative density of sintered sample at different sintering temperatures.

Sintering temperature (ºC)		*1500*	*1600*	*1700*	*1800*	*1900*
Relative density (%)	2 Min sintering	90-93	93-97	100	100	100
	3 Min sintering	91-93	93-98	100	100	100

Source: Author.

Figures 4.32 and 4.33 show the XRD patterns of sintered samples in different temperatures for 2 and 3 minutes, respectively. All peaks related to WC are still completely clear but in most of the samples only one of the peaks related to Co is visible. The same explanation given before about the Co peaks disappearing in mixed powder can be applied here. However, for samples sintered at 1800 and 1900 ºC for 3 minutes there is another Co

peak very close to the WC peak at 2θ ≈ 46°. It can be related to Co grain growth at higher temperature which provides better detection and more intensive peaks.

Figure 4.32 XRD patterns of samples sintered for 2 minutes at different temperatures.

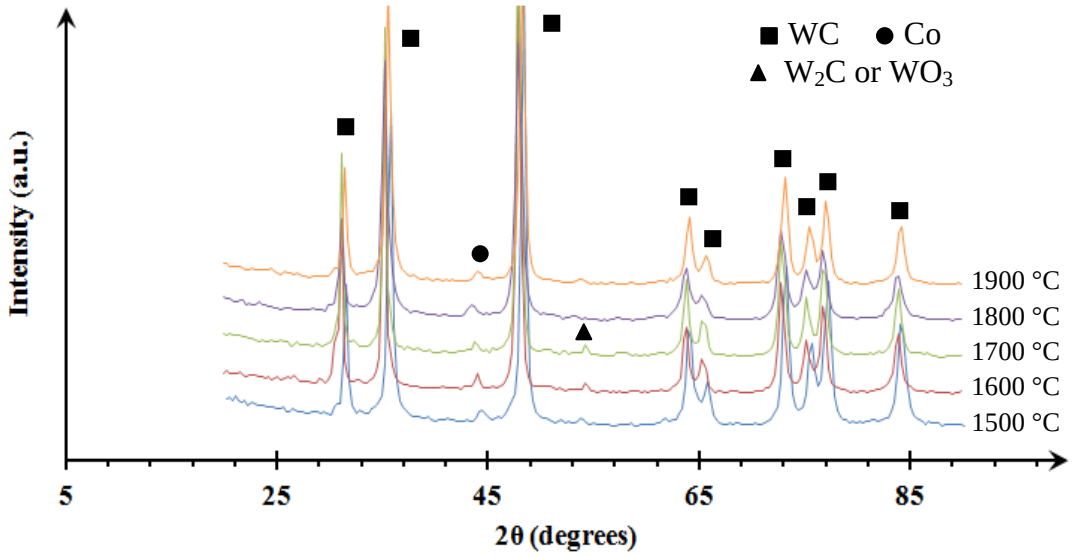

Source: Author.

Figure 4.33 XRD patterns of samples sintered for 3 minutes at different temperatures.

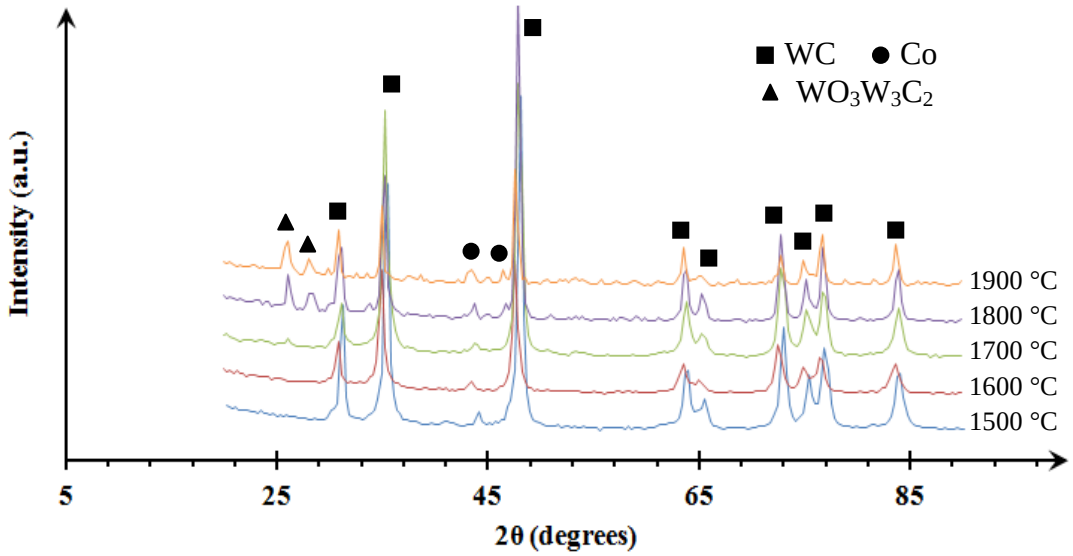

Source: Author.

There are also some peaks not related to none of the primary powders and did not exist in the XRD pattern of the mixed powders (Figure 4.29). Sample sintered at 1500, 1600 and 1700 ºC for 2 minutes had a very small peak at 2θ ≈ 53° related to W_2C or WO_3. Forming

intermediate phases during the WC/Co hardmetal sintering has been reported in various studies [106-109]. Peaks are small, compared to WC peaks which show that there is only small amount of these phases in the microstructure. These phases were formed at early stages of sintering process, as sintering has not been done in vacuum and no excess carbon was used.

As it can be seen in figures 4.32 and 4.33, this peak at $2\theta \approx 53°$ did not appear in samples sintered at 1800 and 1900 ºC for 2 minutes and all the other samples sintered for 3 minutes. It seems that higher sintering temperature and longer sintering time can dissolve these phases in the microstructure.

In figure 4.33, there are two peaks at $2\theta \approx 26°$ and 28° in the samples sintered at 1800 and 1900 ºC, showing some intermediate phase (Co_3W_3C) was formed during sintering. Other studies [106, 109] also reported this intermediate phase in hardmetal microstructure. As there is no peak related to this phase in samples sintered for two minutes at any temperature and also in samples sintered for 3 minutes at 1500 to 1700 ºC, it seems that this intermediate phase cannot form at low sintering temperature or short sintering time. In low sintering temperature and short sintering time condition, there was not enough carbon from WC to diffuse and subsequently form Co_3W_3C. It is important to note that this intermediate phase is formed due to a decrease in WC carbon content as a result of carbon reaction with adsorbed oxygen, almost instantly during a very quick HPHT sintering.

For IFT calculations, it is recommended to take into account the true (load independent) hardness of the material. It is well known that the apparent hardness decreases with the increase of indentation load and approaches a constant value at a relatively high load level [110]. The data resulted from Vickers hardness test at different testing load are listed in Table 4.9 and were used in IFT calculation. The results are also plotted versus sintering parameters in Figures 4.34 and 4.35.

An ideal tool material should have high hardness and high toughness. However, both the properties are inversely proportional to each other. Both properties are structure sensitive, so microstructure of the samples plays a very important role. Past research has also tried to optimize the combination through conventional and advanced sintering techniques. Controlling particle size/ microstructure is of great importance for all the sintering processes [111].

The hardness of WC-10 wt% Co hardmetals was almost independent on applied load but was sensitively dependent on the sintering temperature. As can be seen in Figure 4.34, the

hardness increases sharply by increasing the sintering temperature from 1500 to 1700 ºC for both sintering time. Increasing sintering temperature up to 1800 ºC for sample sintered for 2 minutes results in a slight increase in hardness but for sample sintered for three minutes results contrary (a slight decrease). There is a notable decrease in hardness by increasing sintering temperature from 1800 to 1900 ºC for both sintering time.

Table 4.10 Sintering parameters, hardness and fracture toughness of sintered samples.

Sample no.	*Sintering Temperature (°C)*	*Holding Time (min)*	*HV 15 kgf/mm²*	*Fracture Toughness HV_{15} MPa/m$^{1/2}$*	*HV 30 kgf/mm²*	*Fracture Toughness HV_{30} MPa/m$^{1/2}$*
1	1500	2	1247	12.60	1195	12.08
2	1600	2	1364	13.47	1373	12.94
3	1700	2	1579	15.36	1545	15.85
4	1800	2	1623	16.34	1563	16.04
5	1900	2	1478	16.66	1460	16.40
6	1500	3	1285	12.79	1310	12.39
7	1600	3	1480	13.73	1434	14.01
8	1700	3	1652	15.48	1673	15.89
9	1800	3	1583	17.13	1510	16.52
10	1900	3	1327	17.85	1250	16.91

Source: Author.

Figure 4.34 Vickers hardness as a function of sintering temperature for different sintering time of 2 and 3 minutes.

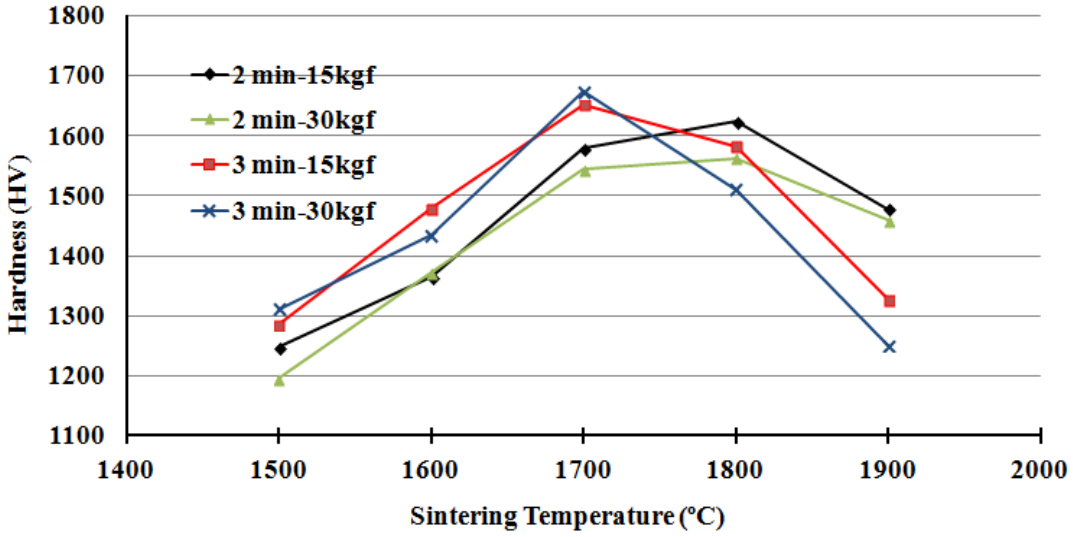

Source: Author.

Figure 4.35 IFT as a function of sintering temperature for different sintering time of 2 and 3 minutes.

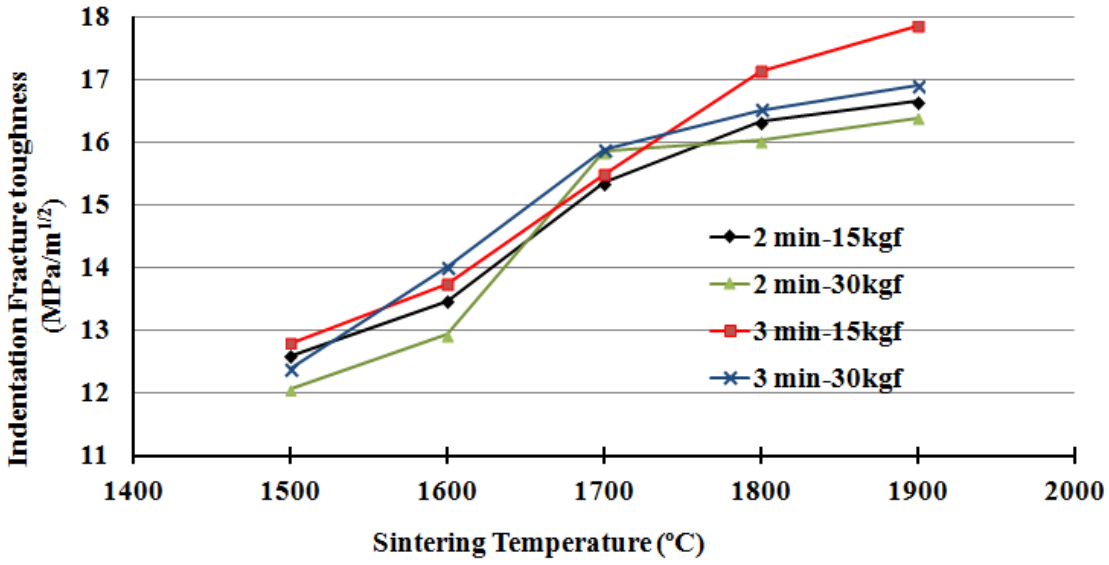

Source: Author.

The rapid increase of hardness above 1500 ºC seems to occur due to the formation of a liquid phase during sintering which leads to an increase in relative density and decrease in porosities. Moreover, the hardness slightly decreases above 1700 ºC for sample sintered for 3 minutes. It can be attributed the fact that the sintered density reaches the saturated value, but the grain size of WC considerably increases at higher temperatures. For samples sintered for 2 minutes, it seems that considerable increasing in the grain size of WC started above 1800 ºC. Hardness decreases dramatically for samples sintered at higher temperature and longer time due to negative effects of grain growth and formation of intermediate phases at higher temperature (Figure 4.33).

The highest hardness value around 1670 HV and fracture toughness of 15.89 MPa/m$^{1/2}$ were observed in samples sintered at 1700 °C/3 min. Samples sintered at 1800 and 1900 °C, with holding time of 2 minutes, presented higher fracture toughness that is in accordance with low hardness and grain growth of these samples. For samples sintered at 1500 and 1600 °C, with holding time of 2 and 3 minutes, higher fracture toughness was expected. Nevertheless, as can be seen in Figure 4.35, the fracture toughness is nearly low. It seems that presenting porosity and incomplete sintering reduced the fracture toughness. Intermediate phase (W_2C or WO_3) formation also can play a negative role in fracture toughness.

Kumar and Singh [111] collected some hardness and fracture toughness combinations obtained by some researchers, when hardmetals sintered by different techniques. Those results along with results achieved by Kumar and Singh [111] are listed in Table 4.10. The results are in good agreement with HPHT sintering of this study.

Table 4.11 Comparison of hardness and fracture toughness combinations obtained with different techniques [111].

Composition	*Sintering method*	*Hardness (kgf/mm^2)*	*Fracture toughness ($MPa/m^{1/2}$)*	*Sintering temperature (°C)*	*Holding time (min.)*
WC-10Co	HFIHS	1280	16.4	1150	1
WC-9.2Co	HFIHS	1992	11.9	1150	1
WC-10Co-0.7VC	CLPS	1610	10	1370	60
WC-10Co-0.7VC	CLPS	1610	10	1410	60
WC-10Co	CLPS	1310	13	1370	60
WC-10Co	CLPS	1410	11.8	1410	60
WC-11Co	CLPS	1782	9.4	1390-1470	-
WC-17Co	CLPS	1591	11	1390-1470	-
WC-21Co	CLPS	1483	12.3	1390-1470	-
WC-12Co	CLPS	1748	9.2	1390-1470	-
WC-20Co	CLPS	1359	13.6	1390-1470	-
WC-14Co	CLPS	1426	11.8	1390-1470	-
WC-17Co	CLPS	1335	13.8	1390-1470	-
WC-21Co	CLPS	1264	20.8	1390-1470	-
WC-13Co	CLPS	1395	12	1390-1470	-
WC-12Co-0.4VC	HIP	1340–1381	12.62–18.62	1390	60
WC-10Co-2VC	HIP	1430	14	1260	30
WC-20Co	CLPS	1582	14.3	1350	1
WC-20Co-2.5VC	CLPS	1693	14.1	1350	1
WC-20Co-5VC	CLPS	1709	15.1	1350	1
WC-20Co-7.5VC	CLPS	1870	14.4	1350	1
WC-20Co	CLPS	1566	15.5	1400	1
WC-20Co-2.5VC	CLPS	1701	13.8	1400	1
WC-20Co-5VC	CLPS	1649	14.7	1400	1
WC-20Co-7.5VC	CLPS	1687	12.4	1400	1

CLPS – Conventional liquid phase sintering, HIP – Hot iso-static pressing, HFIHS – High frequency induction heated sintering.

Figures 4.36 and 4.37 show the effect of sintering temperature on yield strength and compressive strength, respectively. Result values are all in same order of magnitude with result obtained by Santos [112] study of the mechanical properties of nanostructured WC-10Co hardmetal, with and without grain growth inhibitors (VC and Cr_3C_2).

Figure 4.36 Yield Strength as a function of sintering temperature for different sintering time of 2 and 3 minutes.

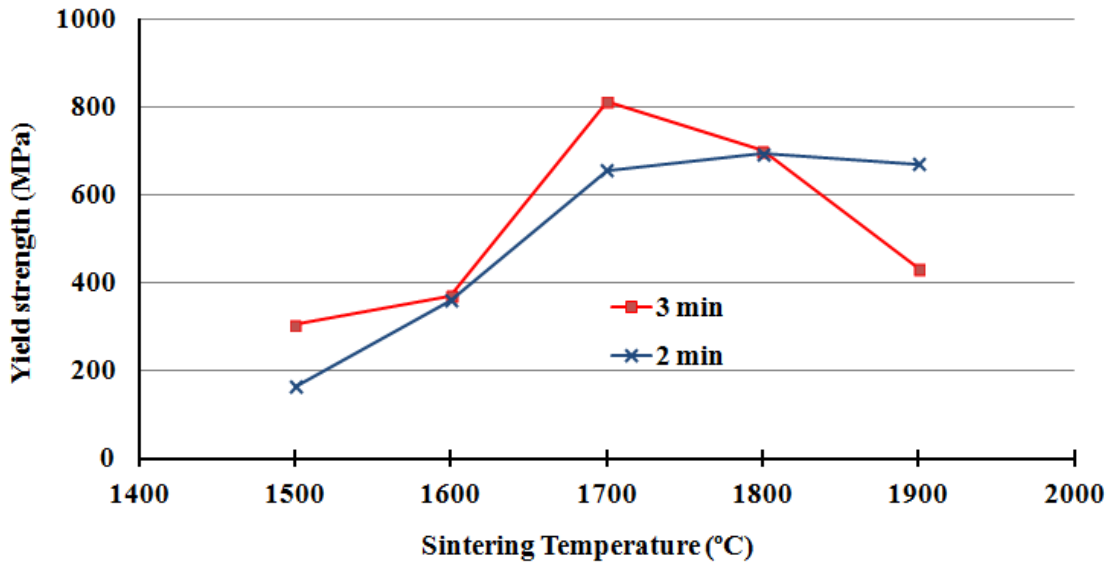

Source: Author.

Figure 4.37 Compressive strength as a function of sintering temperature for different sintering time of 2 and 3 minutes.

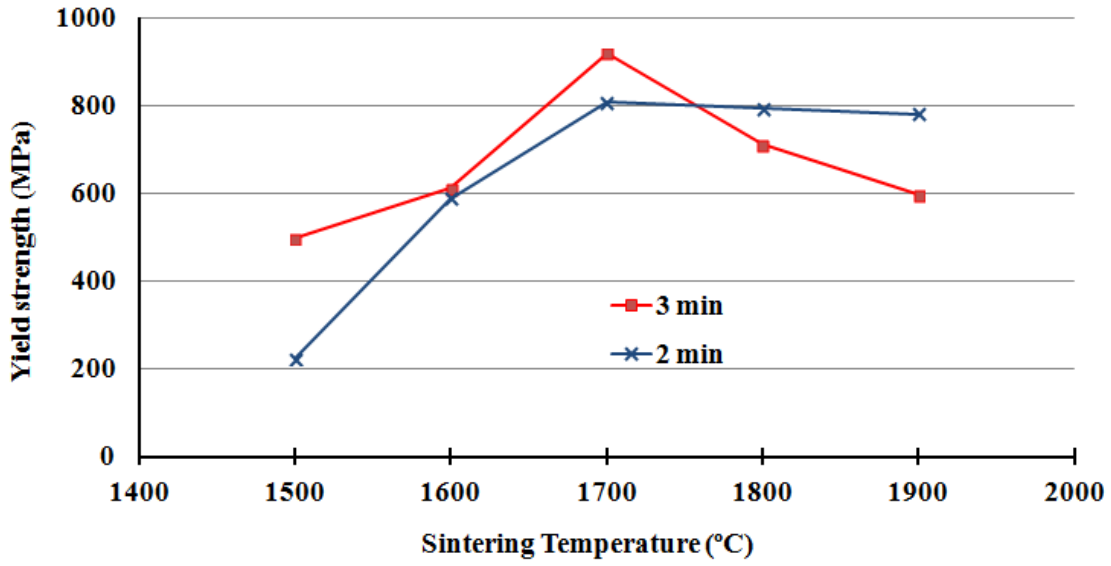

Source: Author.

The trend in both graphs is almost the same as hardness results and same explanation can be applied here as well. According to hardness and compression test results, it seems sintered density reached to saturated value at sintering temperature of 1700 and 1800 ºC for sintering time of 3 and 2 minutes, respectively. After this point, the WC particle size starts to grow, which affects mechanical properties such as hardness and compression strength. These results are completely in compliance with results from density measurement and microstructural study (Table 4.8 and Figures 4.30 and 4.31).

All the above achieved results show that the best HPHT sintering conditions, with a good combination of hardness and fracture toughness are 1700 °C/7.7 GPa/3 min, and 1800 °C/7.7 GPa/2 min. that are close to what found in previous section for sintering diamond powders.

4.3 Third stage - Triple layer PDC

Results from two previous stages were used to produce our final product that was triple layer PDC. The common problem in this kind of materials (layered) is separation between layers. Prepared samples were cross cut to study the layers and interface. Actually, cross cutting was the first test showing that the layers are adhered firmly because no separation was observed between layers specially between diamond and substrate. Figure 4.38 shows the mounted PDC samples. As can be seen three different layers are clear and connected.

Figure 4.38 Mounted PDC samples.

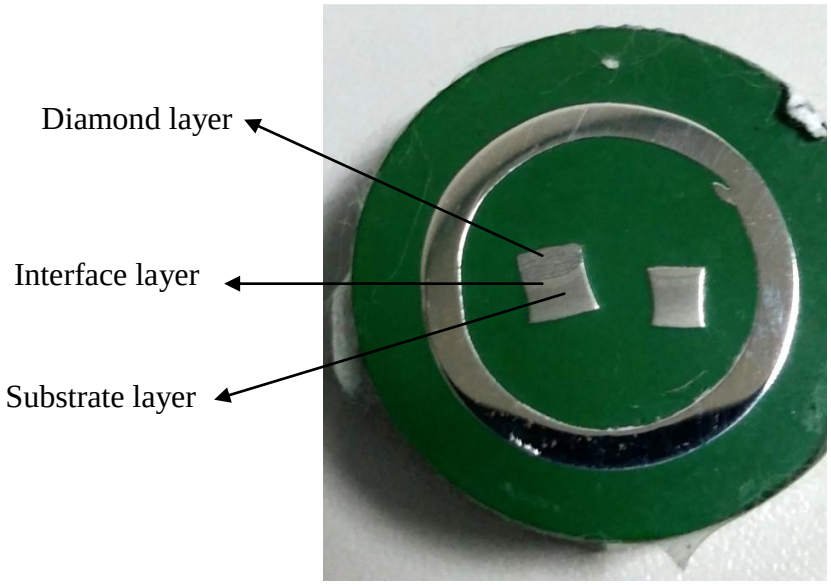

Source: Author.

SEM micrograph of produced PDC samples with different holding time in low magnification are shown in Figure 4.39. No cracks were found an microstructure even near the interfaces were it was at high risk of cracking because of the difference between thermal expansion coefficient of layers.

Figure 4.39 SEM micrograph of PDC samples. Holding time of 6 min (a) and 9 min (b).

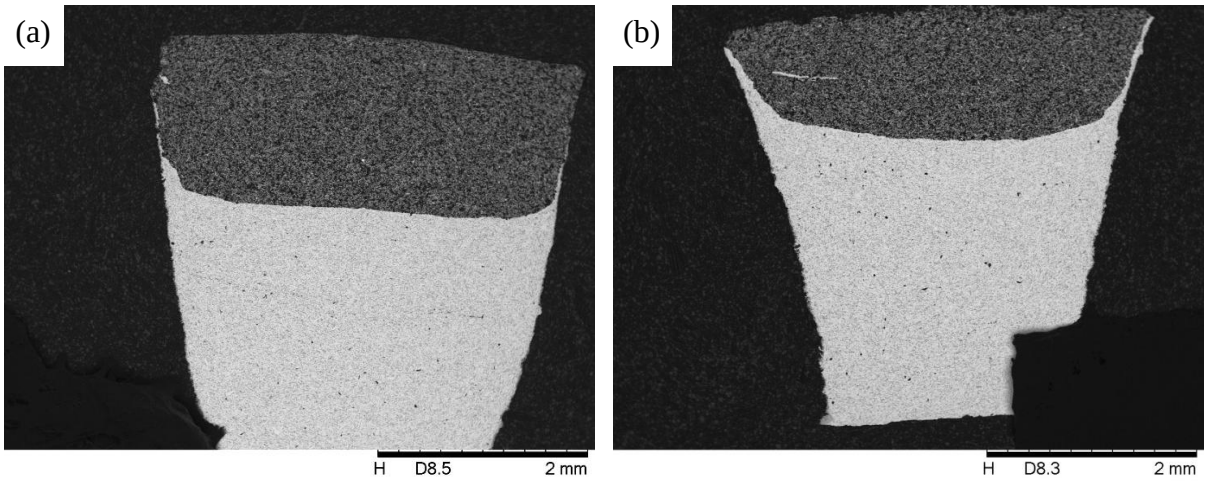

Source: Author

SEM Analyses show uniform dispersion of Niobium binder in diamond layer, for both holding time of 6 and 9 minutes, like what was seen in stage I for Niobium binder. No micro cracks and separation were also found in interfaces even at higher magnifications. Figures 4.40 and 4.41 show the diamond layer and interface of PDC samples sintered at 1750 °C/ 7.7 GPa/ 6 min and 1750 °C/ 7.7 GPa/ 9 min, respectively.

Figure 4.40 Diamond layer (a) and interface of diamond layer (b) an PDC sample sintered at 1750 °C/ 7.7 GPa/ 6 min.

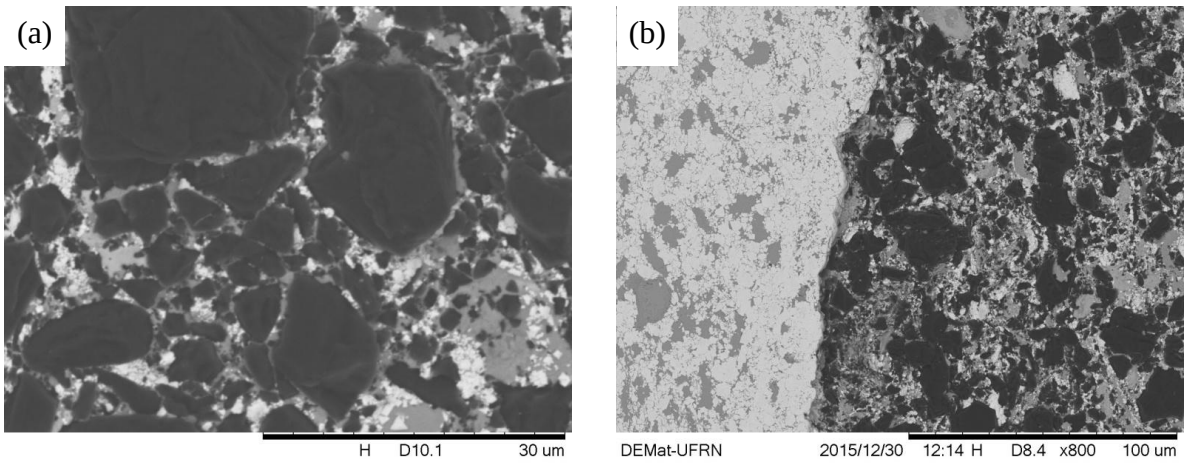

Source: Author

Figure 4.41 Diamond layer (a) and interface of diamond layer (b) an PDC sample sintered at 1750 °C/ 7.7 GPa/ 9 min.

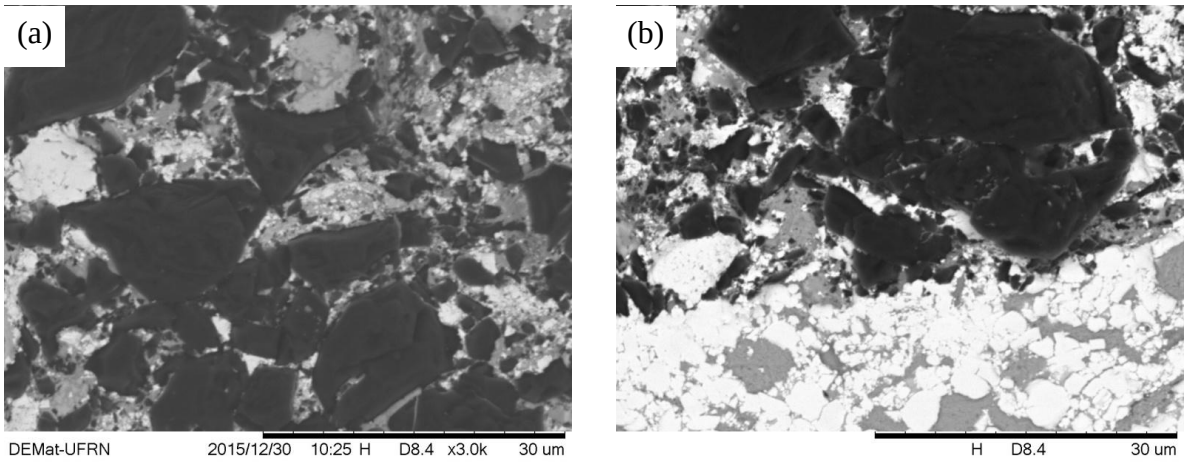

Source: Author.

There is no trace of graphitization (collapsing of binder, diamond transformation and cracks ...) at diamond layer even near the interfaces. The interface between substrate and interface layers was not really clear because this interface was made of two almost similar hardmetal (WC/Co and WC/Ni/Nb) however no cracks found in the entire microstructure of both hardmetals.

Nickel can diffuse into the diamond layer and, as this element is a metallic catalyst, it can cause graphitization in the diamond layer. Linear chemical analysis (Figure 4.42) via EDS around the interface shows the diffusion of Nickel into the diamond layer. Despite the diffusion of Nickel in the diamond layer, it seems that sintering parameters (Pressure, temperature and holding time) were correctly chosen to avoid graphitization for both holding time of 6 and 9 minutes.

The interface was not smooth because of the filling method of the mold (capsules). A rough interface line helps better adhesion between layers by mechanical locking between the different powder particles). Connection between metallic binder (Nb) that exist in the diamond and interface layers can also helps the better adhesion of layers. In addition to Niobium, WC and Nickel also diffused into the diamond layer, thus, they also have significant role in improving the inter layers bonding and reducing the chance of the inter layers separation. Figure 4.43 shows a map analyses done via EDS for a sample sintered at 1750 °C/ 7.7 GPa/ 9 min. Bonding the Niobium binder of the layers and the diffusion of WC and Ni can be seen in this figure.

Figure 4.42 Linear chemical analysis via EDS at interface of the PDC sample sintered at 1750 °C/ 7.7 GPa/ 9 min.

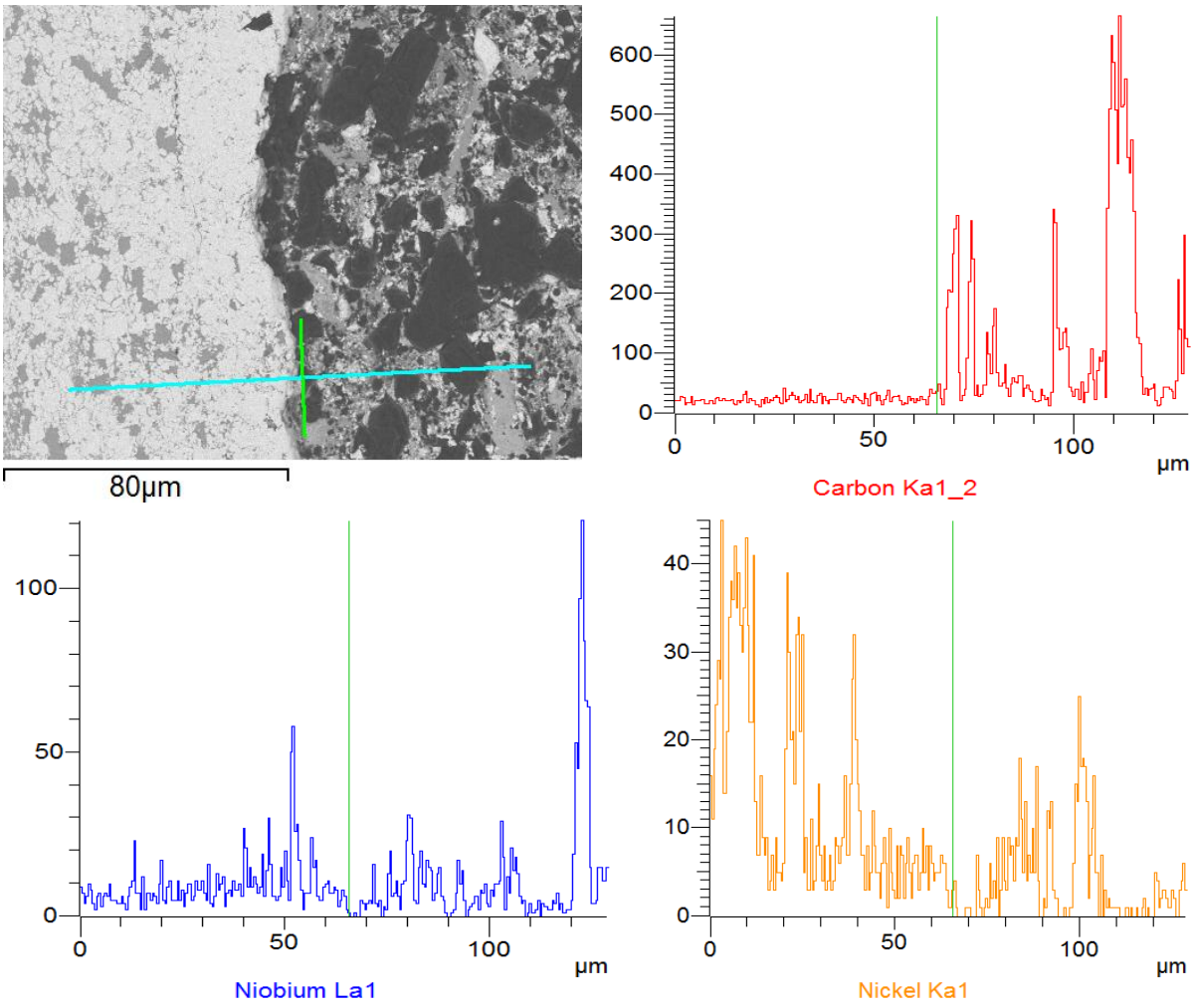

Source: Author.

Microhardness results showed the hardness in the range of 4500-6000 HV in the diamond layers for both holding time that is close to the hardness obtained befor, in stage I. Table 4.12 shows the microhardness results for two different sintering parameters and in the three different layers.

Lower hardness in substrate of the samples sintered with longer holding time can be related to grain growth of WC and binders (Co, Ni and Nb), as it was also observed in the studies explained at the stage II.

It is important to notice that the harness close to the interface line between diamond and interface layer was different with the other parts of microstructure. In the diamond layer, the hardness close to the interface was lower (around 400 HV) than the distant part of the

diamond microstructure. It can be related to the diffusion of Nickel and WC into this layer that results in the softening of diamond.

Figure 4.43 Map Analysis via EDS at the interface for the sample sintered at 1750 °C/ 7.7 GPa/ 9 min.

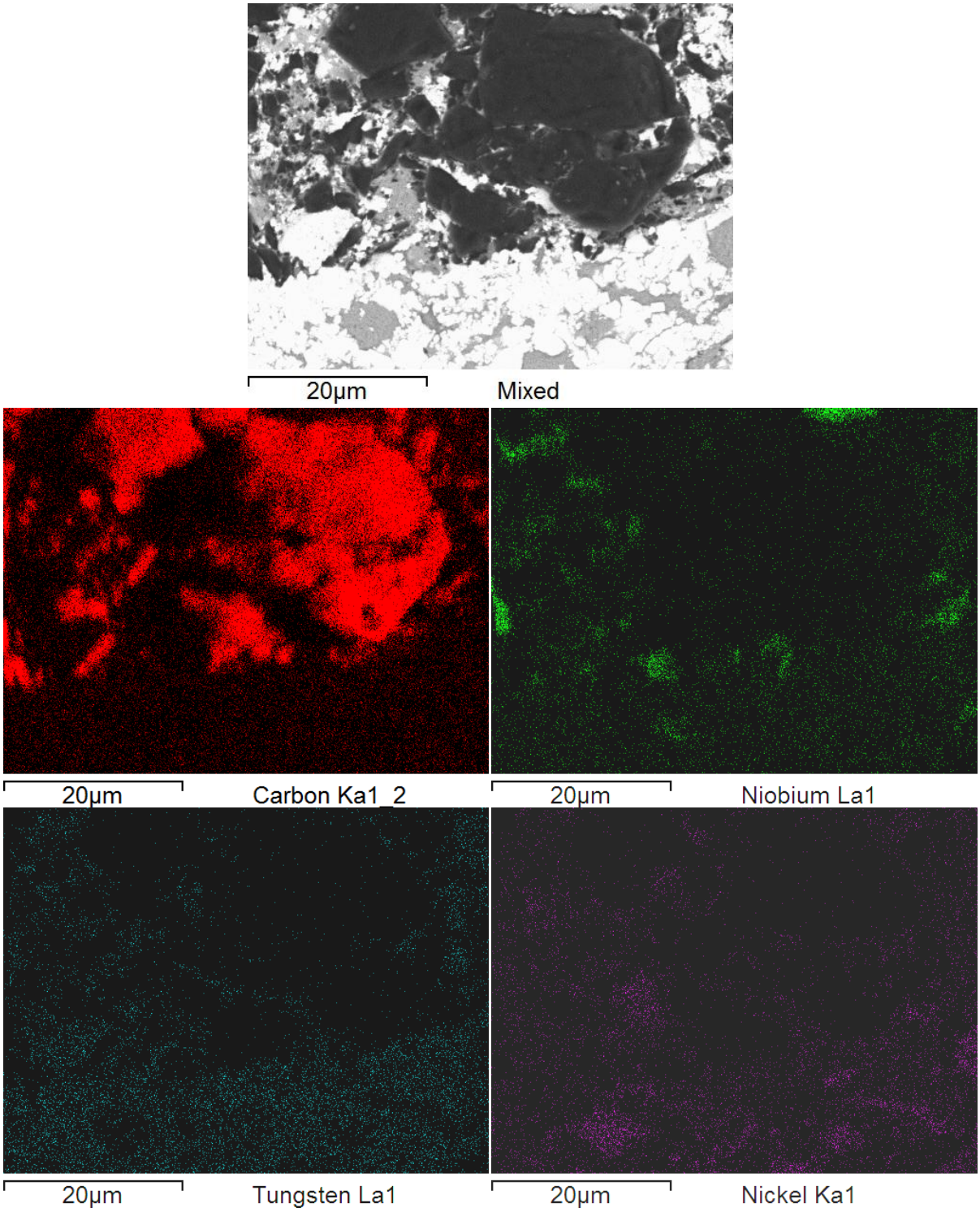

Source: Author.

Unlike diamond layer, in the interface layer, the hardness close to the interface line is higher (around 200 HV) than the distant parts of the microstructure. Like before, It can be explained by diffusion of elements, but in this case, it can be related to diffusion of Carbon from diamond layer to the interface layer. This Carbon can form some carbide such as NbC and increase the hardness.

Table 4.12 Microhardness ranges in different layers for samples sintered at 1750 °C/ 7.7 GPa for different holding times.

Holding time (min)	*Microhardness range (HV)*		
	Diamond layer	***Interface layer***	***Substrate layer***
6 (3 x 2)	4500-6000	1542-1660	1412-1532
9 (3 x 3)	4750-5800	1432-1638	1278-1330

Source: Author.

Chapter 5:

Conclusions

5. Conclusions

It is clear that producing new cutting tools such as bits, saw blades, PCDs, PDCs, etc and improving the available one is an important goal for research centers and industries. Thus, this research project aimed to obtain a new polycrystalline diamond compact with three different layers and with different composition. The main achievements of the present work are listed below:

- The triple layer polycrystalline diamond compact can be successfully produced by HPHT sintering method.

- Diamond layer with pure Nb as binder, which showed the best result during sintering, is the best option for top layer of PDCs.

- For this project WC 10wt % Co was used as substrate and resulted in good adhesion with interface.

- Interface of WC with Nb/Ni binder worked perfectly as a barrier for infiltrating of Co from substrate and as a result, no trace of Cobalt was found in the diamond layer.

- Nb in interface helped to make a better adhesion between diamond and interface layers.

- Microstructure of Produced PDC had no graphitization, cracks or interlayer separations.

- Nb/Fe binder caused graphitization of diamond during sintering even at high pressure but, Nb/Ni and Nb/Co binders showed no or little amount of graphitization during sintering.

- Diamond sintered with Nb/Ni and Nb/Co binders did not achieve to high hardness.

- Among Nb/Ni and Nb/Co binders, the first had better results according to hardness and microstructure.

- Diamond sintered with pure Nb had the best result between all binders.

- The best sintering parameters were 1750 °C/7.7 Gpa with holding time longer than 6 min.

- Hardmetal substrate sintered by HPHT method showed abnormal grain growth at higher temperature.

- The best combination of hardness and fracture toughness for hardmetal substrate achieved at 1700 and 1800 °C.

Recommendations

More research should be done in order to have a comprehensive knowledge about this new kind of cutting tool. Different compositions in layers and different sintering parameters can be considered to produce different tools with different properties suitable for different applications. Followings are some recommendations for pursuing the project.

- Laboratory scale producing of some triple layer tools (bits, PDC, …).
- Tribological studies or other performance tests in order to comparing with conventional tools.
- Study the diamond sintered body with different amount of Nb binder.
- Study different interface composition.
- Study the effect of pre-prepared hardmetal substrate.
- Study the effect of different hardmetal composition.

References

[1] J.L. Wise et al, Effects of Design and Processing Parameters on Performance of PDC Drag Cutters for Hard-rock Drilling, Technical Report, Sandia National Laboratories and US Synthetic Corporation, 2002.

[2] J.T. Finger, D.A. Glowka, PDC Bit Research at Sandia National Laboratories, Technical Report, Sandia National Laboratories, 1989.

[3] H.P. Bovenkerk et al., Preparation of Diamond, Nature, 184, 1959, 1094–1098.

[4] P. Boryczko, Drill Bit Selection and Optimization in Exploration Well 6507/6-4A in the Nordland Ridge Area, Master's Thesis, Faculty of Science and Technology, University of Stavanger, 2012.

[5] D. Belnap, A. Griffo, Homogenous and Structured PDC/WC-Co Materials for Drilling, Diamond and Related Materials, 13(10), 2004, 1914-1922.

[6] C.H. Cooley, N. Meany, C. Hughes, The Development of a Fracture Resistant PDC Cutting Element, SPE Annual Technical Conference and Exhibition, New Orleans, Louisiana, USA, 1994, 25-28,

[7] S.G. Moseley, K.P. Bohn, M. Goedickemeier, Core Drilling in Reinforced Concrete using Polycrystalline Diamond (PDC) Cutters: Wear and Fracture Mechanisms, Int. Journal of Refractory Metals and Hard Materials, 27(2), 2009, 394 - 402.

[8] T. Lin, G.A. Copper, M. Hood, Fatigue Test on Polycrystalline Diamond Compacts, Materials Science and Engineering: A, 163, 1993, 23-31.

[9] K. Zacny, Fracture and Fatigue of Polycrystalline Diamond Compacts, Society of Petroleum Engineers, 27(1), 2012, 145-157.

[10] Z. Fang, et al., Fracture Resistant Super Hard Materials and Hardmetals Composite with Functionally Designed Microstructure, Int. Journal of Refractory Metals and Hard Materials, 19(4), 2001, 453-459.

[11] Z. Fang et al., Chipping Resistant Polycrystalline Diamond and Carbide Composite Materials for Roller Cone Bits, SPE Annual Technical Conference and Exhibition, New Orleans, Louisiana, USA, 2001.

[12] M. Petrovic et al., The Mechanical Properties of Polycrystalline Diamond as a Function of Strain Rate and Temperature, Journal of the European Ceramic Society, 32, 2012, 3021-3027.

[13] E.H.L. Falcao, F. Wudl, Carbon Allotropes: Beyond Graphite and Diamond, Journal of Chemical Technology and Biotechnology, 2007, 82, 523–531.

[14] F.P. Bundy et al., The Pressure-Temperature Phase and Transformation Diagram for Carbon, Carbon, 34(2), 1996, 141–153.

[15] Properties of Diamond, De Beers Industrial Diamond Division, Special publication K4000, 5, 1989.

[16] J. Konstanty**,** Powder Metallurgy Diamond Tools, Elsevier Science, Amsterdam, Netherlands, 2005.

[17] J.E. Field, C.S.J. Pickles, Strength, Fracture and Friction Properties of Diamond, Diamond and Related Materials, 5, 1996, 625-634.

[18] J.E Field, The Properties of Natural and Synthetic Diamond, Academic Press, London, UK, 1992.

[19] E.M. Wilks, J. Wilks, The Abrasion Resistance of Natural and Synthetic Diamond, Wear, 81, 1982, 329 - 346.

[20] A. Mainwood, M.E. Newton, M. Stoneham, Science's Gem: Diamond Science, Journal of Physics-Condensed Matter, 21(36), 2009, Article No. 360301.

[21] S. Iijima, Y. Aikawa, M. Baba, Early Formation of Chemical Vapor Deposition Diamond Films, Applied Physics Letter, 57(25), 1990, 2646-2648.

[22] Z. Nitkiewicz, M. Zwierzy, Tin influence on Cutting Behavior of Diamond Sawblades for Stone Cutting, 13th Int. Scientific Conference on Achievements in Mechanical and Materials Engineering, Poland, 2005, 467-470.

[23] R.C. Burns, G.J. Davies, Growth of Synthetic Diamond, Academic Press, London, UK, 1992, 395–422.

[24] R. Chattopadhyay, Surface Wear: Analysis, Treatment and Prevention, ASM International, Materials Park, OH, USA, 2001.

[25] Y. Sato, M. Kamo, Synthesis of Diamond from Vapor Phase, Academic Press, London, UK, 1992, 423–470.

[26] V. Tatsii, A.V. Bochko, G.S Oleinik, Structure and Properties of Dalan Detonation Diamonds, Combust, Explosion and Shock Waves, 45(1), 2009, 95–103.

[27] H.T. Hall, The Synthesis of Diamond, Journal of Chemical Education, 38(10), 1961,1-7.

[28] C.S. Kennedy, G.C Kennedy, The Equilibrium Boundary Between Graphite and Diamond, Journal of Geophysical Research, 81(14), 1976, 2467-2470.

[29] H. Katzman, W.F. Libby, Sintered Diamond Compacts with a Cobalt Binder, Science, 172(3988), 1971, 1132-1134.

[30] E.H. Hughes, The Early History of Diamond Tools, Industrial Diamond Review, 40(6), 1980, 405-407.

[31] E. Hughes, Diamond Grinding of Metals, Industrial Diamond Information Bureau, Ascot, 1978.

[32] S. Tolansky, Early Historical Uses of Diamond Tools, In Proceedings of the International Industrial Diamond Conference 'Science and Technology of Industrial Diamonds', edited by J. Burls, Industrial Diamond Information Bureau, London, 2, 1967, 341-349.

[33] E. Gauthier, Diamond Lap, US Patent 1625463, 1927.

[34] W.D. Jones, Fundamental Principles of Powder Metallurgy, Edward Arnold Publishers Ltd., London, 1960.

[35] E.E. Brock, Abrasive Implement and Method of Making Same, US Patent 1537454, 1925.

[36] B. Sanford, Abrasive Wheel and a Method of Making the Same, US Patent U.S. 1981970, 1934.

[37] E. Lundblad, Swedish Synthetic Diamond Scooped the World 37 Years ago, Indiaqua, 55(1), 1990, 17-23.

[38] F.P. Bundy et al., Man-made Diamond, Nature, 176, 1955, 51-55.

[39] H.E. Bovenkerk et al., Preparation of Diamond, Nature, 184, 1959, 1094-1098.

[40] H.T. Hall, H.M. Strong, R.H. Wentorf, Method of Making Diamonds, US. Patent 2947610, 1960.

[41] M. Jennings, And the Next 50 Years?, Industrial Diamond Review, 63(1), 2003, 15-20.

[42] J. Konstanty, A Review of Diamond and CBN Sizing and Standards. Industrial Diamond Association of America, Inc., Skyland, USA, Publication No. S&S593 5M.

[43] L. Bjerregaard et al., Metalog Guide, Struers Tech A/S, Rødovre, Copenaghen, Denmark 1992.

[44] H. Prekwinkel, Single-crystal Diamond Tools for Laminated Floors, Industrial Diamond Review, 57(2), 1997, 44-46.

[45] E.A. Bex, Syndie Wire Drawing Die Blanks, In Advances in Ultrahard Materials Application Technology, Edited by P. Daniel, De Beers Industrial Diamond Division, Ascot, 2, 1983, 81-91.

[46] S.A. Herbert, Micron Diamond - an Advancing Technology, In Advances in Ultrahard Materials Application Technology, Edited by P. Daniel, De Beers Industrial Diamond Division, Ascot, 2, 1983, 112-125.

[47] I.E, Clark, E.K. Sen, Advances in the Development of Ultrahard Cutting Tool Materials, Industrial Diamond Review, 58(2) 1998, 40-44.

[48] R. Ladd, Manufactured Large Single Crystal Diamond, Paper Presented During Intertech 2003, Vancouver, Canada, 2003.

[49] P.K. Sen, Synthetic Diamond Dresser Logs: Serving the Future Needs of Industry, Industrial Diamond Review, 62(3), 2002, 194-202.

[50] P.R. Heus, The Applications and Properties of Monocrystal, Industrial Diamond Review, 57(1), 1997, 15-18.

[51] M. Musu-Colman et al., Surface Processing of Ultrahard Materials Used for Embedding in Resin or Metallic Matrices, In Proceedings of Powder Metallurgy World Congress and Exhibition, Granada, Spain, 4, 1998, 234-239.

[52] B.A. Cooley, Vitrified Bonds: no Longer a Synonym for Conventional Abrasive Tools, Society of Manufacturing Engineers, Chicago, USA 1985.

[53] A. Bakori, A. Szymariski, Practical Uses of Diamond, Ellis Horwood and Polish Scientific Publishers, Warsaw, 1993, 124-130.

[54] Micron Products, SANDVIK Hyperion, Product information leaflet GES 91-968.

[55] Antonini E, Vitrified bonds Diamante Applicazioni & Tecnologia, 1994, 1(2), 16-17.

[56] G.I. Harris, Long Life Resin Bond Wheels, In Ultrahard Materials in Industry - Grinding Metals, De Beers Industrial Diamond Division, 1991, 2-4.

[57] M. Jennings, Special Tooling for Specialist Tools, Industrial Diamond Review, 59(1), 1998, 6-7.

[58] M.W. Bailey, R. Garrard, H.O, Juchem, Characteristics of Diamond and Their Effect on Grinding Behaviour, Industrial Diamond Review, 59(1), 1999, 10-19.

[59] V. Mackensen et al., Fine Grinding with Diamond and CBN, Industrial Diamond Review, 57(2), 1997, 40-43.

[60] G. Schwan, R. Zimmerer, Economic Polishing of Granite, Industrial Diamond Review, 58(1), 1998, 4-5.

[61] K. Przyklenk, Diamond Impregnated tools - Uses and Production, Industrial Diamond Review, 53(4), 1993, 192-195.

[62] W. Tillmann, Trends and Market Perspectives for Diamond Tools in the Construction Industry, Int. Journal of Refractory Metals & Hard Materials, 18, 2000, 301-306.

[63] B.V. Derjaguin, D.V. Fedoseev, Low Pressure Diamond Growth, Industrial Diamond Review, 50(3), 1990, 155-160.

[64] Syndie & Monodic - the Largest Die Blank Range in the World, Industrial Diamond Review, 51(4), 1991, 168-172.

[65] M.W. Cook, Diamond Machining of MMC Engineering Components, Industrial Diamond Review, 58(1), 1998, 15-18.

[66] I.E. Clark, PCD Wood Tools - a New Design Concept, Industrial Diamond Review, 53(2), 1993, 73-76.

[67] R. Feenstra, Status of Polycrystalline Ddiamond Compact Bits: Part 1 – Development, Journal of Petroleum Technology, 40(6), 1988, 675-684.

[68] J.C. Walmsley, A.R. Lang, TEM Study of SYNDAX3, Compared with SYNDITE and AMBORITE, In Advances in Ultrahard Materials Application Technology, Edited by C. Barrett, De Beers Industrial Diamond Division, Ascot, 4, 1988, 61-75.

[69] I.E. Clark, Polycrystalline Diamond Drill bits in Mining Applications, In Advances in Ultrahard Materials Application Technology, Edited by C. Barret, De Beers Industrial Diamond Division, Ascot, 4, 1988, 17-35.

[70] E.N. Tomlinson, I.E. Clark, SYNDAX3 Pins - New Concepts in PCD Drilling, Industrial Diamond Review, 52(3), 1992, 109-114.

[71] A. Ersoy, M.D. Waller, Drilling Detritus and Operating Parameters of Thermally Stable PCD Core Bits, Int. Journal of Rock Mechanics and Mining Sciences, 34(7), 1997, 1109-1123.

[72] J.N. Boland, X.S. Li, Microstructural Characterisation and Wear Behaviour of Diamond Composite Materials, Materials, 3, 2010, 1390-1419.

[73] H.S. Li et al., High-Pressure Synthesis and Characterization of Thermal-Stable Boron-doped Diamond Single Crystals, Int. Journal of Refractory Metals & Hard Materials, 27, 2009, 564–570.

[74] T.N. Sexton, C.H. Cooley, Polycrystalline Diamond Thrust Bearings for Down-Hole Oil and Gas Drilling Tools, Wear, 267, 2009, 1041–1045.

[75] J.E. Westraadt, N. Dubrovinskaia, Thermally Stable Polycrystalline Diamond Sintered with Calcium Carbonate, Diamond Related Materials, 16, 2007, 1929–1935.

[76] D.E. Scott, The History and Impact of Synthetic Diamond Cutters and Diamond Enhanced Inserts on the Oil and Gas Industry, Industrial Diamond Review, 1, 2006, 48–55.

[77] S.G. Moseley, K.P. Bohn, M. Goedickemeier, Core Drilling in Reinforced Concrete using Polycrystalline Diamond (PCD) Cutters: Wear and Fracture Mechanisms, Int. Journal of Refractory Metals & Hard Materials, 27, 2009, 394–402.

[78] D. Belnap, A. Griffo, Homogeneous and Structured PCD/WC-Co Materials for Drilling, Diamond Related Materials, 13, 2004, 1914–1922.

[79] Z. Fang et al., Fracture Resistant Superhard Materials with Functionally Designed Microstructure, Int. Journal of Refractory Metals & Hard Materials, 19, 2001, 453–459.

[80] V. Kanyanta, S. Ozbayraktar, K. Maweja, Effect of Manufacturing Parameters on Polycrystalline Diamond Compact Cutting Tool Stress-state, Int. Journal of Refractory Metals & Hard Materials, 45, 2014, 147–152.

[81] K.E. Bertagnolli, R. Vale, Understanding and Controlling Residual Stress in Thick Polycrystalline Diamond Cutters for Enhanced Durability, Finer Points, USA, 2000.

[82] K.C. *Bach, An Improved Cube Cell Assembly for the Use With High Pressure/High Temperature Cubic Apparatus* in Manufacturing Polycrystalline Diamond Compact Inserts, Master's thesis, School of Technology, Brigham Young University, 2009.

[83] R. Riedel, Handbook of Ceramic Hard Materials, Wiley, VCH, 2000.

[84] S. Ozbayraktar, PCD Sintering Model, Element Six (Pty) Ltd Internal Research Report, 1995.

[85] Amanda Lynne McKie, Carbon Enriched Thermal Sprayed Hardmetal Coatings Used in PCD Sintering, PhD thesis, Faculty of Engineering and the Built Environment, University of the Witwatersrand, 2012.

[86] K. Naidoo, Polycrystalline diamond abrasive compact, US Patent US 20110214921 A1, 2011.

[87] J.D. Belnap, Thermally-stable polycrystalline diamond materials and compacts, US Patent 2009/0114454 A1, 2009.

[88] M.M. Karimi, U.U. Gomes, M. Filgueira, Triple Layer Cutting Composite Formed of Cemented Carbide Substrate and Sintered Diamond Body Connected with an Interface, Brazilian Patent BR 10 2016 019214 5, 2016.

[89] M.D. Dennis, Cutting Element Having Composite Formed of Cemented Carbide Substrate and Diamond Layer and Method of Making Same, US Patent 4784023, 1988.

[90] H.D. Richard, Polycrystalline Diamond Body with Enhanced Surface Irregularities and Methods of Making the Same, European patent 0133386 A2, 1985.

[91] R.H. Wentorf, Jr., W.A. Rocco, Diamond Tools for Machining, US Patent Re 32380 E, 1987.

[92] H. Ishizuka, Method for Producing Composite of Diamond and Cemented Tungsten Carbide, US Patent 4411672, 1983.

[93] H. Ishizuka, Method for Producing Diamond Compact, US Patent 4440573, 1984.

[94] F. Cverna, ASM Ready Reference: Thermal properties of metals, ASM International, 2002.

[95] ASTM International Standard, Standard Test Methods for Density of Compacted or Sintered Powder Metallurgy (PM) Products Using Archimedes' Principle, ASTM B962, 2013.

[96] International Organization for Standardization, Hardmetals - Vickers hardness test, ISO 3878, 1983.

[97] International Organization for Standardization, Hardmetals - Compression test, ISO 4506, 1979.

[98] Shetty D.K, Wright IG, Mincer P.N, et al. Indentation fracture of WC–Co cermets. J Mater Sci. 1985; 20:1873–1882.

[99] A.B. Kurdumov, A.B. Biliankevich, Physical transformation of carbon and boron nitride, Metallography 6, 1989, 186–189.

[100] O.N. Breusov et al., Effect of High Temperature Vacuum Annealing on Properties of Detonation Synthetic Diamond, Proceedings of International Symposium on Physico-chemical Properties of Ultra-hard Materials, Academy of Science, Kiev, 1987, 48– 53.

[101] J. Qian et al., Graphitization of Diamond Powders of Different Sizes at High pressure–high temperature, Carbon, 42, 2004, 2691–2697.

[102] B.D. Cullity, Elements of X-ray diffraction, Pearson Education, Nov 2013.

[103] R. Jenkins, R.L. Snyder, Introduction to X-Ray Powder Diffractometry, J. Wiley, New York, 1996.

[104] A. Petersson, J. Agren, Rearrangement and Pore Size Evolution During WC–Co Sintering Below the Eutectic Temperature, Acta Materialia, 53, 2005, 1673–1683.

[105] Mi. Karbasi, A. Saidi, M.H. Fathi, The Effect of Sintering Temperature on Microstructure and Hardness of the Milled WC-20 Wt.% Equiatomic (Fe,Co) Cemented Carbides, Journal of Advanced Materials and Processing, 3, 2015, 29-38.

[106] C.M.F.G. Marques, G.S. Bobrovnitchii, J.N.F. Holanda, Phase Analysis by X-ray Diffraction on the WC-10Co Doped with Rare-earth Elements Obtained under High Pressure, Matéria, 18, 2013, 10-18.

[107] M.F. Rodrigues et al., High Pressure Sintering of the WC/10Co Alloy, Matéria, 11, 2006, 174-180.

[108] X.L.Shi et al., Mechanical Properties, Phases and Microstructure of Ultrafine Hardmetals Prepared by WC–6.29 Co Nanocrystalline Composite Powder, Materials Science and Engineering: A, 392, 2005, 335–339.

[109] P. Peetsalu et al., Characterization of WC-Co Composite Thermal Spray Powders and Coatings, Proceedings of the Estonian Academy of Sciences and Engineering, 12, 2006, 435–444.

[110] F. Sergejev, M. Antonov, Comparative Study on Indentation Fracture Toughness Measurements of Cemented Carbides, Proceedings of the Estonian Academy of Sciences and Engineering, 12(4), 2006, 388–398.

[111] D. Kumar, K. Singh, High Hardness - High toughness WC-20Co Nanocomposites: Effect of VC Variation and Sintering Temperature, Materials Science and Engineering: A, 663, 2016, 21–28.

[112] C.M. Santos, Effect of Grain Growth Inhibitors in the Mechanical Properties of WC-10 wt% Co from Nanostructured WC, Master's thesis, Northern Fluminense State University, 2011.